

# Case Study of Convection Lines During GATE

By

R.N. Mower

Department of Atmospheric Science  
Colorado State University  
Fort Collins, Colorado

**Colorado  
State**  
University

**Department of  
Atmospheric Science**

Paper No. 271



CASE STUDY OF CONVECTION LINES DURING GATE.

by

R. N. Mower

Research Report supported by

The Global Atmospheric Research Program,  
National Science Foundation and the  
GATE Project Office, NOAA under grant  
OCD-74-21678.

Principal Investigators: A.K. Betts and S.K. Cox

Department of Atmospheric Science  
Colorado State University  
Fort Collins, Colorado  
80523.

June 1977.

Atmospheric Science Paper No. 271



## ABSTRACT

### CASE STUDY OF CONVECTION LINES DURING GATE

A semi-quantitative case-study of 2 September 1974 (Julian Day 245) is presented. As many data sources as possible were used to describe the dynamics and thermodynamics of two lines of active convection located within the GATE B-scale ship array. The northern line and southern line were located to the north and south of the C-scale array respectively. Data relative to the lines from a total of five aircraft flying on north-south legs have been composited and indicate a region of strong convergence near the surface ahead of the line ( $\sim 10^{-3} \text{ s}^{-1}$ ) with a somewhat weaker divergence to the rear associated with a region of downdraft air. Both lines seem to indicate that 3-dimensional motions may be important in their development and an analysis of the composited data show the lines to be similar in one respect to tropical squall-lines with block inflow to the south and block outflow to the north. The lines have a travel speed of  $\sim 6 \text{ ms}^{-1}$  southwards with no conclusive evidence of the steering level suggested by Pestaina-Haynes and Austin (1976). At present, no attempt has been made to explain their origin and formation except to suggest that an adequate supply of high  $\theta_E$  air extending from the surface to at least cloud base is required for their maintenance. The low-level divergence and vorticity also seem to be important. No observable temperature change can be found across the lines except near the surface indicating the presence of a shallow density current with an origin between 900 mb and 800 mb which spreads out when it reaches the surface. A density current model is solved for the travel speed using the observed temperature change (Miller and Betts,



1976). This gives a value of  $\sim 3.5 \text{ ms}^{-1}$  showing that this model probably does not apply to this type of convection.

The fact that the lines travel southwards at  $6 \text{ ms}^{-1}$  is not clearly understood except to comment that they appear to be embedded in feeder bands to a well defined vortex to the NE of the A/B-scale array and it is possible that their movement is closely related to the large-scale dynamics of the vortex although no conclusive evidence is presented in this paper.



## ACKNOWLEDGEMENTS

The author wishes to express his gratitude for the financial support, invaluable guidance and encouragement given by Dr. Alan K. Betts during the course of this research. The advice of Drs. W. M. Gray and J. E. Cermak is very much appreciated. Special thanks are due to Ms. Sandy Wunch, Ms. Renee Jorgensen, Ms. Pauline Martin and Mr. Steve Knox for their assistance in manuscript typing, drafting, data acquisition and computer programming. The author is also grateful to the members of the NCAR GATE Group for many helpful discussions. I would also like to thank Dr. G. Austin of McGill University for supplying me with processed Quadra radar data.

This research was supported by the Global Atmospheric Research Program of the National Science Foundation, and the GATE Project Office, NOAA, under grant OCD-74-21678.



## TABLE OF CONTENTS

	<u>PAGE</u>
ABSTRACT	ii
ACKNOWLEDGEMENTS	iv
TABLE OF CONTENTS	v
LIST OF TABLES	vii
LIST OF FIGURES	viii
LIST OF SYMBOLS	xi
I. INTRODUCTION	1
1.1 The GATE experiment	1
1.2 Objectives of this report	3
1.3 Previous studies	3
1.4 Contents of this report	7
1.5 Data	8
1.6 Further data reduction	12
II. SYNOPTIC-SCALE PICTURE	16
III. PHYSICAL FEATURES OF THE LINES	33
3.1 Quadra radar cross-sections	33
3.2 Aircraft cross-sections	36
3.3 Line travel speeds	38
3.4 Cross-sections through the southern line from boom and aircraft data	40
3.5 Cloud - subcloud layer features	47
3.6 Vertical profiles	59
3.6.1 Wind profiles	60
3.6.2 Thermodynamic profiles	63
3.6.3 Vorticity and divergence	67



TABLE OF CONTENTS - Continued

	<u>PAGE</u>
3.6.4 Discussion	71
3.7 Density current model	71
IV. DATA INTERCOMPARISON	74
4.1 Aircraft and Quadra radar	74
4.2 Dallas BLIS - aircraft - Dallas boom	74
4.3 BLIS, aircraft and rawinsonde data	77
V. CONCLUSIONS	86
REFERENCES	90



## LIST OF TABLES

<u>TABLE</u>		<u>PAGE</u>
1	Altitudes flown by the GATE aircraft.	8
2	Quality flags for aircraft data.	9
3	Comparison of averaging methods for Dallas 0300Z, 245.	11
4	Sources of errors in parameters from which wind is derived.	13
5	Differences in wind components before and after corners for CV-990 and L-188.	14
6	Rainfall rates from Z-R relationship.	35
7	Data sources and their associated features.	40
8	Number of runs with good data at each level for both lines.	43
9	Corrections for the trends in u and v.	60
10	Characteristics of layers associated with this line of convection.	70
11	3 km mean wind intercomparison.	76
12	3 km mean specific humidity and potential temperature intercomparison.	77



## LIST OF FIGURES

<u>FIGURE</u>		<u>PAGE</u>
1	Location of the GATE ship arrays.	2
2	Visible photograph from SMS-1 satellite at 1300Z.	17
3	Visible photograph from SMS-1 satellite at 1500Z.	18
4	Visible photograph from SMS-1 satellite at 1800Z.	19
5	Oceanographer radar at 1500Z.	20
6	Quadra radar precipitation intensities at 1500Z.	21
7	Rawinsonde and BLIS 1200-2100Z average vorticity and divergence. (Reeves and Ropelewski, 1976).	23
8	Surface streamline analysis at 1200Z day 245.	24
9	700 mb streamline analysis at 1200Z day 245.	25
10	200 mb streamline analysis at 1200Z day 245.	26
11	Maximum and mean cloud-top heights for northern line.	28
12	Maximum and mean cloud-top heights for southern line.	29
13	SMS-1 satellite brightness data for 1200Z.	30
14	SMS-1 satellite brightness data for 1600Z.	31
15	Quadra radar cross-sections along 22.8°W at 1229Z, 1329Z and 1529Z.	34
16	(a) Temperature, dew point and LWC traces for DC-6 along one leg. (b)	37
17	Plotted wind-vectors for DC-6 along the flight tracks.	39
18	Time sequence of events measured by different systems for northern line.	41
19	Time sequence of events measured by different systems for southern line.	42
20	Pressure, LCL and incoming solar radiation relative to the southern line from 3-minute Dallas boom data.	44



LIST OF FIGURES - Continued

<u>FIGURE</u>		<u>PAGE</u>
21	Thermodynamic and wind parameters relative to the southern line from 3-minute Dallas boom data.	45
22	Mean of 2 runs through southern line at 985 mb for DC-6.	48
23	Mean of 4 runs through southern line at 960 mb for DC-6.	49
24	Mean of 4 runs through southern line at 900 mb for L-188.	50
25	Mean of 4 runs through southern line at 810 mb for L-188.	51
26	Mean of 2 runs through southern line at 720 mb for US-C130.	52
27	Mean of 7 runs through southern line at 640 mb for US-C130.	53
28	Wind components relative to the southern line from 3 minute Dallas BLIS data.	55
29	Equivalent potential temperature ( $\theta_E$ ) relative to the southern line from 3 minute Dallas BLIS data.	57
30	Potential temperature ( $\theta$ ) relative to the southern line from 3 minute Dallas BLIS data.	58
31	Average zonal wind component for southern line from aircraft data.	61
32	Average meridional wind component for southern line from aircraft data.	62
33	Average specific humidity for southern line from aircraft data.	64
34	Average potential temperature for southern line from aircraft data.	65
35	Average equivalent potential temperature for southern line from aircraft data.	66
36	Mean 2-dimensional divergence computed from aircraft data.	68



LIST OF FIGURES - Continued

<u>FIGURE</u>		<u>PAGE</u>
37	Mean 2-dimensional vorticity computed from aircraft data.	69
38	Mean inflow to southern line from Dallas boom (sfc) and aircraft data.	72
39	Comparison of aircraft specific humidity and Quadra precipitation intensity at (I) 1214Z, (II) 1229Z and (III) 1314Z at 4 km.	75
40	BLIS, aircraft, boom and rawinsonde potential temperature intercomparison for 1221Z.	78
41	BLIS, aircraft, boom and rawinsonde specific humidity intercomparison for 1221Z.	79
42	Quadra and aircraft potential temperature intercomparison at 1202Z and 1505Z.	81
43	Quadra and aircraft specific humidity intercomparison at 1202Z and 1505Z.	82
44	u wind-component intercomparison between the Vize 1130Z sounding and proximate aircraft values.	83
45	v wind-component intercomparison between the Vize 1130Z sounding and proximate aircraft values.	84
46	Schematic of stream-tubes and characteristics of this line of convection.	88



## LIST OF SYMBOLS

$\theta$	Potential temperature
$\theta_E$	Equivalent potential temperature
$q$	Specific humidity
$u$	Zonal wind component
$v$	Meridional wind component
$p$	Atmospheric pressure
LCL	Lifting condensation level
INSOL	Incoming solar radiation
BLIS	Boundary layer instrument systems
A/C	Aircraft
nm	Nautical miles



## I. INTRODUCTION

### 1.1 The GATE experiment

Prior to the GATE experiment, which was conducted in the summer of 1974, there was a serious deficiency both in the quality and quantity of meteorological data in the tropics. Consequently, much of the research in the tropics to date has had to employ a compositing technique where data relative to a number of similar atmospheric phenomena are averaged together. (Although this is a useful numerical tool to study large-scale atmospheric systems, sub-synoptic and mesoscale systems should be studied case-by-case because any form of averaging may disguise important features.) This meant that we were unable to understand one of the unresolved problems in tropical meteorology -- namely scale-interaction. In an attempt to fill in this gap in our knowledge, a massive data network was set up between East Africa and Brazil with sufficient density to monitor weather systems ranging from the cumulus scale to the wave, (or planetary) scale.

The experiment was focused in the eastern Atlantic where a network of 3 nested ship arrays were set up. These are indicated in Figure 1.

In decreasing order of size we have:

- |                    |   |                            |
|--------------------|---|----------------------------|
| a) A/B-scale array | ~ | synoptic scale             |
| b) B-scale array   | ~ | sub-synoptic scale         |
| c) C-scale array   | ~ | mesoscale or cumulus scale |

The experiment consisted of three separate phases when the ships released rawinsondes at regular intervals -- every six hours and every three hours during intensive periods. These data were supplemented with the use of thirteen highly instrumented aircraft which flew coordinated

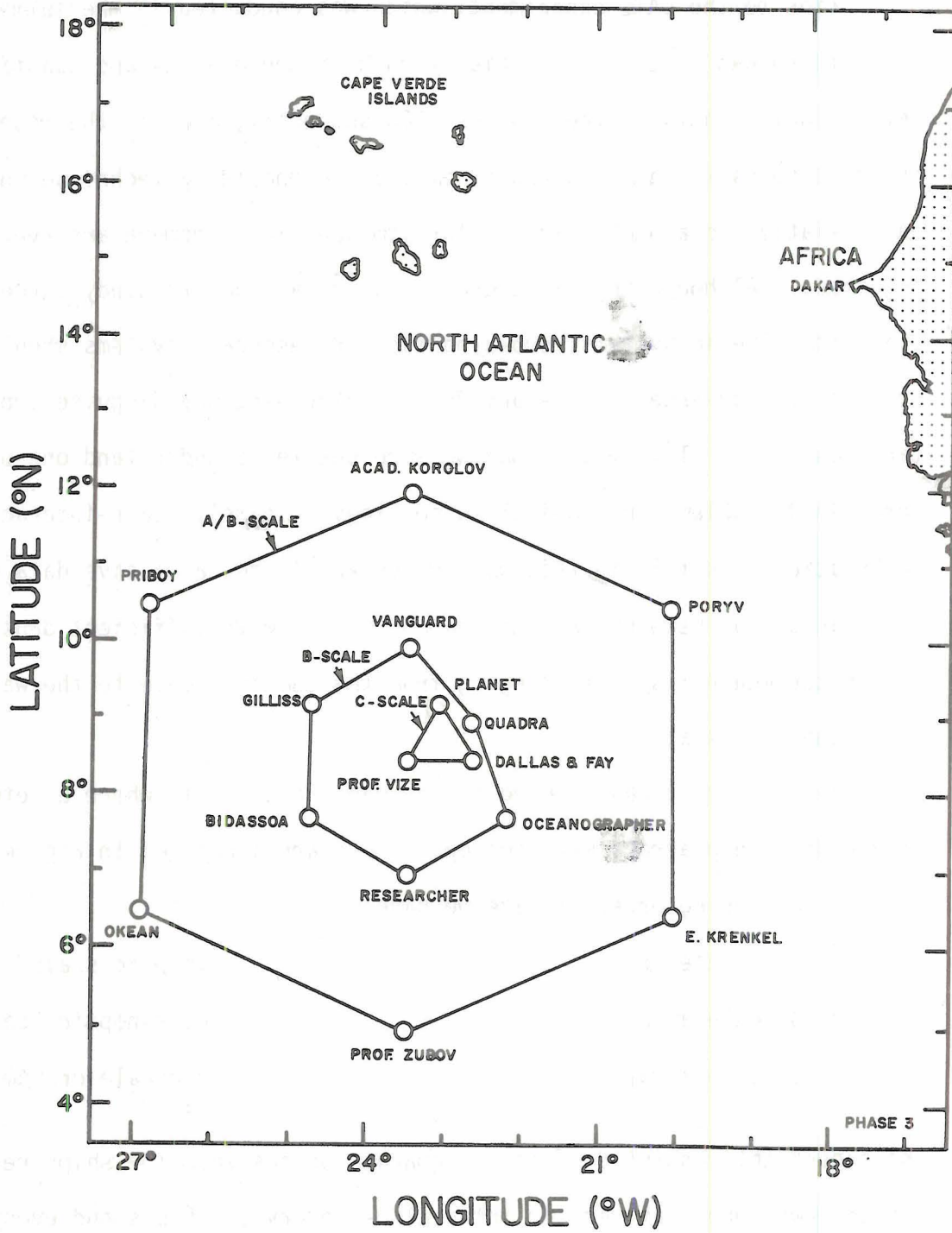


Figure 1. Location of the GATE ship arrays.

missions through regions of active convection located within the ship arrays. Other instrumentation systems include tethered balloons, structure sondes and meteorological buoys, which are useful in studies which require a high degree of resolution in the sub-cloud layer. The development of weather systems was also monitored by ship radar and the SMS-1 satellite which provided twenty-four hour coverage. Thus, we now have a valuable data set from which we should be able to answer questions regarding scale-interaction and to improve our present numerical models of the global circulation.

### 1.2 Objectives of this report

The goal of this research is two-fold. First, an attempt has been made to describe the thermodynamic and dynamic features of lines of convection which appeared with surprising regularity within the GATE ship arrays. Secondly, as many independent data sets as possible were used so that an intercomparison of the data sets will serve to validate the data. In an experiment of this nature, several different data systems were used to measure the same parameters thereby introducing problems of instrument calibration and intercomparison. Since the experiment, our main concerns have been data intercomparison and validation.

### 1.3 Previous studies

Recent research efforts in tropical meteorology have been directed towards the study of tropical cloud clusters and their relationship to easterly waves. Cloud clusters have been studied extensively by Riehl (1947, 1954) and Williams and Gray (1973). Reed and Recker (1971) and Burpee (1972, 1974), described the structure and properties of wave disturbances using a compositing technique and found the convection to

be closely correlated with the location of the wave-axis. More recent studies by Reed et al. (1977) showed similar results using GATE data composited relative to eight wave disturbances during phase III. However, the GATE has provided large quantities of data on all space-scales ranging from cumulus-scale to planetary (or wave) scale. It is now possible to conduct more detailed studies of the small scale weather systems which are individual components of a cloud cluster. The convection line is one such component.

It is the small, organized weather systems which account for a high percentage of the rainfall in the tropics (Krishnamurti, 1968) even though their area coverage may be only a few percent. Studies using high altitude observations, conducted by Kuettner (1959, 1971), showed mesoscale organization of small tropical cumulus into cloud bands which had a definite spacing. One such band is a squall-line. The air flow becomes highly organized in these systems thus enabling them to propagate for hours. Studies, to date, notably Zipser (1969) and Betts in a series of papers on Venezuelan squalls, have been primarily concerned with air flow through these systems and its consequent modification.

In a case study using data from the Line Islands Experiment, Zipser (1969) showed that the development of tropical disturbances requires a high degree of organization. The convergence/divergence patterns were most intense in the lowest 500 m consistent with the idea of Gray (1968) that large sub-cloud layer convergence is fundamental to producing intense convection.

Moncrieff and Green (1972), Browning (1962) have already stressed the importance of the slope of the main updraft (in the upshear sense) in the maintenance of line-type convection.

Zipser (1977), and Miller and Betts (1977) stressed the importance of the downdraft in the energetics of the system. Air enters the squall from the front, most of which rises into the active towers. The consequent precipitation induces downdraft activity on two different scales. The cloud-scale downdraft has its origins beneath the main updraft and is near saturated as it reaches the surface. The mesoscale downdraft has its origins beneath the anvil to the rear of the main updraft. This downdraft is unsaturated and eventually attains positive buoyancy with the result that it only occasionally is able to reach the surface. The unsaturated air (formed by a mixing process) to the rear of the squall-line increases the fluxes of sensible heat and moisture from the ocean to the atmosphere and is, therefore, very important to the energetics of the tropics.

Papers by Betts (1976) (observational) and Moncrieff and Miller (1976) (theoretical) describe the transformation of the atmosphere after the passage of a squall-line. The transformations are closely related to the level of origin of the downdraft air. This air has its origin in low levels atop the updraft air in the subcloud layer. As the downdraft is accelerated towards the surface, two opposing processes come into operation, i.e. descent produces a warming and drying and evaporation produces a cooling and moistening. Thus, it is possible to observe four different transformations:

- a) warming and drying
  - b) warming and moistening
  - c) cooling and drying
  - d) cooling and moistening.
- a) and c) are the most commonly observed.

With a few exceptions, e.g. 12th September 1974, most of the lines of convection observed during the GATE were of a 'mild' nature having low-level winds of order  $6 \text{ ms}^{-1}$  and so they can hardly be called squall-lines. Cloud tops frequently reached the upper troposphere as a result of large humidities in the mid-troposphere.

Since the GATE there have been several case studies using high resolution aircraft data. Using uncorrected data obtained during the field phase of the experiment, Reed et al. (1975) made a brief analysis of a flight into the ITCZ on August 4, 1974 and found large 2-dimensional convergence where the convective activity was maximum. The convergence attained a value of  $3 \times 10^{-4} \text{ s}^{-1}$ . Most of the changes associated with the ITCZ took place in a small distance ( $\sim 3 \text{ km}$ ). In another paper, Reed (1975) in a case study of a squall on June 28, 1974 found a maximum convergence at the leading edge of the line and a maximum divergence to the rear of the rain band. Pennell (1975) studied an isolated line of cumulus and also observed strong low-level wind shifts. Downdraft activity was also found to be present even though the line was relatively weak.

An intensive study of a mesoscale disturbance during BOMEX (Smith et al., 1975) suggests that these systems are embedded in larger wave troughs. However, two case-studies by Seguin and Garstang (1976) indicated strong cloud layer-subcloud layer coupling on the convective scale. They commented that in the absence of low-level convergence, mesoscale systems will be short-lived. The author feels that this is the case in this study. However, the problem of scale-interaction is still unresolved and the case-study approach could shed some more light on the subject.

#### 1.4 Contents of this report

The 2nd September 1974 (Day 245) was chosen for study because two well developed lines of convection were observed to the west of 'Quadra' in the C-scale array. A stack of six aircraft flew on north-south tracks through both lines in the latter stages of their development, thus enabling aircraft data to be composited relative to the lines. The data for one aircraft (Il-18M) were not available. These data combined with rawinsonde, tethered balloon and structure sonde data have been used to qualitatively describe the 2-dimensional flow through the lines and to determine the consequent dynamic and thermodynamic changes produced upon the environment.

A brief overview of the data used and data reduction techniques is given in Chapter 1. Chapter 2 shows the synoptic-scale picture using several observational systems.

The results are presented in Chapter 3. The meso-synoptic flow in the vicinity of the lines is described from aircraft cross-sections and high resolution tethered balloon data. Some vertical profiles relative to the lines are also presented.

Chapter 4 is devoted entirely to data intercomparison between several platforms. In the first section the aircraft cross-sections are compared to the precipitation intensity cross-sections from the Quadra radar and in the last section an evaluation of the BLIS, rawinsonde, aircraft and boom data has been made.

Finally, some comments about the relationship of the lines to their large-scale environment are given together with some suggestions for future research.

### 1.5 Data

The core of the study consists of

#### (a) Aircraft data:

Table 1. Altitudes flown by the GATE aircraft.

Aircraft	Altitudes (Kft)	Pressures (mb)
DC-6	0.85, 1.3, 2	985, 970, 945
L-188	3.2, 6	900, 810
USC-130	9, 12	720, 640
I1-18C	15	574
CV-990	25, 31, 37	220, 290, 380

Table 1 indicates the five aircraft for which data were available. The DC-6, USC-130, L-188 took data samples every second and the CV-990 every two seconds during their flights. Wind components, ambient and dew point temperatures and atmospheric pressure were the principal parameters measured. The I1-18C did not have the capability of measuring humidity and data values were given every minute only.

Individual data values were given quality flags and are shown in Table 2.

Table 2. Quality flags for aircraft data.

FLAG	DESCRIPTION
1	O.K.
2	Machine flagged questionable - annotator says O.K.
3	Unvalidated
4	Machine flagged questionable
5	Annotator flagged questionable (not flagged by machine)
6	Before take-off and after landing
9	Missing data

(b) Rawinsonde data:

During the intensive periods of the experiment most of the ships in the A/B, B and C-scale arrays launched rawinsondes every three hours and every six hours at other times. Processed data from the U.S.S.R. ships contained parameters at standard and significant levels only while the Canadian and U.S.A. ships contained all dynamic and thermodynamic parameters at 5 mb intervals. These data have been generated from the raw data using a series of processing steps, (see Rasmusson et al., 1976). Several surface reports from merchant ships in the area have been used to fill in data-sparse regions in the arrays.

(c) Radar data:

Approximate locations of the areas of convection were found from photographs of the radar-scope from Oceanographer, Meteor, Researcher and Quadra. This product gave only two intensity levels at best. More accurate locations of the convection were found from a higher quality

product from Quadra showing both precipitation intensity and echo-top height in digital form. Scans were available at fifteen minute intervals throughout the day making it possible to quantitatively describe the time-history of the convection in the region of interest. Further data processing yielded radar cross-sections of precipitation intensity along 22.8°W (flight track). The range of the Quadra radar is 200 km giving adequate coverage over the region of interest.

(d) Satellite data:

SMS-1 gridded images on 35 mm microfilm have been used with resolutions of 0.5, 1 and 2 nm, and typical images at 0.5 nm resolution are shown later. Another product giving satellite brightness values in digital form for a specified area are also shown.

(e) BLIS, boom and mast data:

The BLIS consists of a four second time series. Dry bulb and wet bulb temperatures, relative humidity and atmospheric pressure were computed once every four seconds. The wind speed and direction and tilt angle were sampled once every two seconds. The set contains a time series of all measurements; that is, the four second data taken during the fixed level mode or constant level mode. Finally, the data have been averaged in three minute and hourly blocks and are at four different levels (995, 970, 950, 910 mb) for this day.

A similar procedure was applied to the ship boom data. The boom was located approximately 10 m above the sea surface. In addition, all radiation parameters are given. Data will be presented at the time when the southern line passed over the Dallas and will be used to further supplement and confirm the aircraft data relative to the same line.

Table 3. Comparison of averaging methods for 'Dallas' 0300Z 245.

Level	25 mb		50 mb		60 sec		120 sec		Observed	
	$\bar{u}$	$\bar{v}$	$\bar{u}$	$\bar{v}$	$\bar{u}$	$\bar{v}$	$\bar{u}$	$\bar{v}$	$\bar{u}$	$\bar{v}$
	$\text{ms}^{-1}$									
1000	2.2	-3.7	2.1	-4.0	2.2	-4.0	2.1	-3.8	2.1	-4.3
850	1.9	-3.5	0.9	-3.6	1.6	-3.5	0.8	-3.7	2.4	-3.2
700	-4.1	-1.7	-4.5	-1.6	-4.1	-1.7	-4.3	-1.6	-3.1	-1.4
640	-6.6	-0.5	-5.5	-0.6	-6.6	-0.5	-5.6	-0.5	-7.4	-0.4
500	-6.9	-7.2	-5.4	-7.3	-6.9	-7.2	-6.3	-7.3	-7.2	-7.2
200	-11.8	3.4	-11.3	4.1	-9.9	2.7	-11.8	3.4	-9.9	2.7

## 1.6 Further data reduction

This section describes the averaging and convection methods applied to these data by the author. The reader will recall that these data have been subject to a number of quality checks and processing routines prior to archiving. For a complete discussion see Acheson (1974); Rasmusson et al. (1976).

### (a) Rawinsonde data:

A method for smoothing out wild data points in the wind components is to perform some sort of block averaging process in the vertical. Four block averages (25 mb, 50 mb, 60 sec and 120 sec) were performed on the 0300Z, 245 sounding from Dallas, the results from which are shown in Table 3. The 'observed' column indicates the 5 mb data at the level in question. The zonal wind component is seen to be slightly more sensitive to the averaging process in that the differences between the averaged values are relatively large. However, the differences between the averaged values are generally  $< 1.5 \text{ ms}^{-1}$  which is thought to be less than the observational error. Hence, a 25 mb average was thought to be adequate enough to smooth out wild data points and small enough to preserve natural variations in the wind profiles.

### (b) Aircraft data:

As stated in the previous section, the aircraft data consists of one second values of all parameters with the exception of the IL-18C which only gives wind components at various points along its track, usually every minute and the CV-990 reporting values at two second intervals.

To eliminate a large volume of data and smooth out most of the 'noise' but still preserve natural features in the data, ten second

block averages were taken with poor quality data deleted from the average. With the low-level aircraft flying at  $100 \text{ ms}^{-1}$  and the high level at  $200 \text{ ms}^{-1}$ , this corresponds to an approximate space scale of approximately 1 km and 2 km respectively.

Data with flags 1, 2, 3 and 4 have been included in the ten second averages. If less than three good data values appeared in the average, that average was flagged as questionable by the computer and was used in the analysis with caution. However, in regions of active convection, where large horizontal gradients are known to exist, the annotator's flags may be too restrictive.

There was the additional problem of the apparent change in the wind vector when the aircraft changes heading. A series of parameters measured on board the aircraft (each of which are subject to at least one source of error) are used to determine the wind vector. These parameters and their corresponding sources of error are given in Table 4. (See also Grossman, 1976).

Table 4. Sources of errors in parameters from which wind is derived.

PARAMETER	SOURCE(S) OF ERROR
True Air Speed	Dynamic pressure Static pressure Temperature
Ground Speed	Calibration
True Heading	Compass reading
True Track	Drift angle reading True heading reading

Errors in the wind vectors before and after all corners were particularly noticeable with the L-188 and CV-990. See Table 5.

Table 5. Differences in wind components before and after corners for CV-990 and L-188.

A/C	CORNER	$\Delta u$	$\Delta v$
- ( $\text{ms}^{-1}$ ) -			
CV-990	1		1.2
	2		4.0
	3		0.1
	4		0.8
	5		2.7
	6		8.5
			$\overline{\Delta v} = 2.9 \pm 3.1 \text{ ms}^{-1}$
L-188	1	7.5	0.3
	2	5.7	2.0
	3	7.6	0.7
	4	7.7	0.3
	5	6.9	0.6
	6	6.3	1.8
	7	6.0	0.4
			$\overline{\Delta u} = 6.8 \pm 0.8 \text{ ms}^{-1}$
			$\overline{\Delta v} = 0.9 \pm 0.7 \text{ ms}^{-1}$

$\Delta u$  - change in u after completing a maneuver

$\Delta v$  - change in v after completing a maneuver

For the CV-990 there was no systematic change in u and so this has not been included in the table. For the above calculations, ten data points were used on either side of the corner for both aircraft. This corresponds to 10 km on either side for the L-188 and 20 km for the CV-990. Each pair of wind components were chosen so that they occurred at the same latitudes and the wind field was assumed to remain stationary in time and homogeneous in space. Since each leg was in the north-south direction, it becomes a simple task to correct the wind components

by taking half the difference ( $\overline{\Delta u}/2$ ,  $\overline{\Delta v}/2$ ) and then adding  $\overline{\Delta u}/2$  to the u components on one leg and subtracting  $\overline{\Delta u}/2$  from the u components on the other leg, and similarly for v.

A more sophisticated method for correcting the winds has been used by Ruiz (1975), which uses a simple vector triangle to compute directly the true airspeed error and drift angle error from which the required corrections can be easily computed. This program was developed for an aircraft cloverleaf pattern.

In this study, the corrections remove about  $2.5 \text{ ms}^{-1}$  of bias error from the measured wind. Residual errors of  $1 \text{ ms}^{-1}$  for the L-188 and  $2 \text{ ms}^{-1}$  for the CV-990 are probably still present after correction. There were no observable bias errors in the wind vectors for both the DC-6 and the USC-130.

## II. SYNOPTIC-SCALE PICTURE

Satellite images from the SMS-1 are presented in Figures 2-4. Figure 2 shows there to be an active vortex off the coast of West Africa which is obscured by a dense layer of cirrus. Associated with this vortex are several feeder bands orientated NNE, SSW. The most pronounced of which is located directly over 'Oceanographer'. The two lines (A and B) through which the aircraft flew repeated legs are clearly visible to the west of 'Quadra' within the C-scale array. It appears as if they are components of this synoptic-scale system and their motion may be closely related to the large-scale flow. However, this is beyond the scope of this study since we are merely attempting to describe their characteristics. Figure 3 shows the lines just prior to their maximum intensity and both have moved in a southerly direction towards the southernmost cloud mass which can tentatively be called the ITCZ. Figure 4 again shows the lines at 1700Z when most of the A/B-scale array is covered by a thick layer of cirrus which is the product of the previous active convection. The complete system is now termed a cloud-cluster, the large-scale features of which have been extensively studied by Gray and numerous other authors.

In order to show consistency with other data products, digital scans from 'Oceanographer' and 'Quadra' radar are shown in Figures 5 and 6. These show the lines with the cirrus canopy absent and are well represented on the 'Oceanographer' radar at 1500Z in Figure 5. At this time the southern line appears to be much more active - especially at its 'leading' edge than does the northern line which is located to the NW of the scan. This fact is also shown in the data presented later.

13:00 245:34 01-A-H 0545 2650 A1 DAK 6A4 CH1

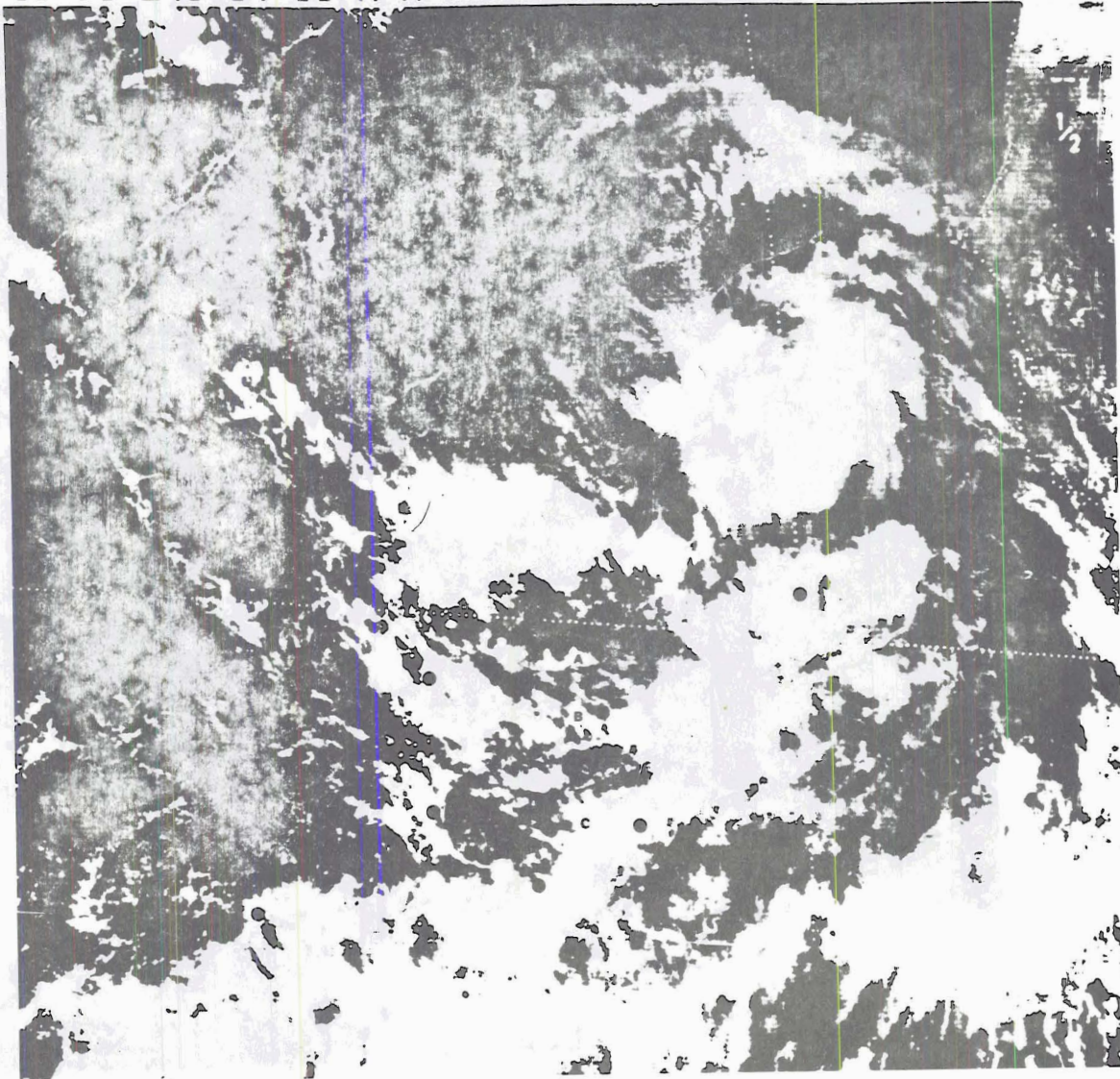


Figure 2. Visible photograph from SMS-1 satellite at 1300Z.

15:00 245:34 01-A-H 0545 2650 A1 DAK 6A4 CH1

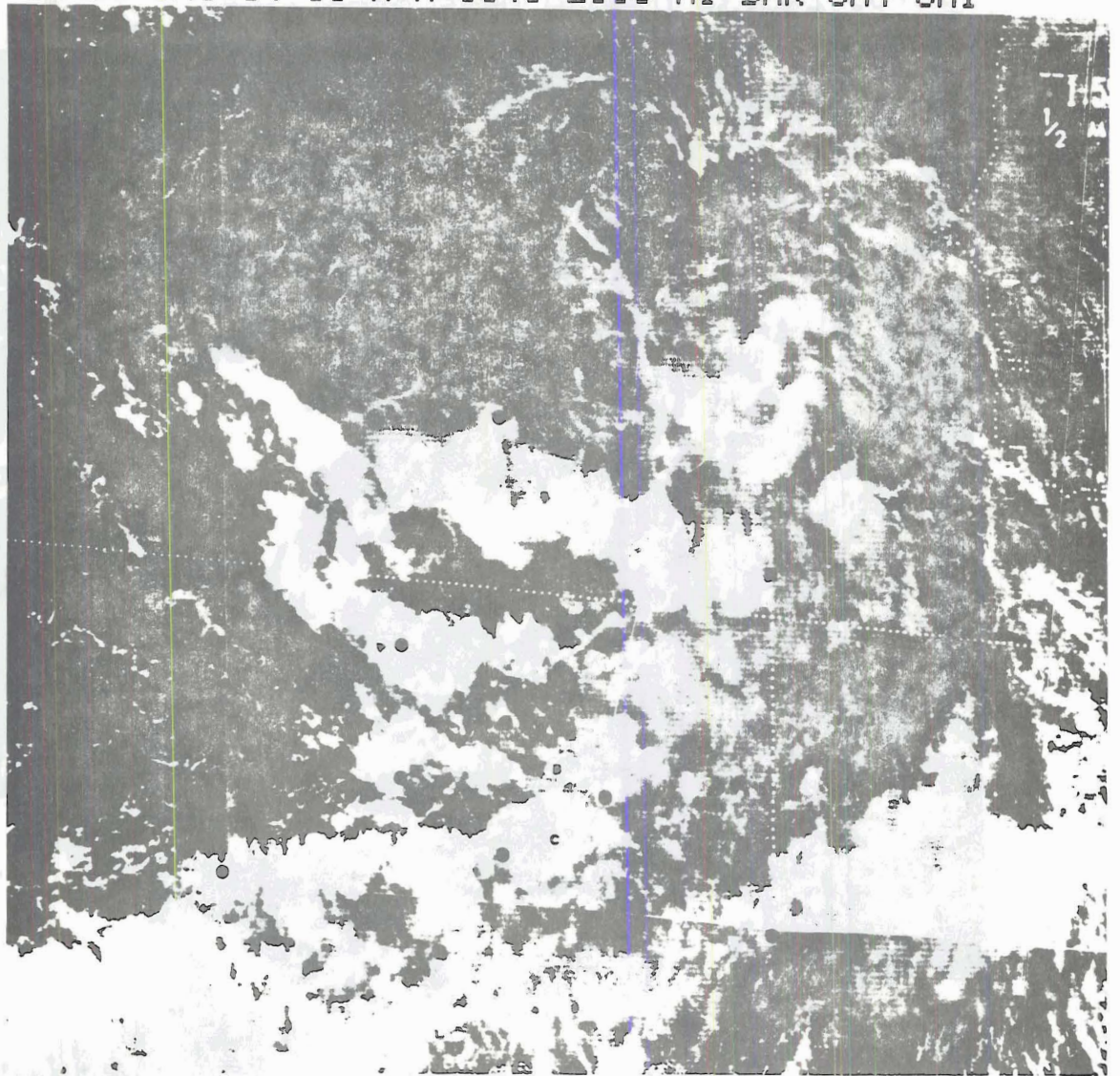


Figure 3. Visible photograph from SMS-1 satellite at 1500Z.

18:00 245:34 01-A-H 0545 2650 A1 DAK 6A4 CH1

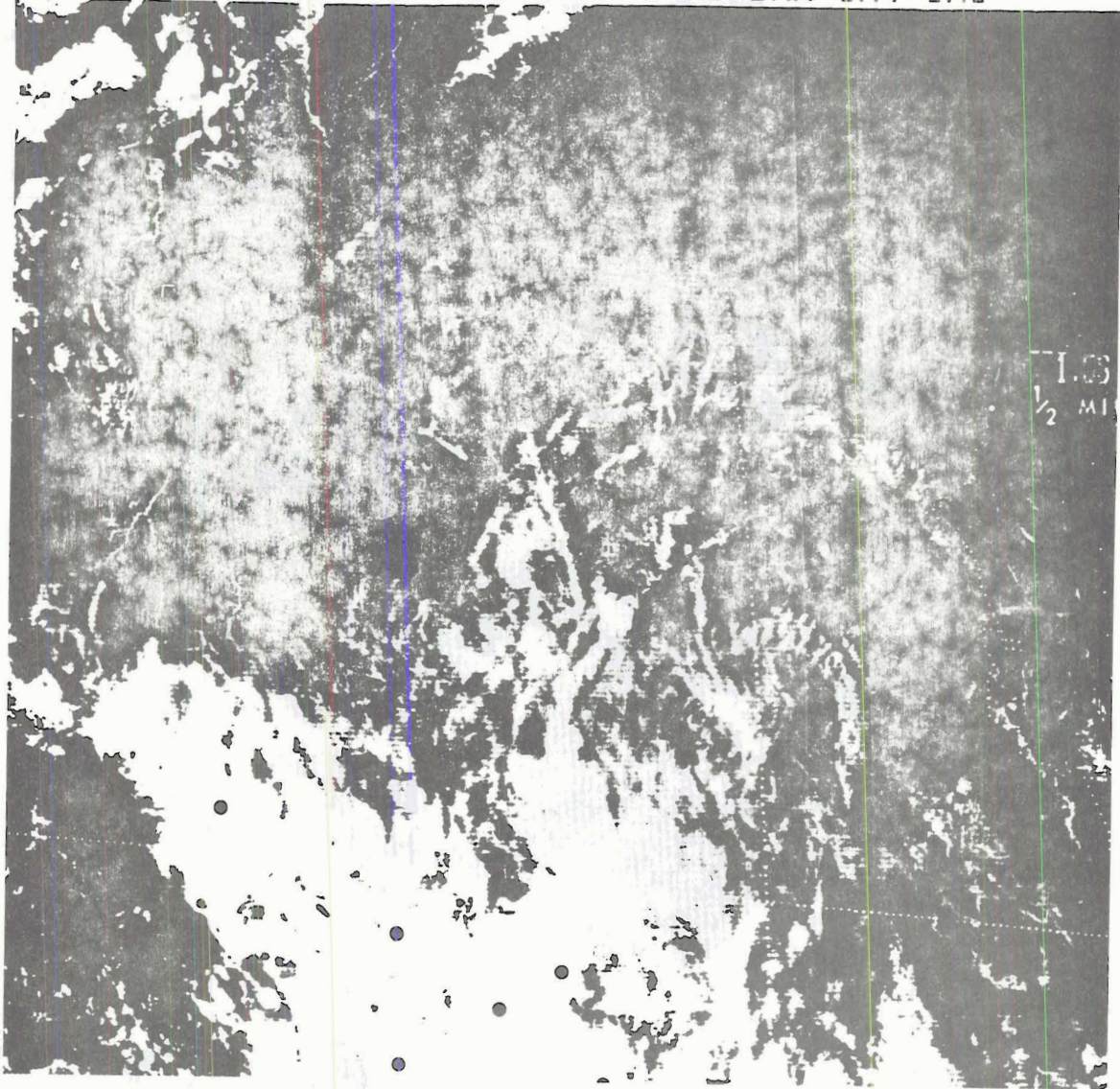


Figure 4. Visible photograph from SMS-1 satellite at 1800Z.

155

### GATE DIGITIZED RADAR DATA

SHIP ID # 4 JULIAN DATE 245 TIME 1500 SHIP POSITION LAT 776 LONG 2222 RANGE MARKER INTERVAL = 110KM  
HYBRID TILT CODE 6 GRID SPACING 4KM X 4KM SHIP HEADINGS T-15 T T+15  
95 267 246

CODE	DBZ	RAINRATE (MM/HR)	CODE	DBZ	RAINRATE (MM/HR)	CODE	DBZ	RAINRATE (MM/HR)	CODE	DBZ	RAINRATE (MM/HR)
BLANK	0	0.00									
x	1-2	0.00 - .02	1	15-18	.18 - .30	o	31-34	3.01 - 5.13	■	47-50	51.28 - 87.23
r	3-6	.02 - .04	6	19-22	.36 - .61	■	35-38	6.12 - 10.41	■	51-54	104.14 - 177.16
s	7-10	.04 - .07	1	23-26	.73 - 1.24	■	39-42	12.43 - 21.15	■	55-58	211.49 - 359.80
1	11-14	.09 - .15	o	27-30	1.48 - 2.52	■	43-46	25.25 - 42.95	■	59-63	429.52 - 872.32

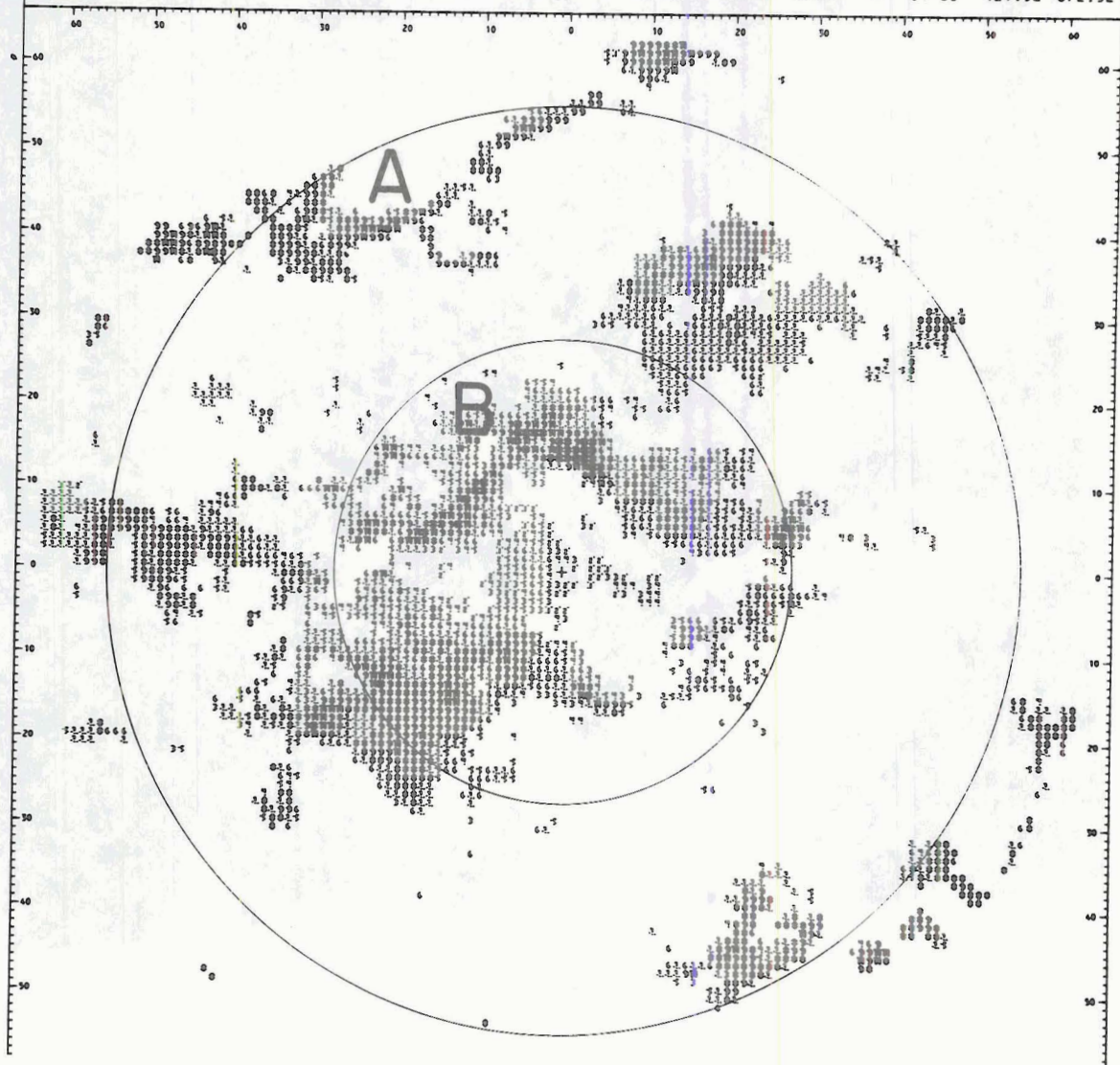


Figure 5. Oceanographer radar 1500Z.



Figure 7 presents the results of a synoptic-scale study of Day 245 by Reeves and Ropelewski, 1976. The profiles are vorticity and divergence obtained from the Dallas, Oceanographer and Researcher triangle and were computed from both the BLIS (tethered balloon) and rawinsonde data. Although the profiles extend to only 880 mb, it can be seen that there is low level convergence with cyclonic vorticity in the region of active convection. This will be substantiated in a later section of this paper.

In addition, Figures 8, 9 and 10 show the streamline analysis for 1200Z. The analysis covers the A/B-scale ship array and with the exception of the surface analysis, the wind vectors are averaged over 25 mb. Aircraft winds have also been plotted at a time when the aircraft were closest to that level. The surface, 700 mb and 200 mb levels are presented. Basically, at the surface there is a sharp convergence zone in the south of the B-scale array with convergence into a vortex just to the west of 'Quadra'. This convergence zone can be regarded as the location of the ITCZ for this day. There is southerly flow into the ITCZ, the air being of southern hemispheric origin. The flow to the north is uniform and from the NE. Winds from the 'Vanguard' and 'Gillis' are in a direction opposed to neighboring stations and are inflow to another system.

At 700 mb the flow is more easterly and the convergence zone much less intense. The mesoscale vortex to the north of 'Oceanographer' is based upon one observation only and so its existence is rather questionable. At 200 mb a ridge in the flow is located over the B-scale array. There appears to be a large vertical shear of the flow between the surface and 700 mb with somewhat weaker shear above this. When the

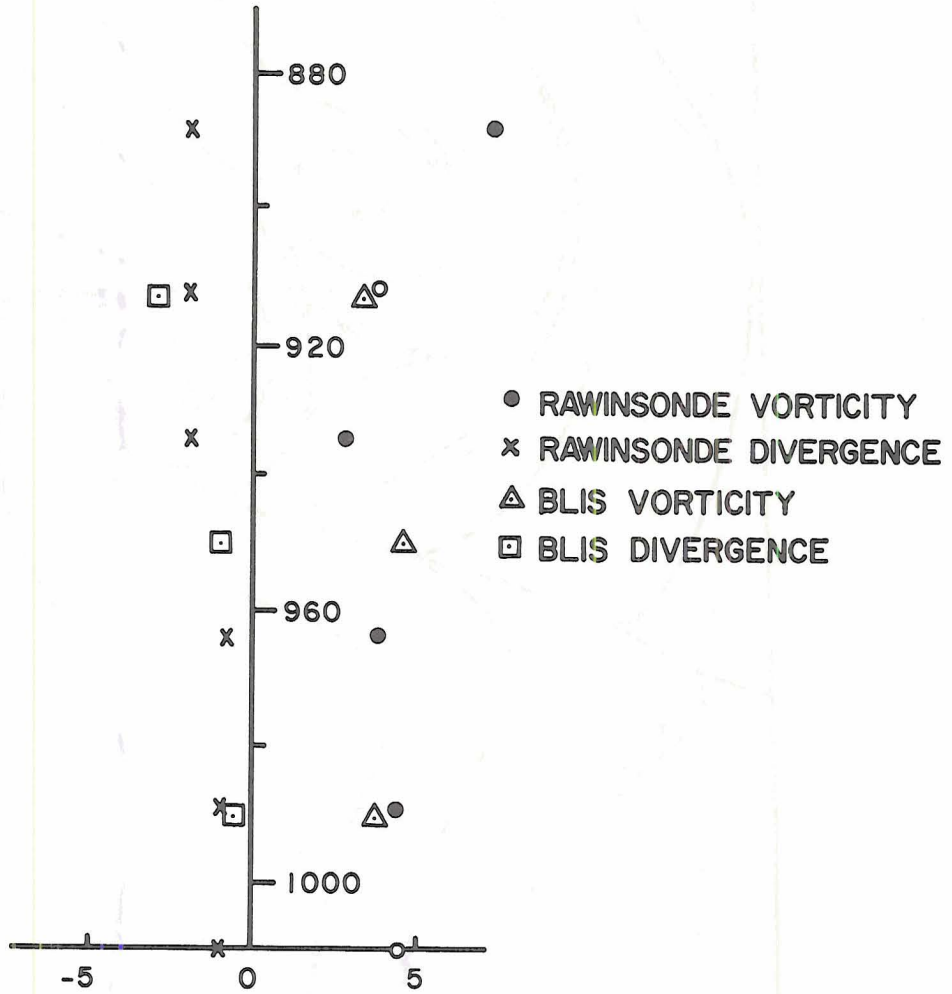


Figure 7. Rawinsonde and BLIS 1200-2100Z average vorticity and divergence. (Reeves and Ropelewski, 1976).

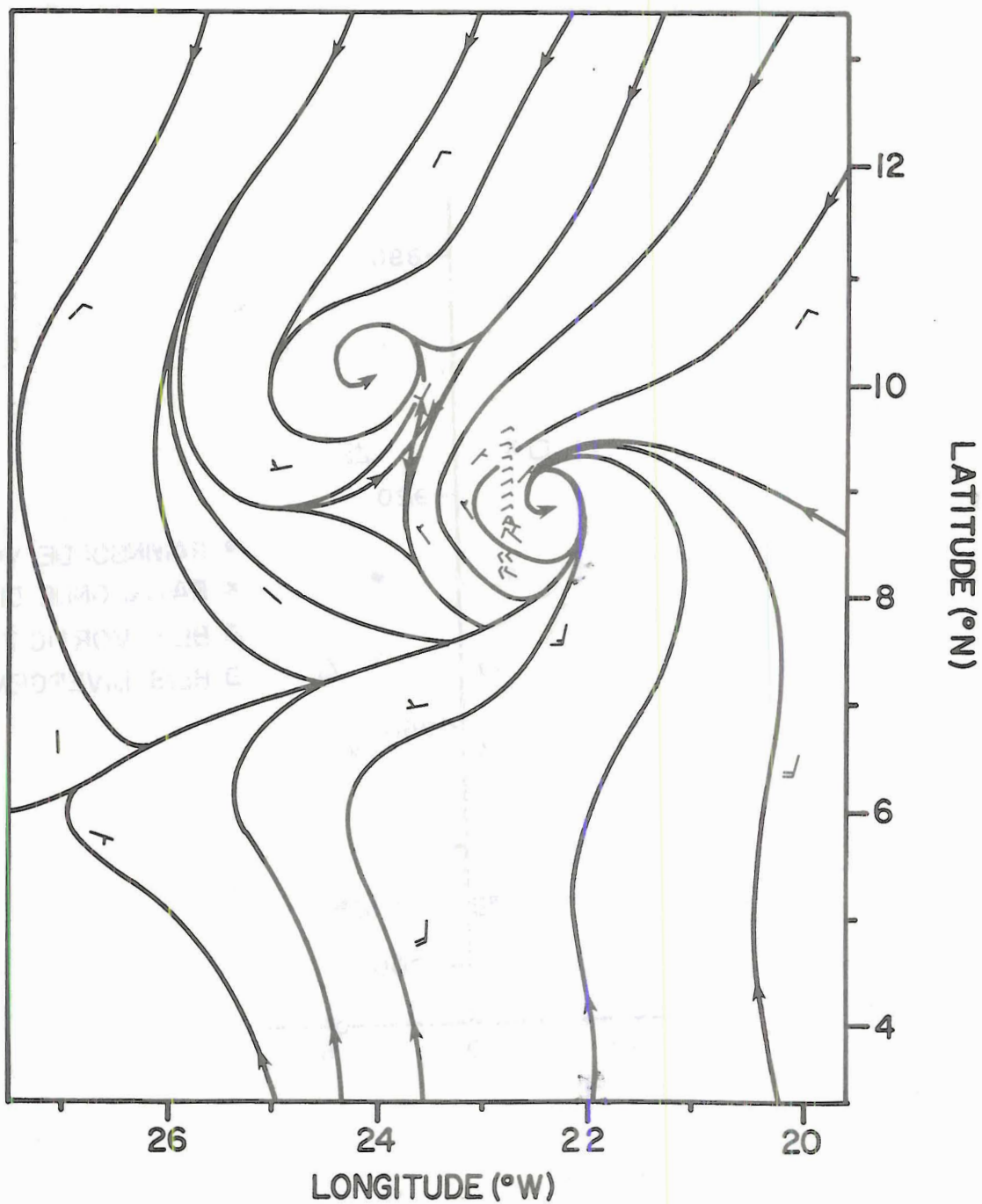


Figure 8. Surface streamline analysis at 1200Z day 245.

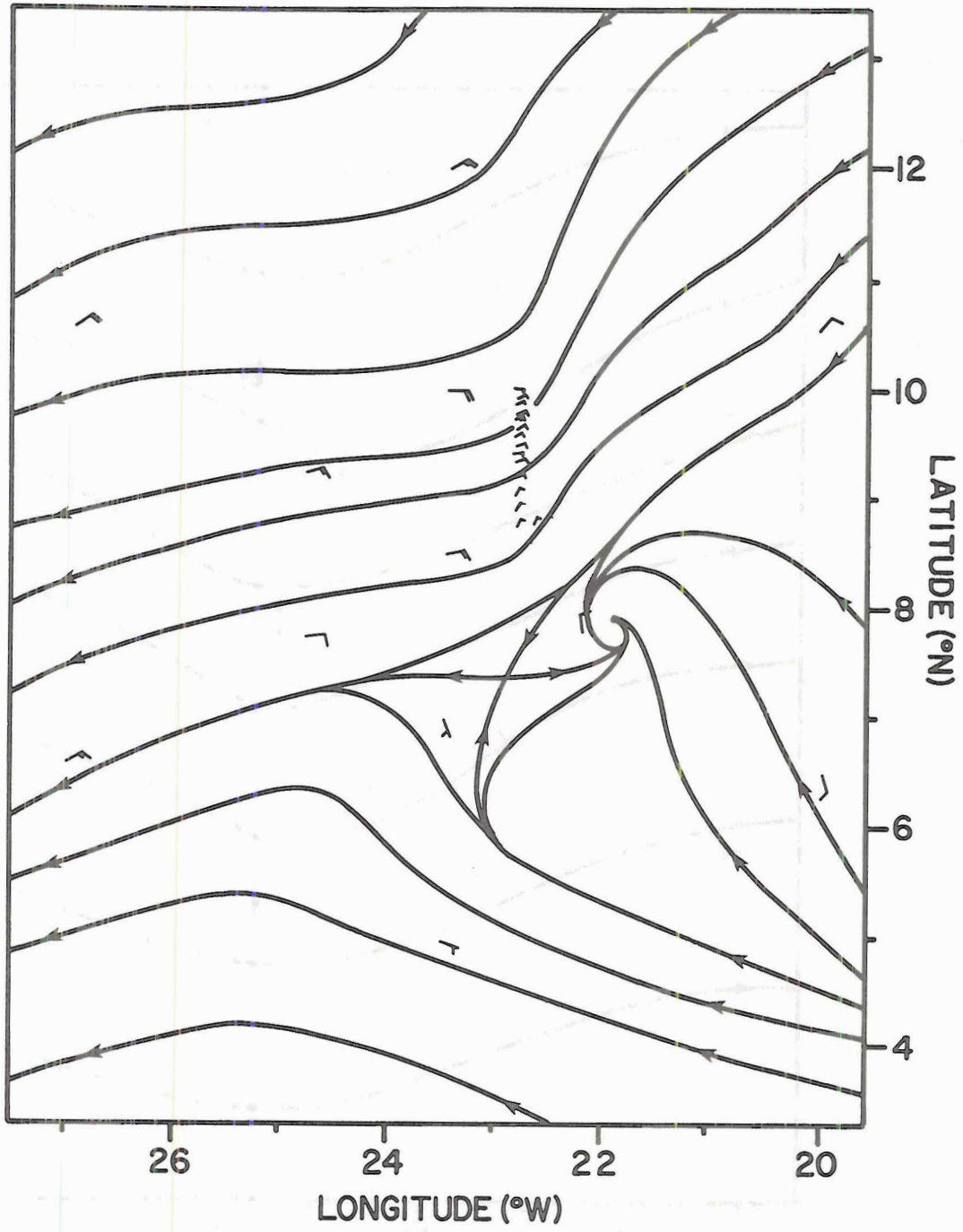


Figure 9. 700 mb streamline analysis at 1200Z day 245.

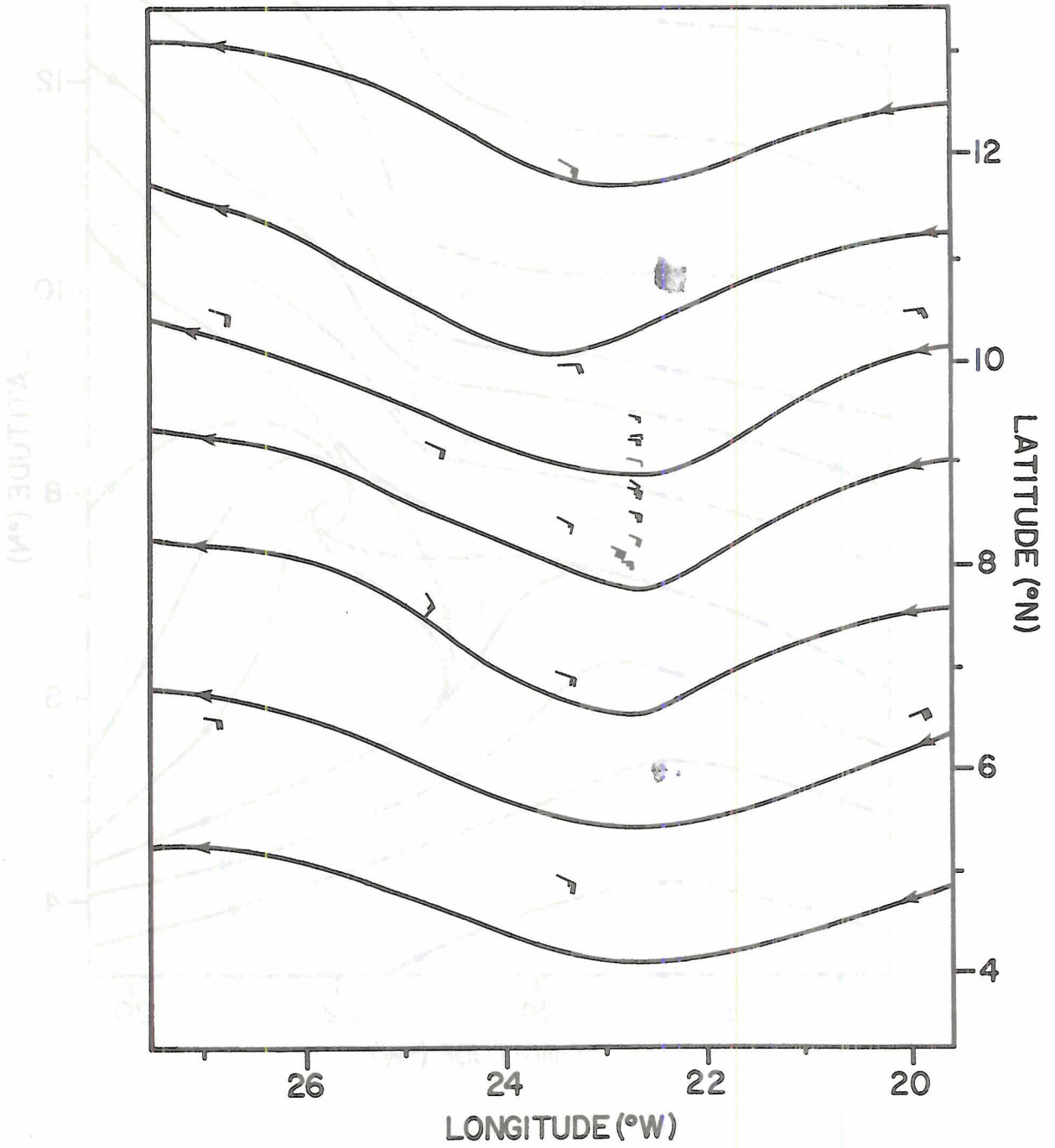


Figure 10. 200 mb streamline analysis at 1200Z day 245.

satellite winds become available for this day, it should fill in data-sparse areas and provide a more reliable analysis.

Fifteen minute scans for the 'Quadra' radar are available throughout most of the day and show precipitation intensities and cloud-top heights, an example of which was given in Figure 6. To place a numerical value on the intensity of each line, the cloud-top heights within  $0.5^\circ$  latitude, longitude squares, centered on the point where the aircraft crossed the leading edge of the lines, have been averaged and plotted against time. Also plotted are the maximum cloud-top heights observed within the squares (see Figures 11 and 12).

It is interesting to see that the mean cloud-top height for both lines reached a maximum value of  $\approx 7.5$  km at 1700Z. The southern line begins to intensify at 1100Z (about one hour before the northern line). Both dissipated at 2300Z. Generally speaking, the growth time is equal to the dissipation time and is approximately six hours.

The last piece of 'visual' data available is the satellite brightness values from the SMS-1 which are shown in Figures 13 and 14 for 1200Z and 1600Z. It is very difficult to define cloud boundaries using these data because the threshold values for cloud type have not yet been determined. However, the technique employed here was to look for regions of maximum brightness gradient. Both lines were, however, located reasonably accurately. The vertical line through both figures represents the aircraft track close to the indicated time and shows that the track passes through the most active portion of the southern line but passes between two active cells in the northern line and this is the reason why sections through the southern line only are presented here (see later).

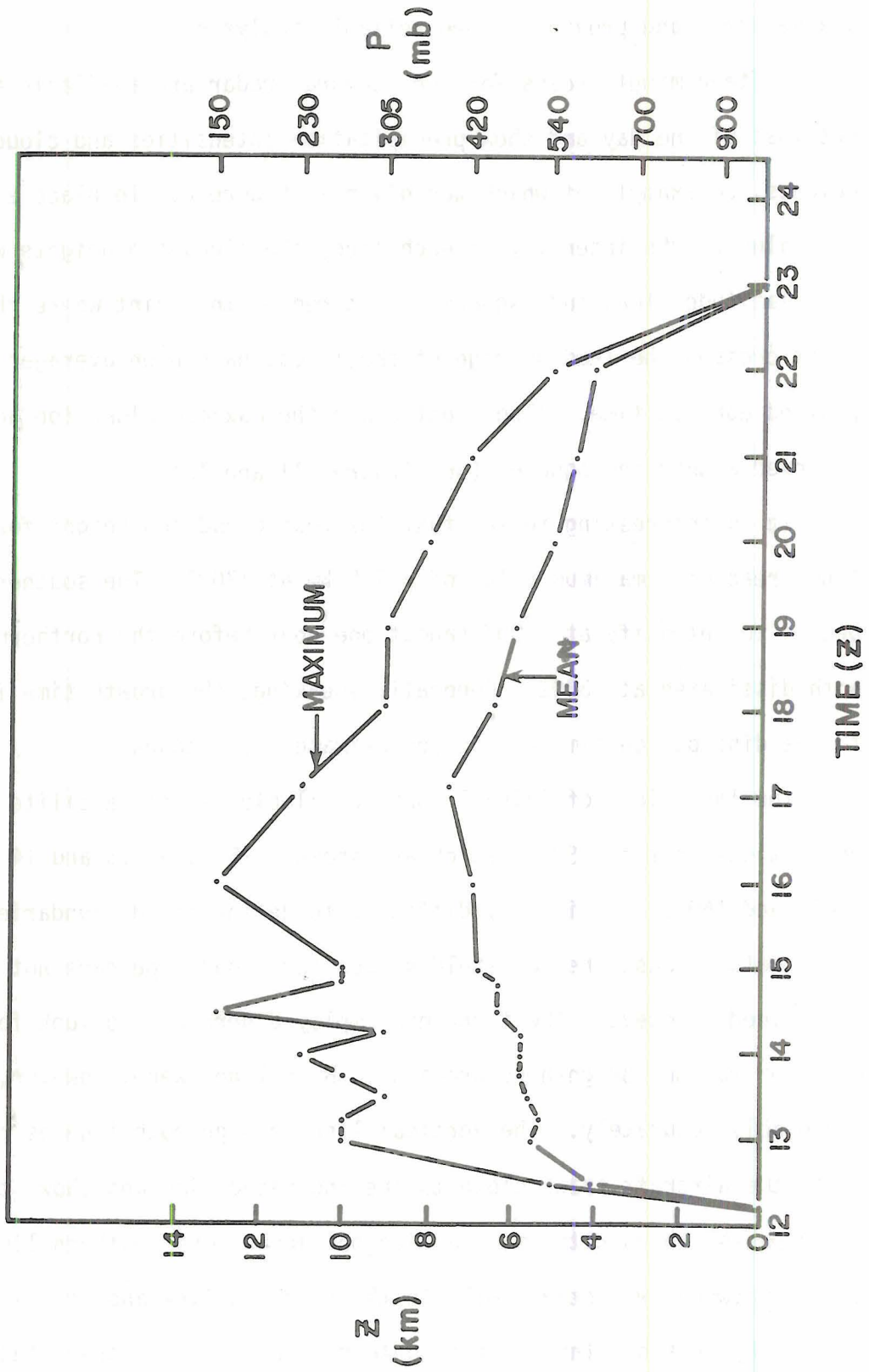


Figure 11. Maximum and mean cloud-top heights for northern line.

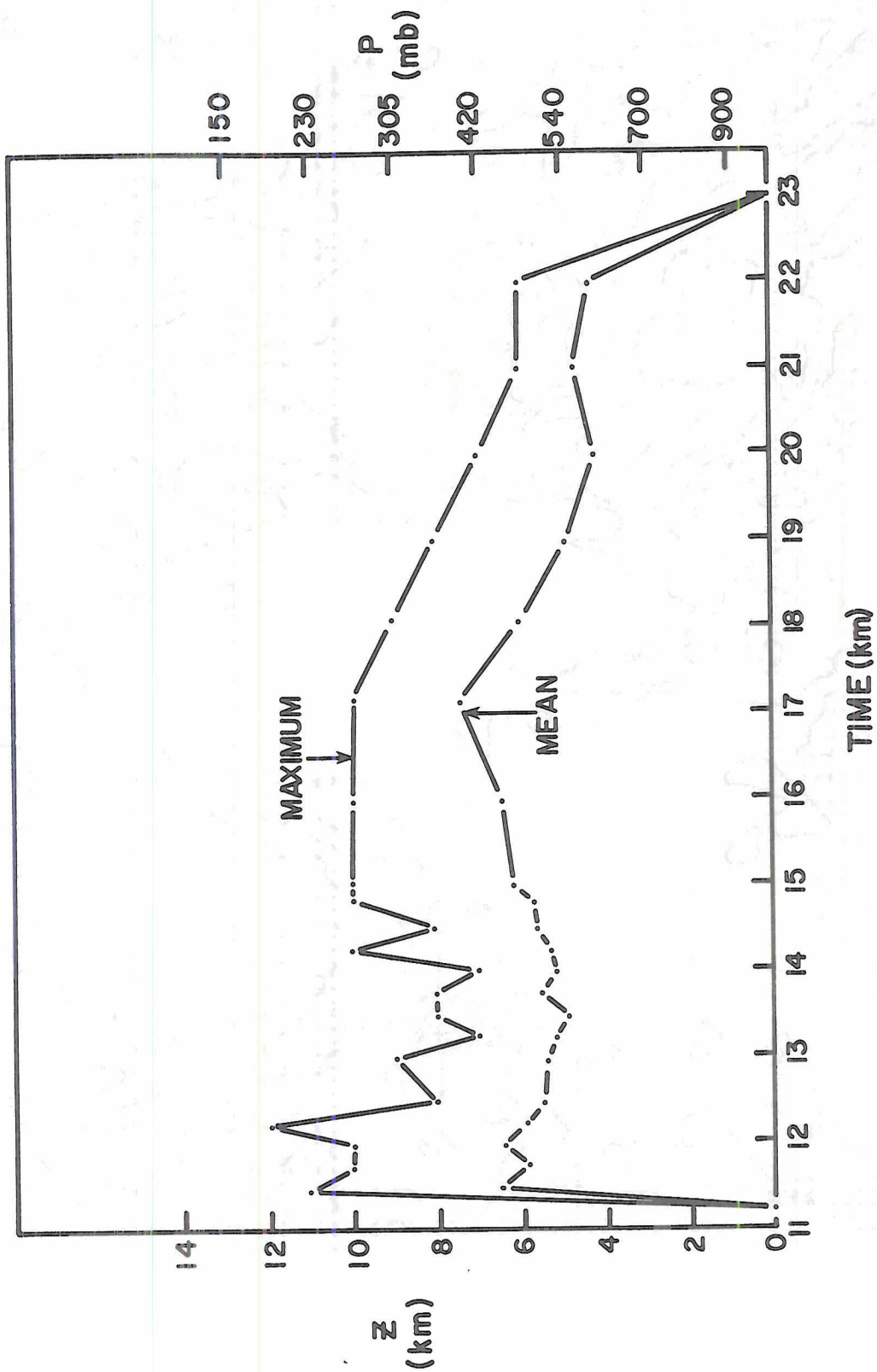


Figure 12. Maximum and mean cloud-top heights for southern line.

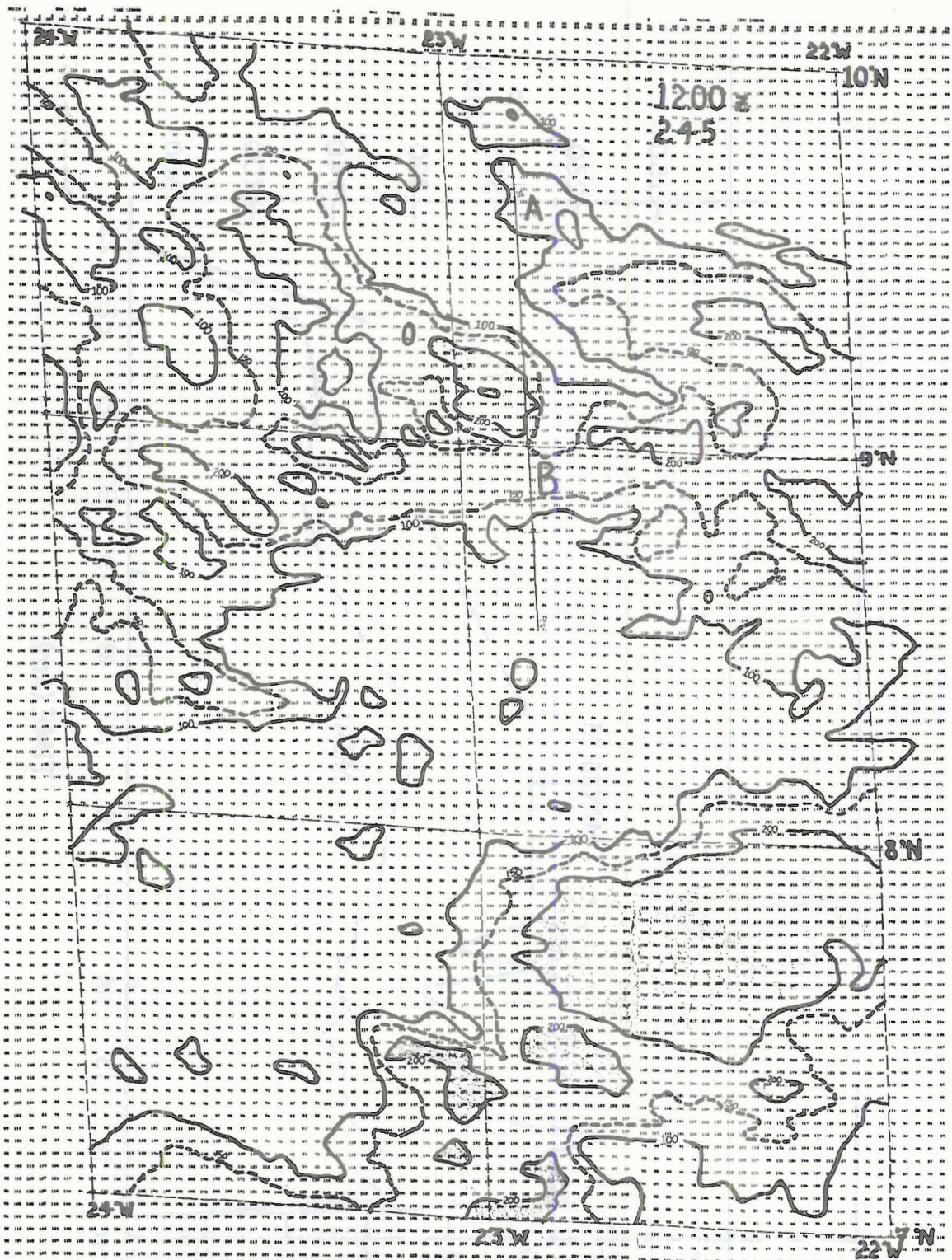


Figure 13. SMS-1 satellite brightness data for 1200Z.

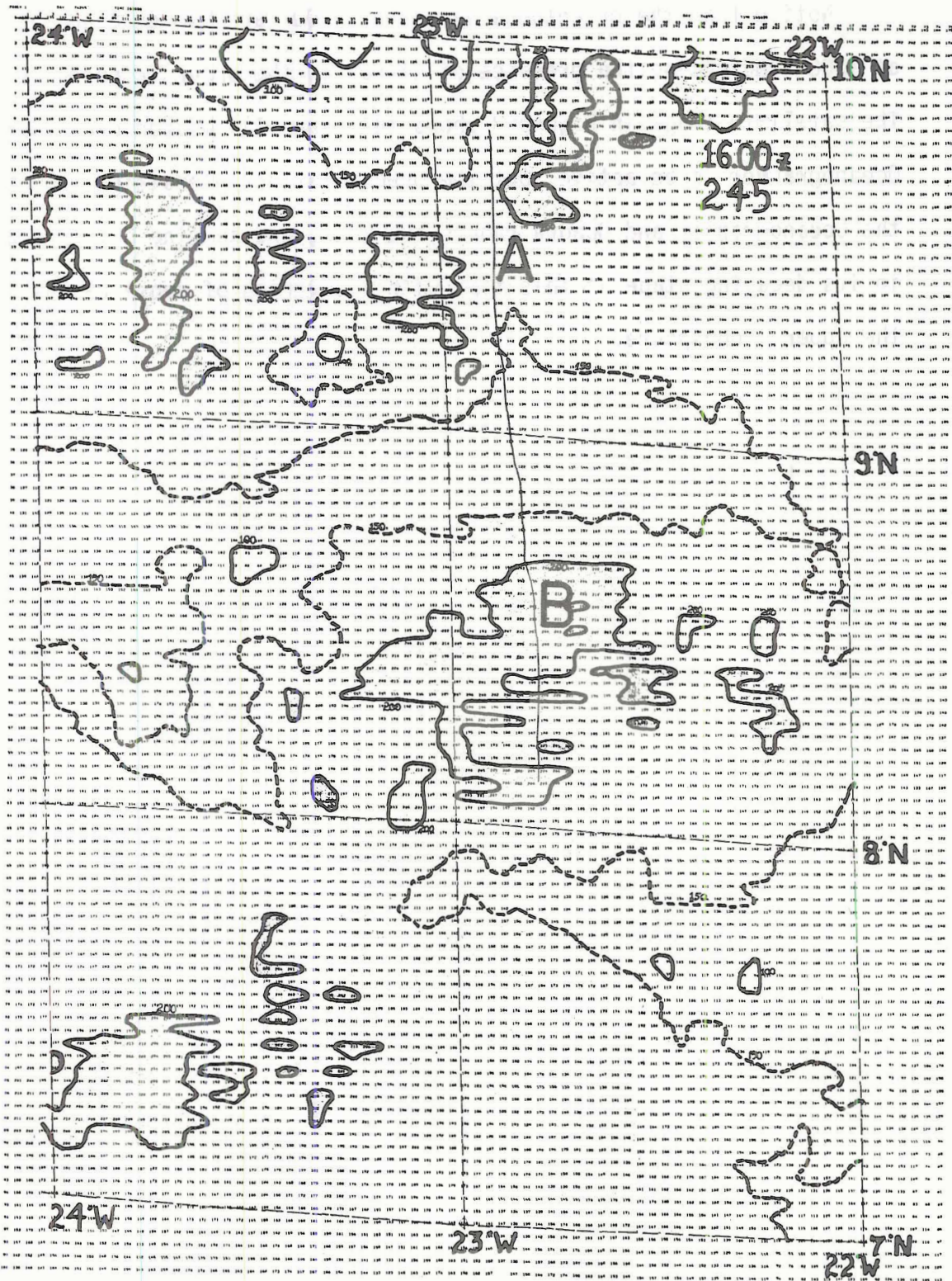


Figure 14. SMS-1 satellite brightness data for 1600Z.

Notice that the brightness values at 1600Z are higher than those at 1200Z indicating the presence of cirrus in the upper troposphere. The satellite image in Figure 3 shows the line (C) located over the Oceanographer to be active, but the precipitation intensities from both the Oceanographer and Quadra radars are weak, and so line C is probably in its decaying stage at this time with a covering of dense cirrus in the upper troposphere.

### III. PHYSICAL FEATURES OF THE LINES

This section presents a detailed analysis of the southern line only based on the ten second aircraft data and three minute BLIS and boom data. All data have been plotted relative to the line and take the form of cross-sections through the line. The Dallas BLIS data and vertical profiles from aircraft data both ahead of and behind the line have been used to diagnose some of the dynamic and thermodynamic transformations of the environment effected by the line.

#### 3.1 Quadra radar cross-sections

Figure 15 shows the digital cross-sections of the Quadra radar along the flight trace (22.8°W). Three frames are presented for 1229Z, 1329Z and 1529Z.

Precipitation intensities are coded from 0 to N and are based on the following reflectivity rainfall-rate relationship

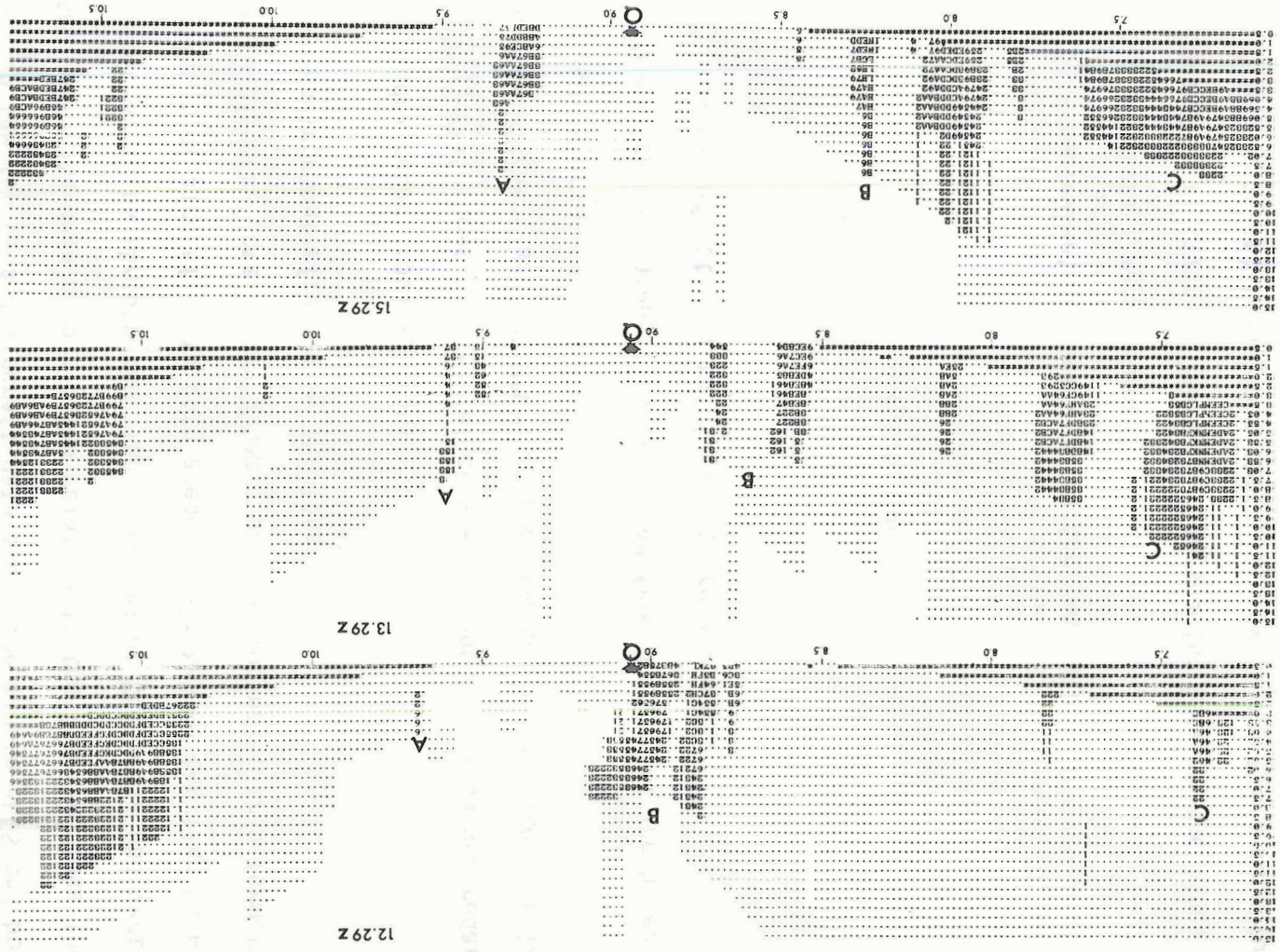
$$Z_e = 232 R^{1.5}$$

where  $Z_e$  - equivalent reflectivity factor ( $\text{mm}^6/\text{m}^3$ )

R - rainfall rate (mm/hr).

The conversion is given in Table 6. The spacing between the lines remains fairly constant throughout their life-cycle and has a magnitude of approximately 60-70 km. The progression southwards of the northern line (A), the southern line (B) and the feeder band to the vortex off Dakar (C) mentioned earlier can be easily seen. Precipitation

Figure 15. Quadra radar cross-sections along 22.8°W at 1229Z, 1329Z and 1529Z.



intensities near the southern edge of the southern line support the Oceanographer radar which shows the maximum intensity at the leading edge. This should be in close proximity to the main updraft.

Table 6. Rainfall rates from Z-R relationship.

SYMBOL	RAINFALL RATE (mm/hr)	SYMBOL	RAINFALL RATE (mm/hr)
0	0.00	A	2.10
1	0.10	B	3.05
2	0.14	C	4.40
3	0.17	D	6.34
4	0.24	E	9.17
5	0.31	F	13.25
6	0.46	G	19.20
7	0.68	H	27.72
8	0.98	K	40.05
9	1.44	L	57.89
		M	83.71
		N	120.99

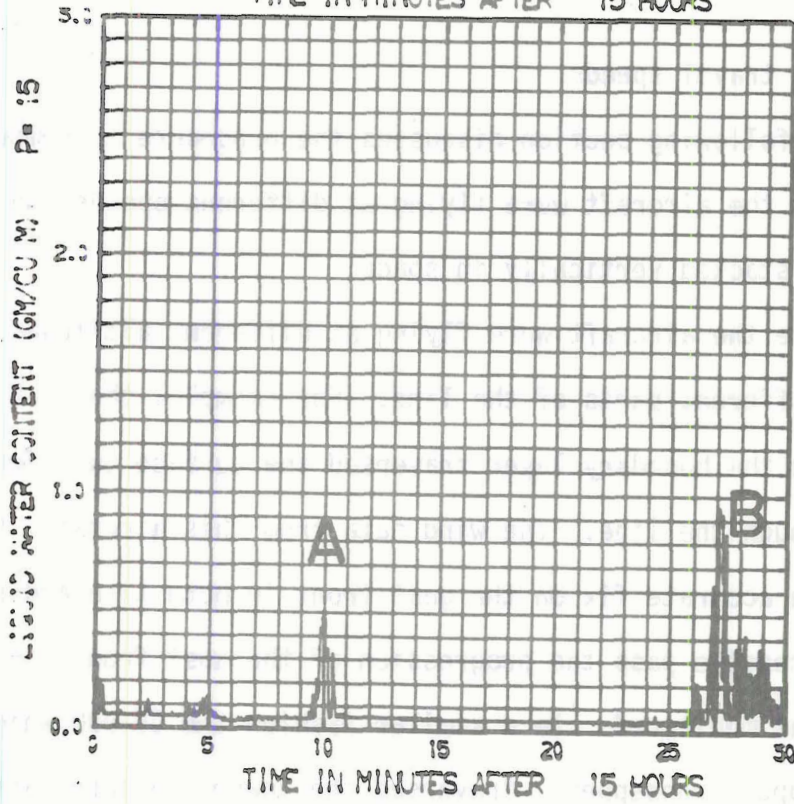
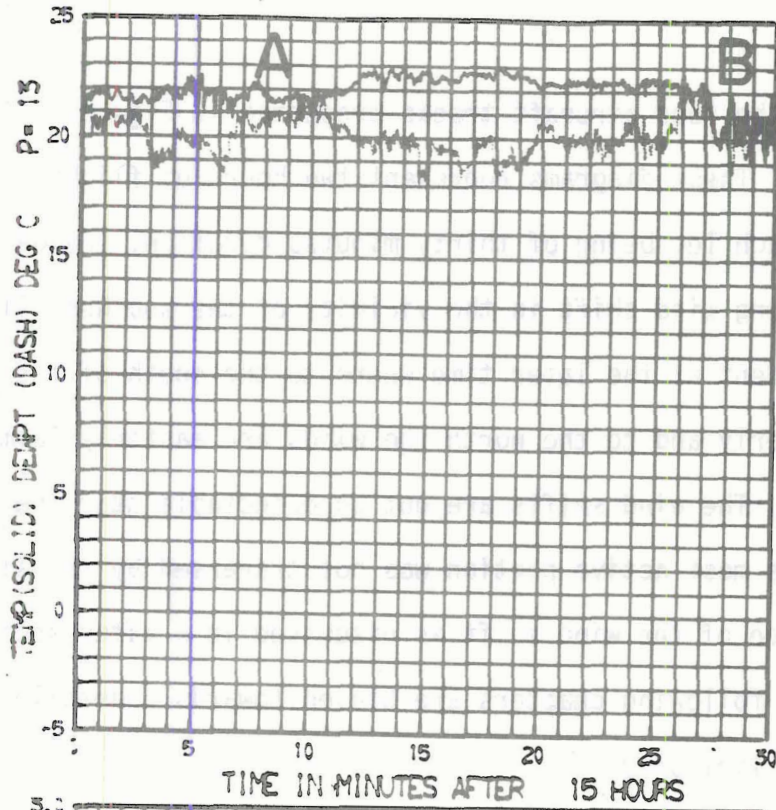
A feature common to all these radar sections on this day is the break in the precipitation some distance away from the leading edge. At 1229Z, line B shows two such breaks in the precipitation. A possible explanation for these is the generation of new cells at the leading edge of the line. The cells to the rear (north) of the leading edge indicate generally lower precipitation intensities and are probably in a state of decay.

The northern line (A) does not appear to be particularly well developed along 22.8°W being only slightly visible at 1229Z. This agrees well with the satellite brightness data at 1200Z and 1600Z in Figures 13 and 14.

In summary then the Quadra radar data provides useful quantitative information on the location of the leading edges of the convection and gives a value for the quantity of precipitation that these systems are capable of producing.

### 3.2 Aircraft cross-sections

Figures 16 (a) and (b) show the unaveraged one second values of temperature and dew point and liquid water content traces respectively as the DC-6 completes one run from south to north through both lines. At around 1510Z the dew point becomes equal to the ambient air temperature while at the same time there is a sharp peak in the liquid water content. The same happens at 1527Z. This sequence of events indicates that the aircraft crosses the 'leading' edges of the lines. In between these events the aircraft passes through some relatively unsaturated air between the lines.



Figures 16 (a), (b). Temperature, dew point and LWC traces for DC-6 along one leg.

On the four aircraft tracks presented in Figure 17 are plotted wind vectors. These diagrams represent two hours of flight from 1331Z to 1530Z, each leg being of thirty minutes duration. Evident on each leg is a strong wind shift in the vicinity of the southern line. This is most evident at the later time where to the south of the line the winds are westerly and to the north the winds are easterly (almost a 180° change). The wind shifts are not so detectable near the northern line since its most active portion was not traversed by the aircraft. The importance of the wind shift is discussed in a later section.

The following chapters are biased towards a detailed study of the southern line only.

### 3.3 Line travel speeds

The following section discusses the procedure to compensate for the fact that the aircraft were flying at different speeds and consequently, were not stacked vertically in space.

Since the aircraft were flying at different altitudes they traversed different parts of the line. For example, the DC-6 which was flying in the boundary layer traversed the surface gust front on each pass through the line. The wind data from this aircraft, therefore, yields an accurate fix on the gust front in both time and space. On each successive pass the progression of the gust front (in time and space) was monitored. In a similar fashion the CV-990 which was flying in the upper troposphere, traversed the towers on each pass. A summary of the data sources and the associated features of the line which they sample are given in Table 7.

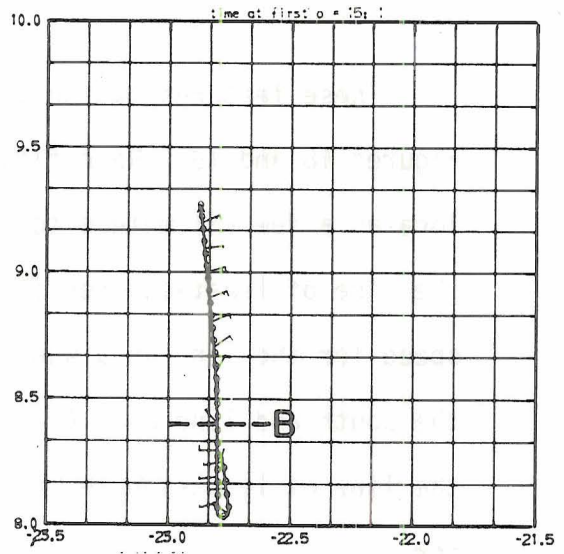
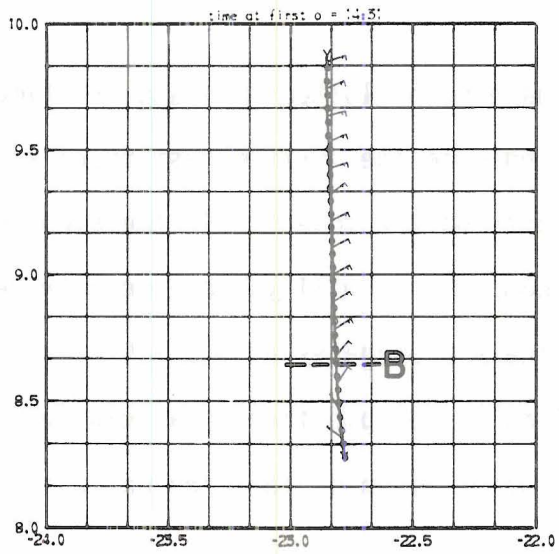
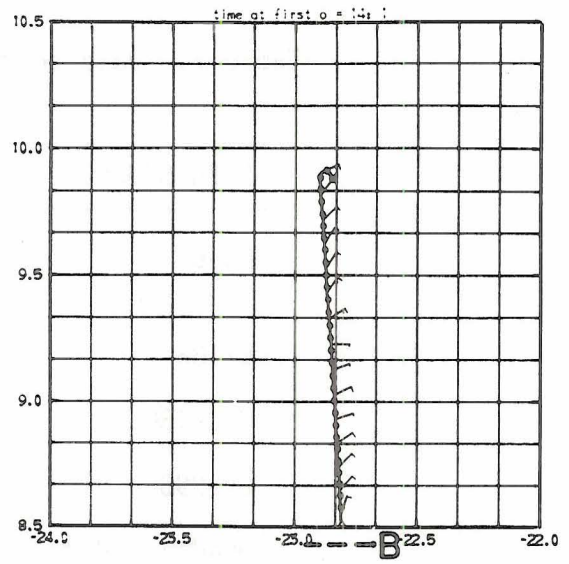
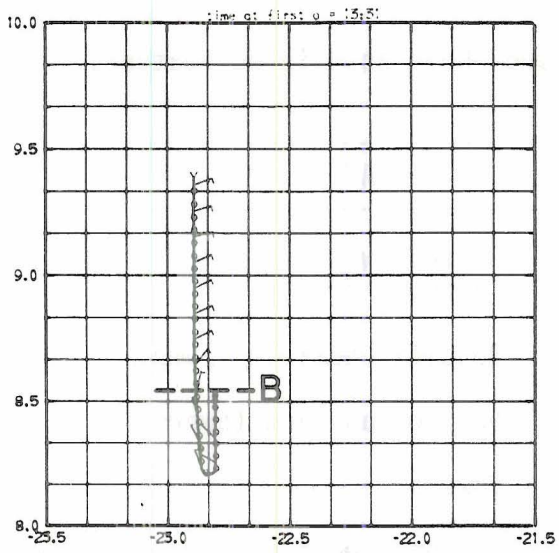


Figure 17. Plotted wind-vectors for DC-6 along the flight tracks.

Table 7. Data sources and their associated features.

DATA SOURCE	FEATURE
DC-6	Surface wind shift (gust front)
L-188	Specific humidity jump
USC-130	$\theta_E$ increase and towers
CV-990	Towers
Quadra radar	Southern edge of precipitation
Dallas boom	Temperature drop and wind shift

These features of the lines have been plotted in space and time in Figures 18 and 19. Both figures indicate the surface gust front to be located a few kilometers to the south of the towers. If the slope of the line of least-squares fit is computed it will yield a mean travel speed for the line as a whole. Line A propagates at  $5.9 \pm 0.1 \text{ ms}^{-1}$  to the south and line B at  $6.1 \pm 0.1 \text{ ms}^{-1}$ . By plotting data relative to the line of least-squares fit the propagation of the line was accounted for.

In physical terms the line of least-squares fit corresponds to a plane in space located a few kilometers to the north of the surface gust front and a similar distance to the south of the towers.

#### 3.4 Cross-sections through the southern line from boom and aircraft data

Both the ten second aircraft data and three minute boom data from the Dallas have been plotted relative to the plane of least-squares fit

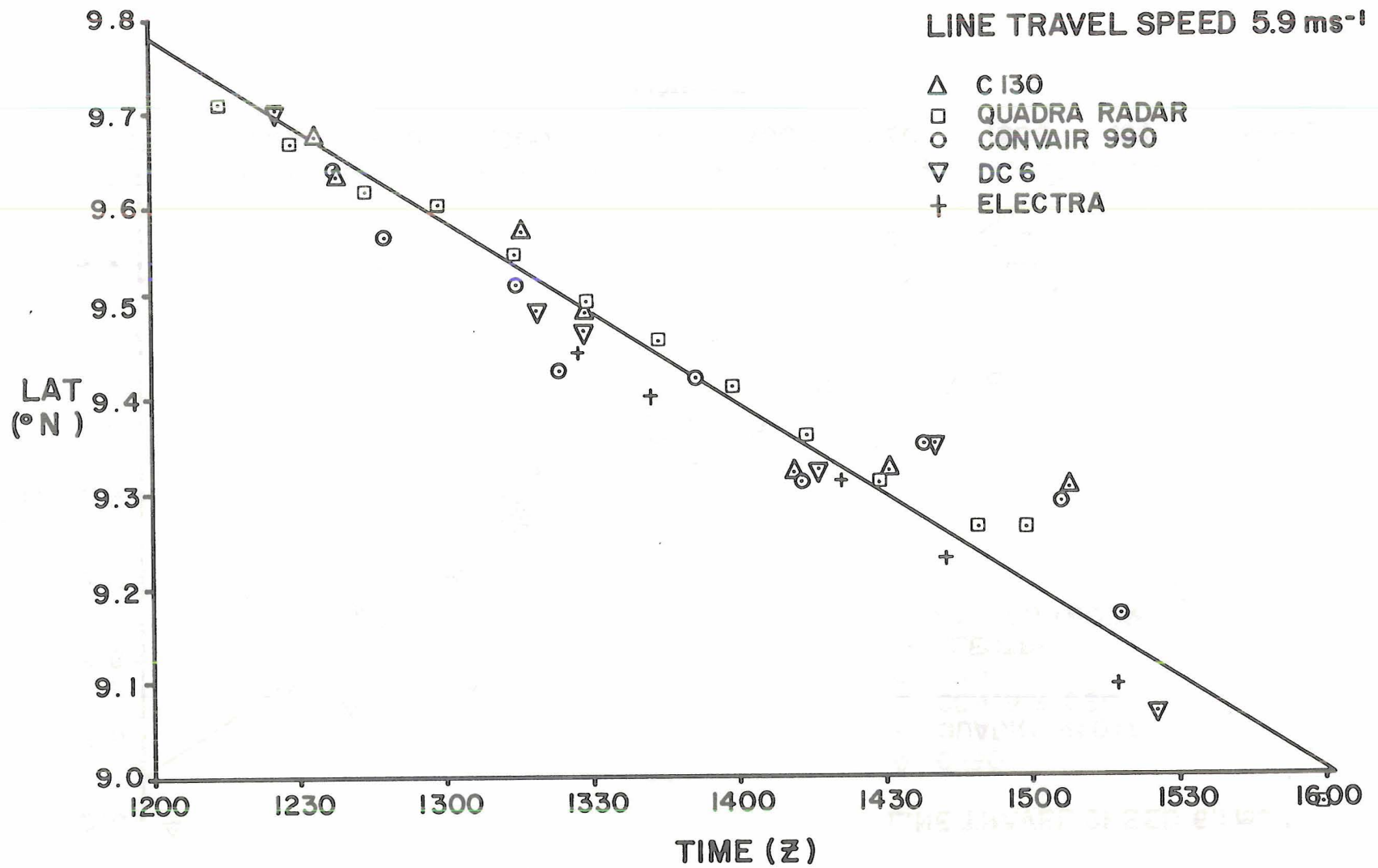


Figure 18. Time sequence of events measured by different systems for northern line.

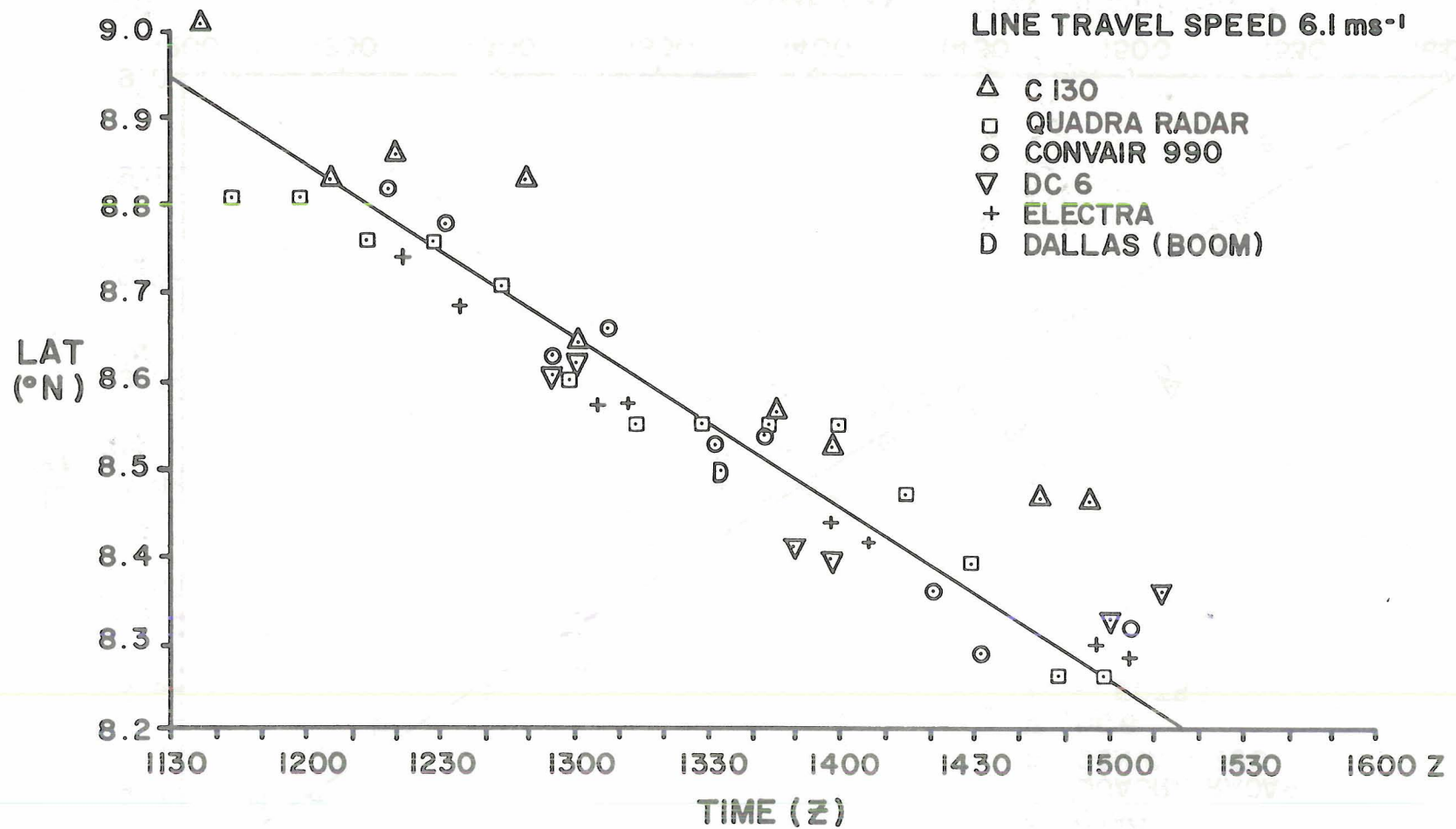


Figure 19. Time sequence of events measured by different systems for southern line.

(see earlier). Each aircraft made several runs through the line at at least one altitude. The number of runs is shown in Table 8.

Table 8. Number of runs with good data at each level for both lines.

Aircraft	Pressure (mb)	Number of Runs	
		Line A	Line B
DC-6	985	3	2
	970	1	2
	945	2	2
L-188	900	2	4
	810	3	4
USC-130	720	2	2
	640	5	7
II-18C	574	5	5
CV-990	380	2	2
	290	3	3
	220	4	4

Cross-sections through the line are shown in the series of Figures 20-26. The distance scale on the abscissa represents distance in kilometers relative to the plane of least-squares fit. Figures 20 and 21 show the passage of the southern line over the 'Dallas' at ~ 1345Z. The plots are derived from the three minute boom data and so differ from the other figures in the sense that each point represents just one data value whereas the other figures are composites.

The diurnal incoming solar radiation curve shows a sharp decrease from over  $1000 \text{ Wm}^{-2}$  to  $400 \text{ Wm}^{-2}$  at the onset of the surface gust front.

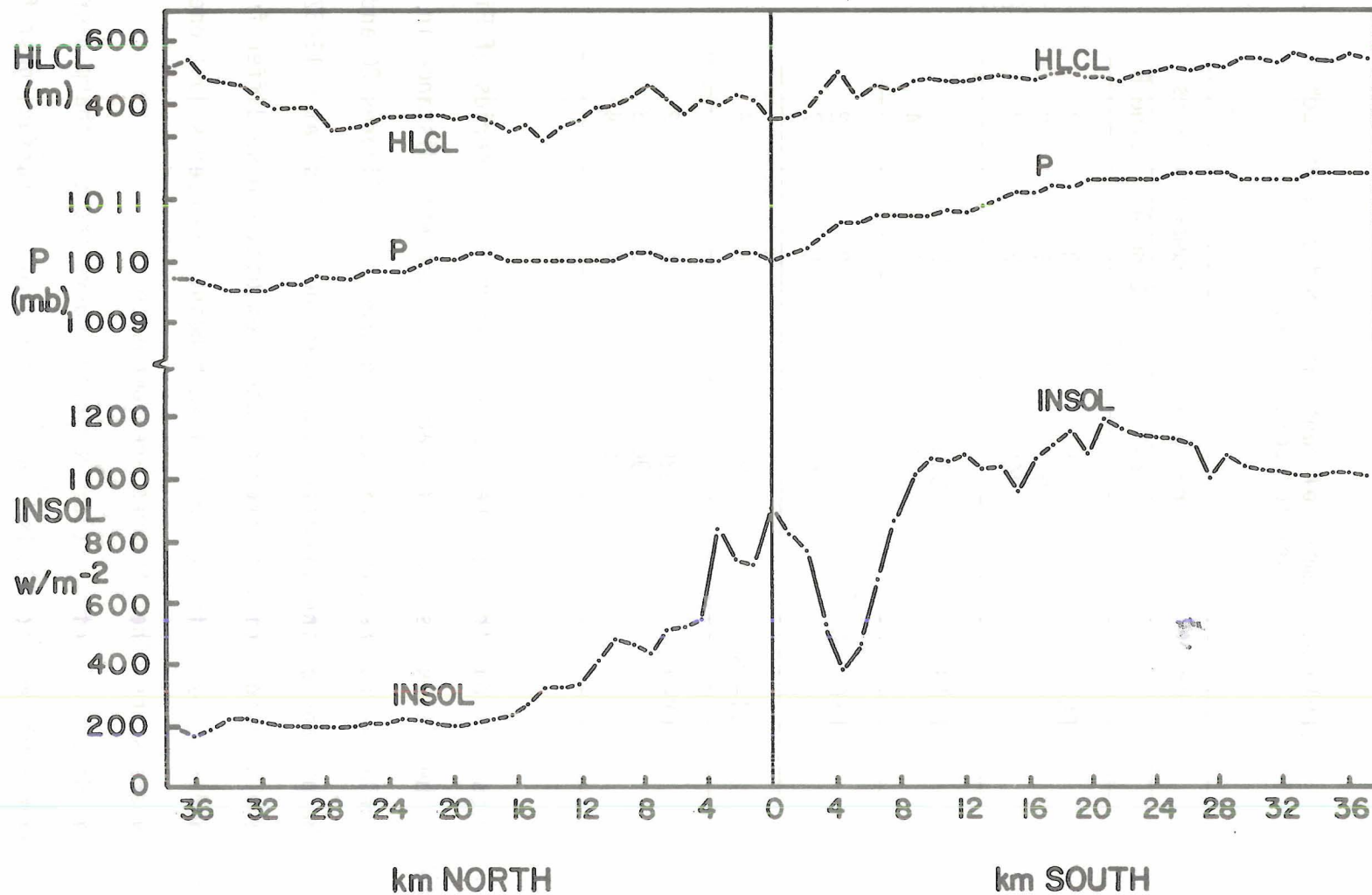


Figure 20. Pressure, LCL and incoming solar radiation relative to the southern line from 3 minute Dallas boom data.

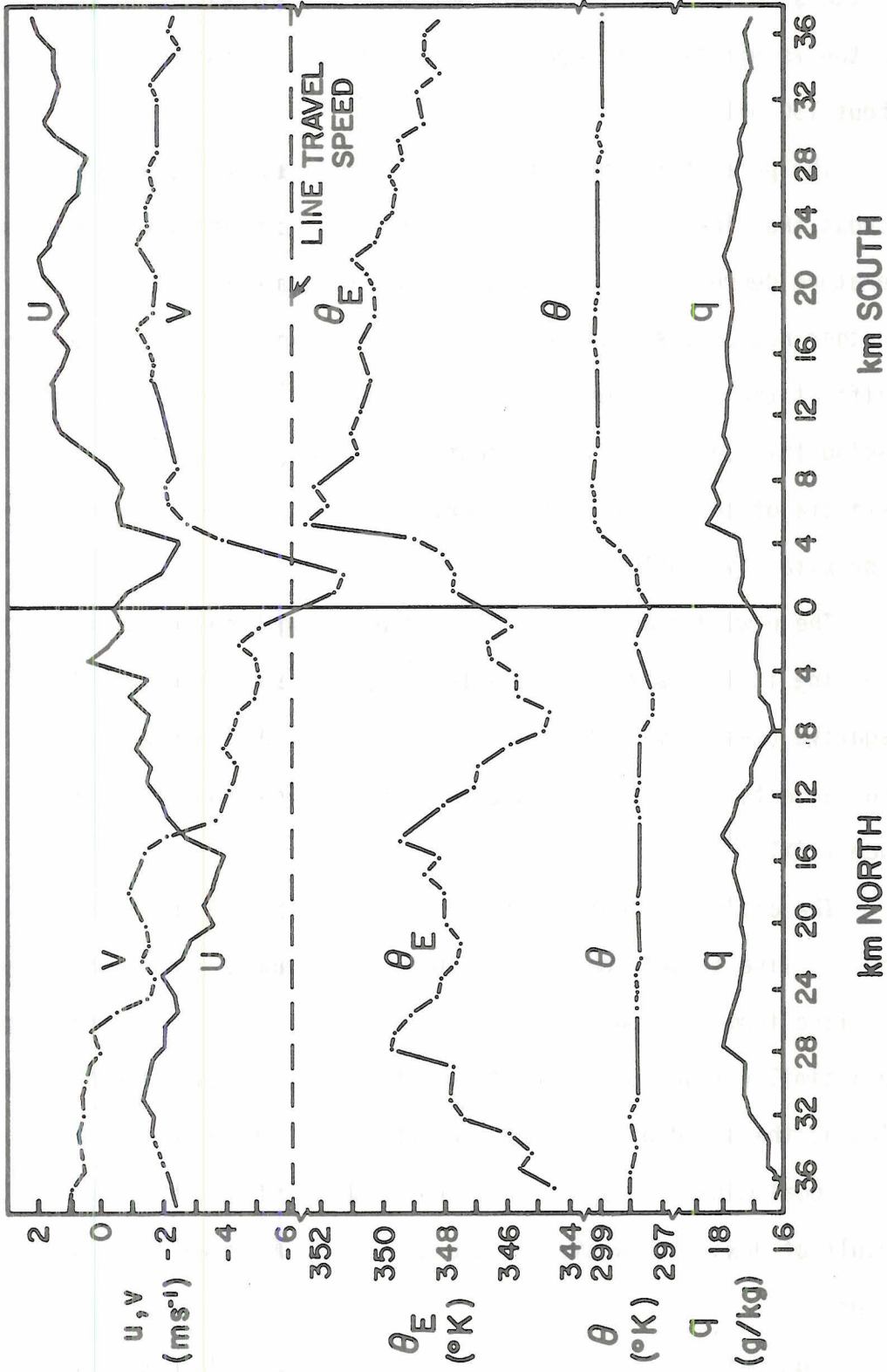


Figure 21. Thermodynamic and wind parameters relative to the southern line from 3 minute Dallas boom data.

At the same instant is a small but detectable pressure drop of  $\sim 0.6$  mb in twelve minutes, accompanied by a decrease in the height of the LCL of about 150 metres.

The parameters shown in Figure 21 indicate a large change in  $\theta_E$  across the line of at least  $7^\circ\text{K}$ . This is a combination of both a temperature decrease of  $1.5^\circ\text{K}$  and a specific humidity decrease of  $2$  g/Kg. Another noticeable feature at this level (surface) is the large wind shift at the surface where  $v$  changes by  $6$   $\text{ms}^{-1}$  in a small time period. Taking this change in  $v$  from south to north ( $y$  increasing) gives an estimate of the 2-dimensional convergence at the gust front and it is approximately  $1.4 \times 10^{-3} \text{ s}^{-1}$ .

The  $u$  wind component is also interesting because to the south of the line it is positive (westerly) and to the north of the line it is negative (easterly). This confirms the wind shifts seen in Figure 17 and suggests that there is cyclonic vorticity across the line of magnitude  $1.6 \times 10^{-4} \text{ s}^{-1}$ .

The difference between the  $v$  component to the south of the line and the line travel speed shows there to be about  $4 \text{ ms}^{-1}$  of inflow into the line from the south and similarly on the north side there appears to be a similar magnitude of outflow. However, the gust front is travelling at the speed of the line and perhaps a little faster.

Local minima in  $\theta_E$  at 8 km and 20 km north of the line are the result of downdraft activity, the origin of which will be discussed later.

From this cross-section alone then we can deduce that there is sharp convergence of warm, moist air into the line from the south with

also been observed by Zipser 1977. The shift in the wind field may be the most important feature of this line. The spreading out of the downdraft (or density current) when it reaches the surface is a likely source for the observed divergence. A likely source for the downdraft air is in the layer between 900 and 800 mb ahead of the line. For this we have to assume that the air parcels descend conserving  $\theta_E$ .

### 3.5 Cloud - subcloud layer features

In order to study processes operating at low levels, the tethered balloon data from 'Dallas' was employed. These data give dense coverage from the surface to 900 mb. Unfortunately, the measurements of wet bulb temperature were beset with problems during the field phase and are incompatible with the relative humidity measurements. The wick used for wet-bulb measurements was often contaminated with sea-salt and periodically dried out. There were also some electronic problems with the recording devices, thereby causing the values to 'stick' and have some preferred values (Ropelewski 1977 - personal communication).

Another rather common occurrence evident throughout many of the BLIS data is rainwater seeping into the instrumentation producing artificially low humidity values. Comparison with rawinsondes launched on other days from Dallas indicate mixing ratio differences as much as 5 g/Kg and the instruments appear to take a long time to recover. On this day only 1 mm of precipitation fell at the Dallas and the author feels that this problem is not evident in the data presented here.

Figure 28 shows a time section across the line for the u and v wind components. There is a large wind shift at 995 mb in both u and v across the line. This shift appears to be confined to a shallow layer

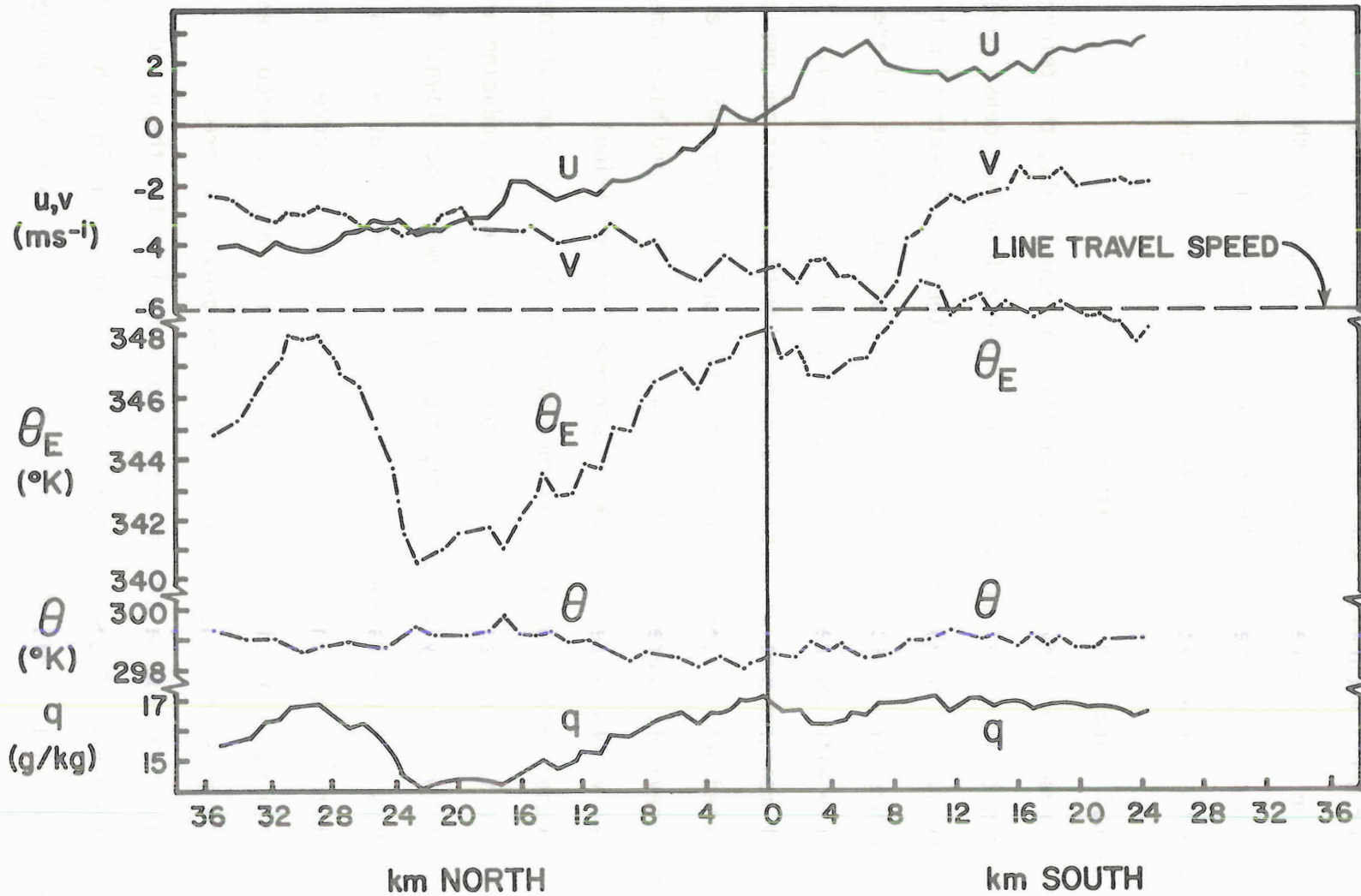


Figure 22. Mean of 2 runs through southern line at 985 mb for DC-6.

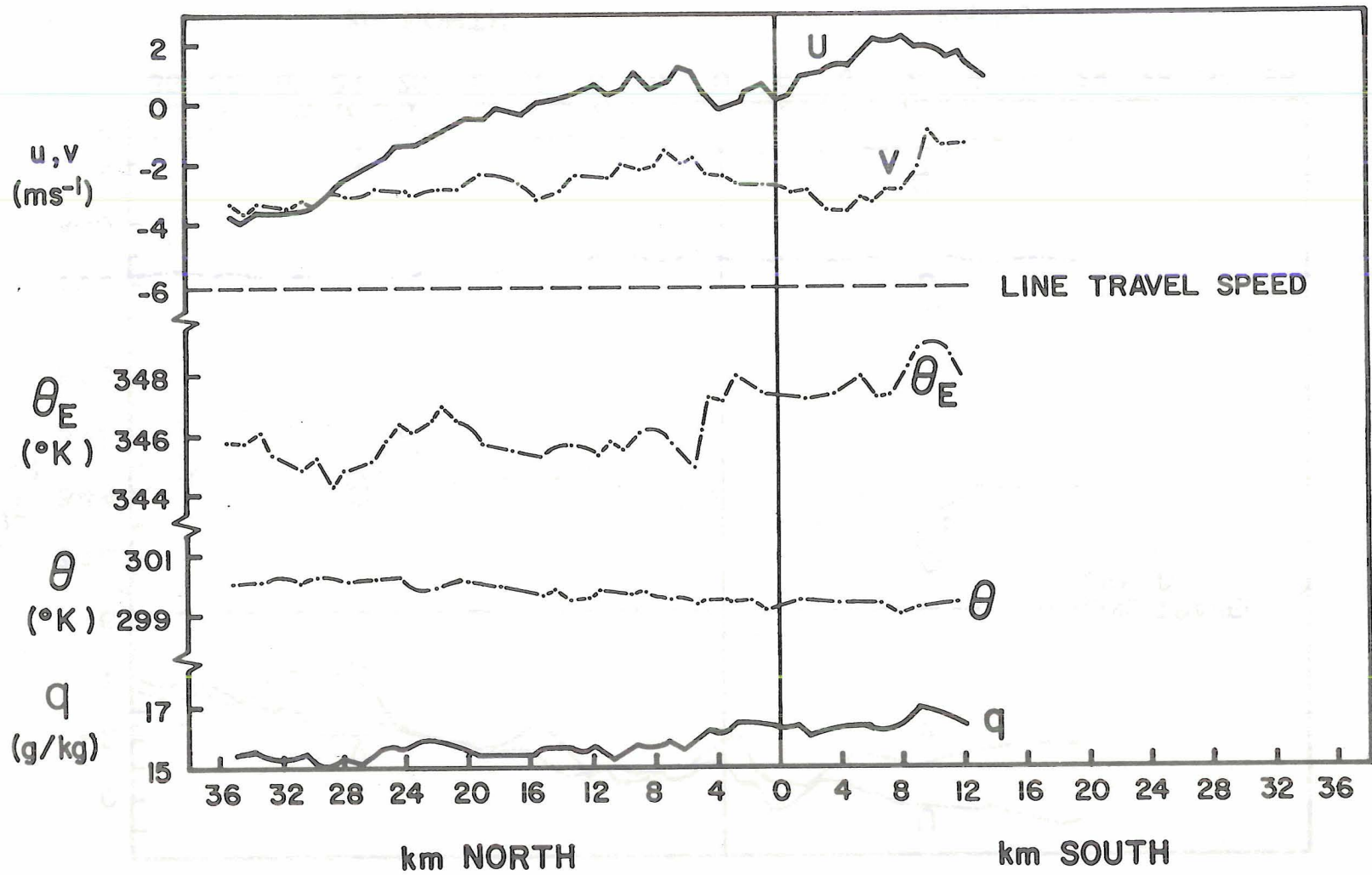


Figure 23. Mean of 4 runs through southern line at 960 mb.

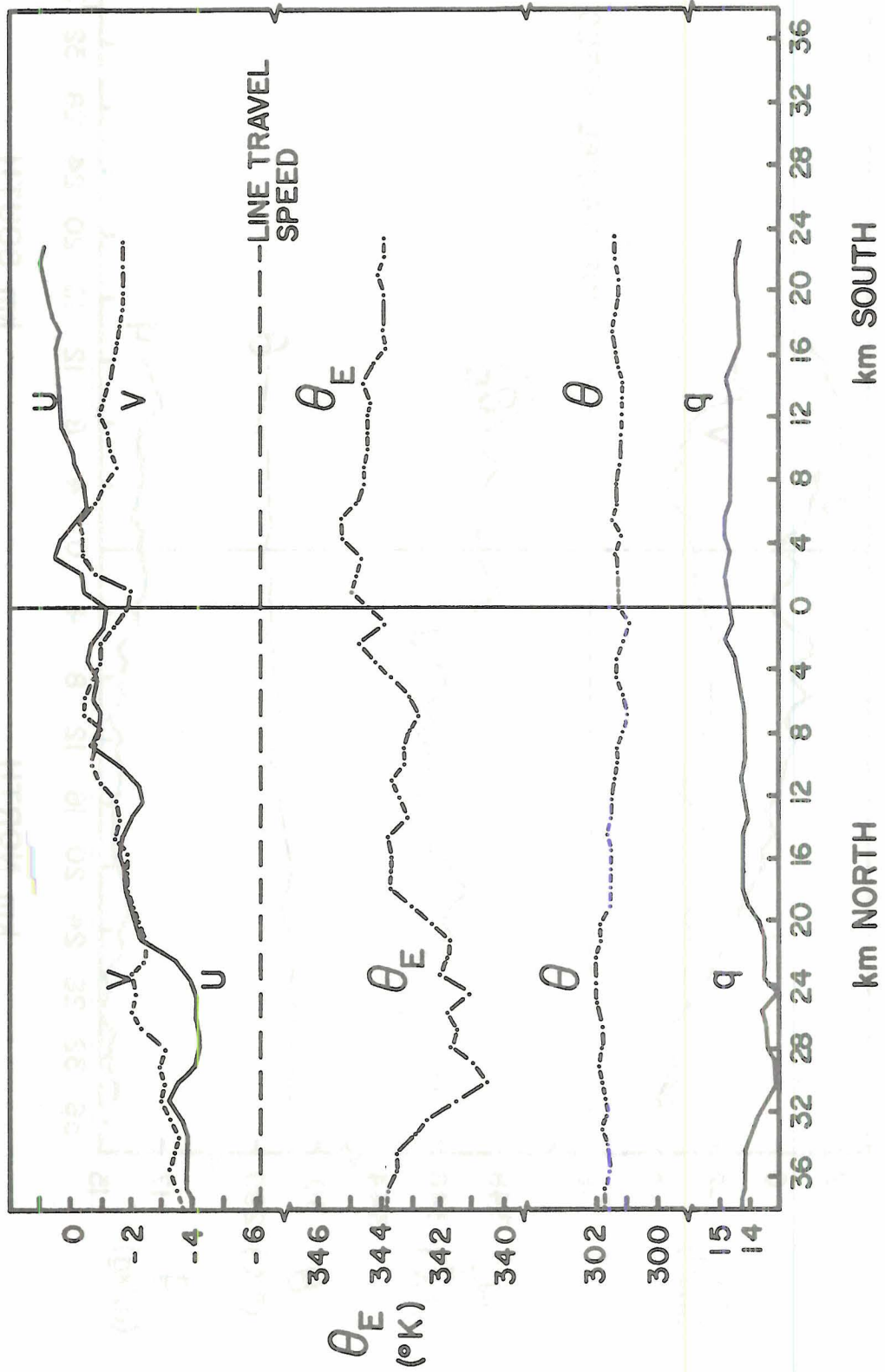


Figure 24. Mean of 4 runs through southern line at 900 mb for L-188.

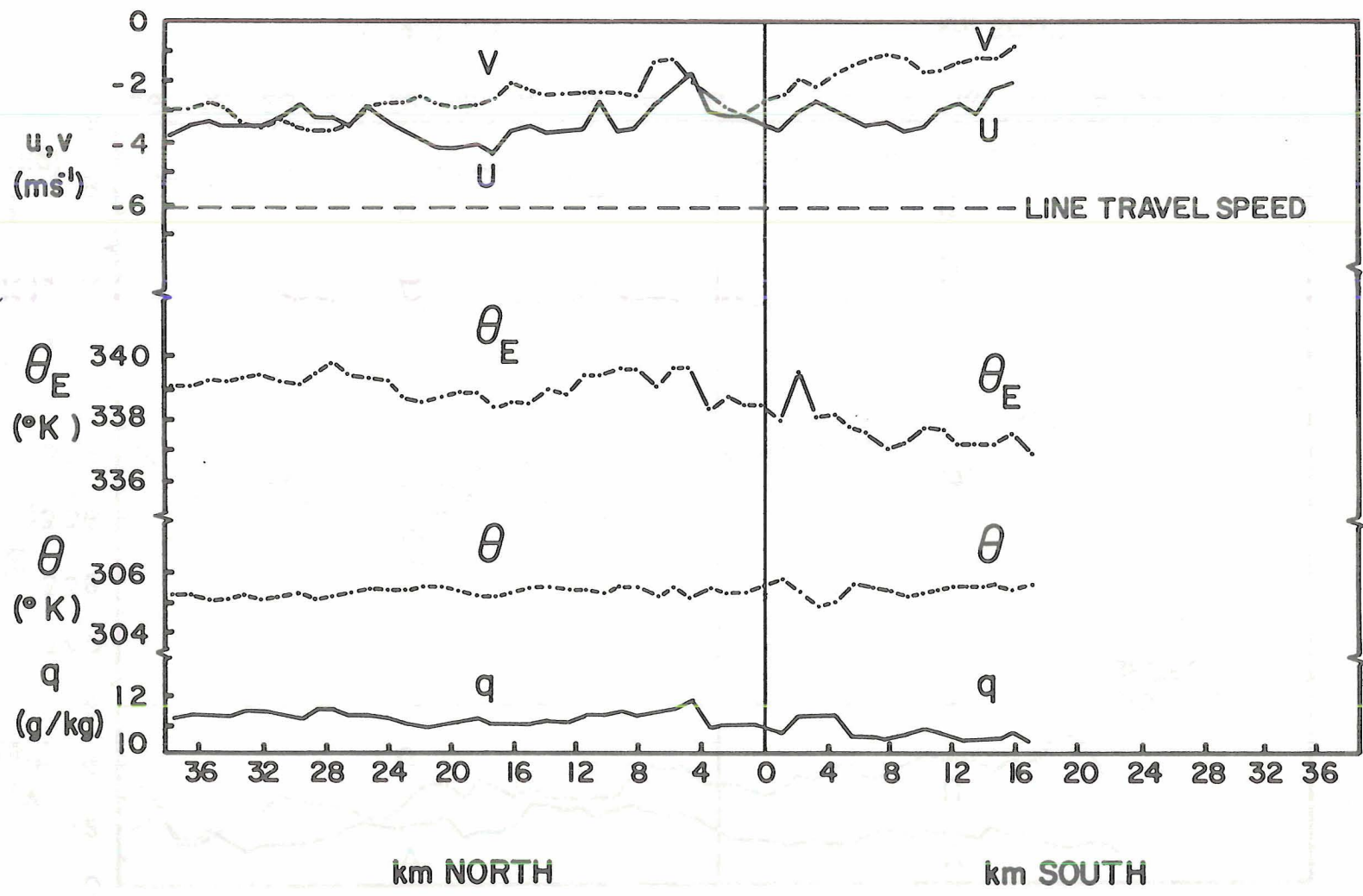


Figure 25. Mean of 4 runs through southern line at 810 mb for L-188.

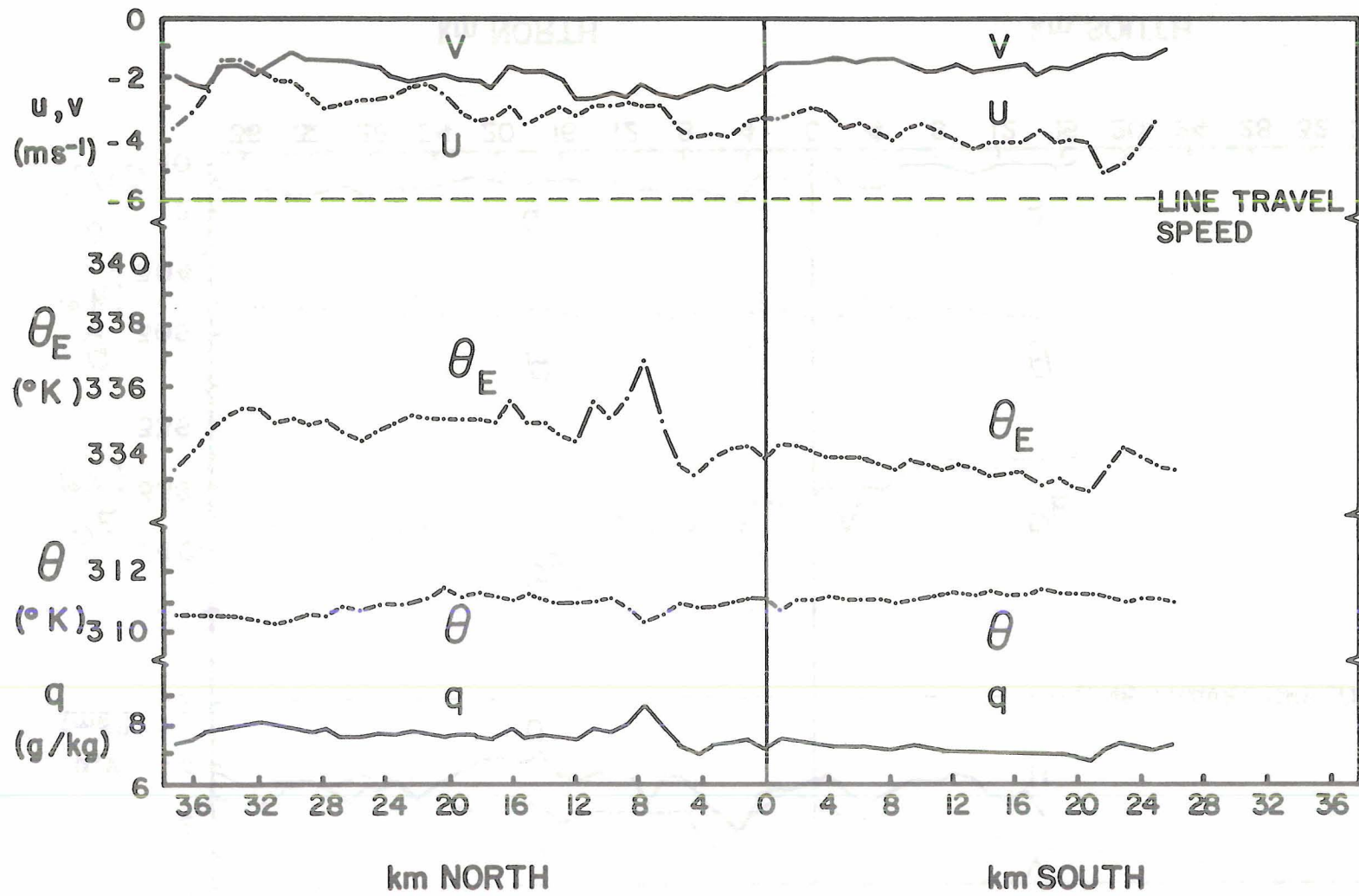


Figure 26. Mean of 2 runs through southern line at 720 mb for US-C130.

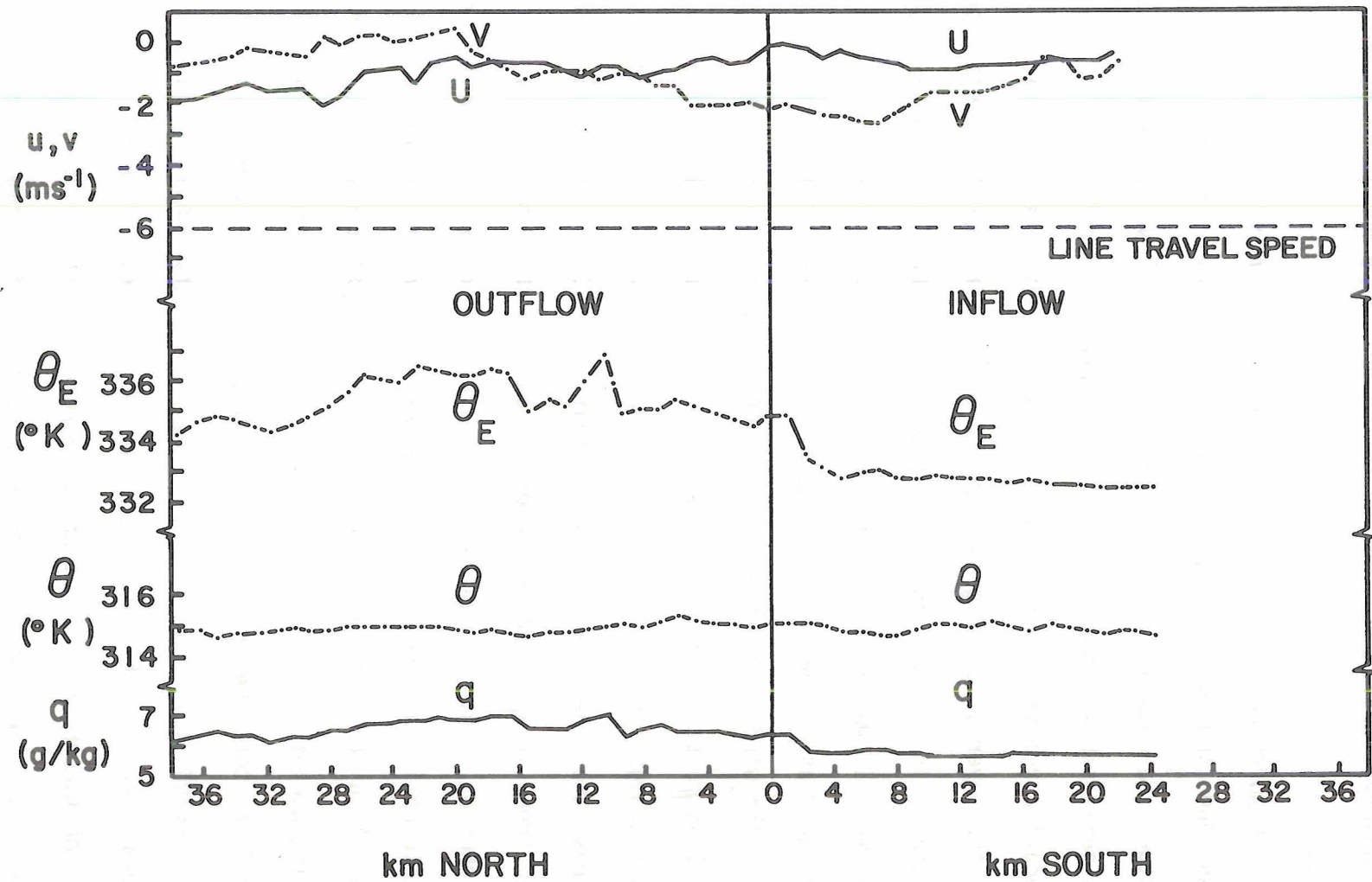


Figure 27. Mean of 7 runs through southern line at 640 mb for US-C130.

an observed cooling and drying to the rear as a result of downdraft activity.

Figures 22-27 represent the composited aircraft data at levels 985, 960, 900, 810, 720 and 640 mb, respectively. The 960 mb level is actually a mean of the 970 and 945 mb levels flown by the DC-6. This is permissible because both levels showed similar features at the same location relative to the line. It is interesting to note that the depth of the layer of cooling is confined to a layer near the surface because a change in  $\theta$  is not observed at any level other than the surface and 985 mb. It would, therefore, be unwise to place this line in the same category as a squall-line owing to its relatively 'mild' nature.

The wind shift at 985 mb and 960 mb is still very much present as well as moist inflow air. The local  $\theta_E$  minimum is also evident at 960 mb although its amplitude has been damped slightly. The decrease in  $\theta_E$  across the line at 900 mb is somewhat less  $\sim 3^\circ\text{K}$ . At and above 810 mb the trend in  $\theta_E$  is in the opposite sense in that the outflow air is of higher  $\theta_E$ . This is due to a gradual rise in  $q$  which is a result of meso-scale uplift behind the line. Superimposed on the general trend of  $\theta_E$  (or  $q$ ) in the outflow are one or two local maxima associated with the existence of growing cumulus towers. Another common feature of Figures 22-27 is that the inflow and outflow to the line are nearly constant with height (block flow). The large, local gradients in the wind components are not observed above the 900 mb level. From the surface to 900 mb though there is strong convergence in the inflow and considering the zonal wind component, there is evidence of 2-dimensional positive (or cyclonic) vorticity up to at least 800 mb. The strong convergence just ahead of the line and somewhat weaker divergence to the rear has

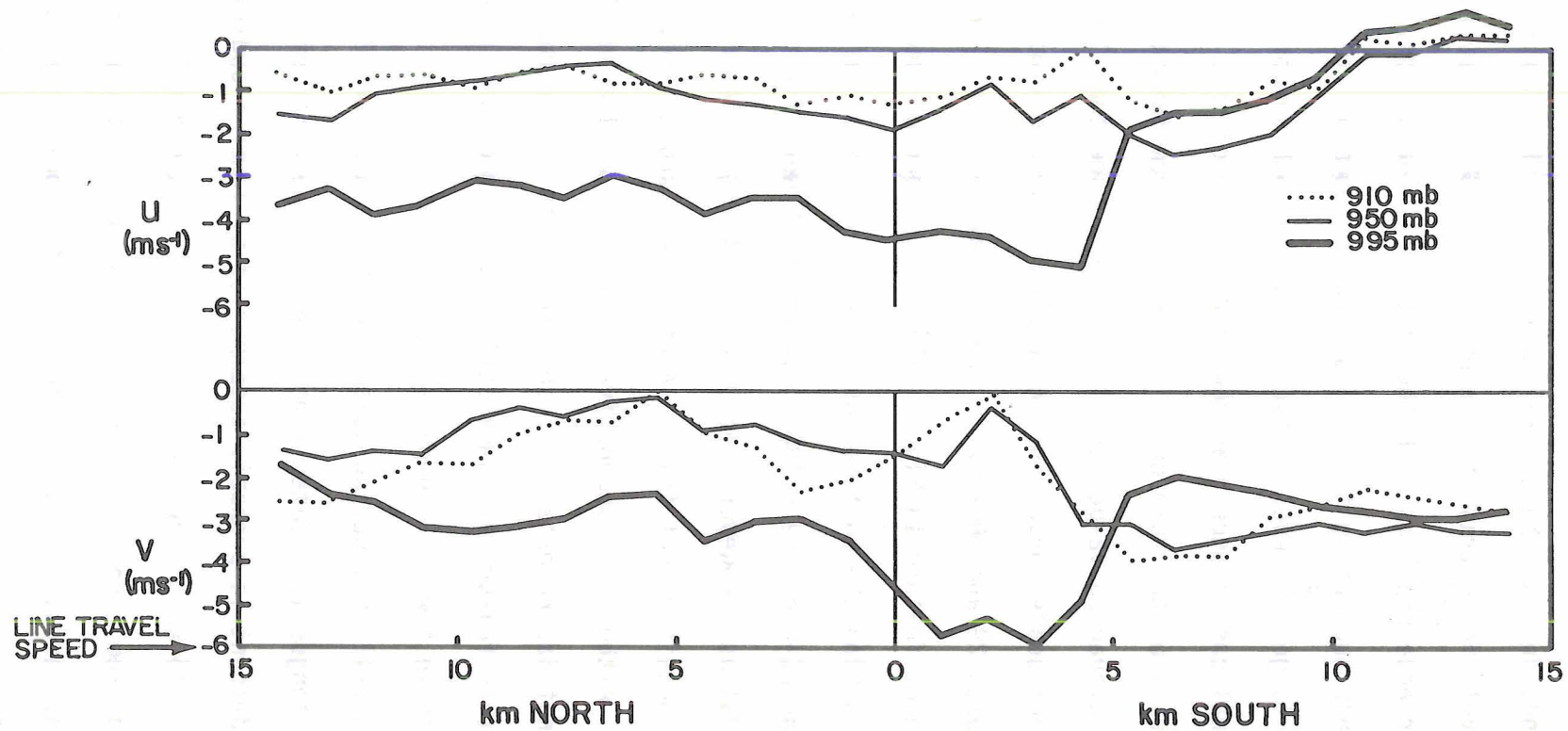


Figure 28. Wind components relative to the southern line from 3 minute Dallas BLIS data.

near the surface because the same feature is not observed at 950 mb and 910 mb and, indeed, the general trend across the line is reversed at these levels in contrast to the DC-6 and L-188. However, the BLIS system did experience problems with the wind direction sensor. The surface shift lends support to the DC-6 and Dallas boom at the lowest level only. There is large low-level vertical shear in both components. The 2-dimensional convergence near the leading edge of this line is  $1.2 \times 10^{-3} \text{ sec}^{-1}$  and is of the same order as computed from the other data sets. By mentally averaging values on either side we see that the line is embedded in a larger scale convergent and cyclonic surface wind field.

Figures 29 and 30 show  $\theta_E$  and  $\theta$  relative to the line respectively. The dominant feature in Figure 29 is the tongue of low  $\theta_E$  (warm, but dry) air just behind the surface gust front. This feature was not observed by either the DC-6 or the L-188, both of which were flying about 20 km to the west of Dallas. However, the DC-6 was flying at 945 mb at 1500Z only and so it is possible that this is a relatively short-lived feature and occurs locally. Although no supportive evidence is available, it is likely that this is not instrumental because recovery is rather rapid. The origin then of this feature is compensating subsidence (dry adiabatic descent) around active towers. Comparison of the position of this tongue with the sharp fall in incoming solar radiation in Figure 20, it can be seen that the tongue is located immediately to the north of the minimum and so this descent is probably accompanied by lower cloudiness.

About 15 km to the rear of the line is another local fall in  $\theta_E$  resulting from a downdraft which spreads as it reaches the surface and moves southwards, the southernmost boundary being the surface gust front. This, in turn, forces air of high  $\theta_E$  out of the sub-cloud layer

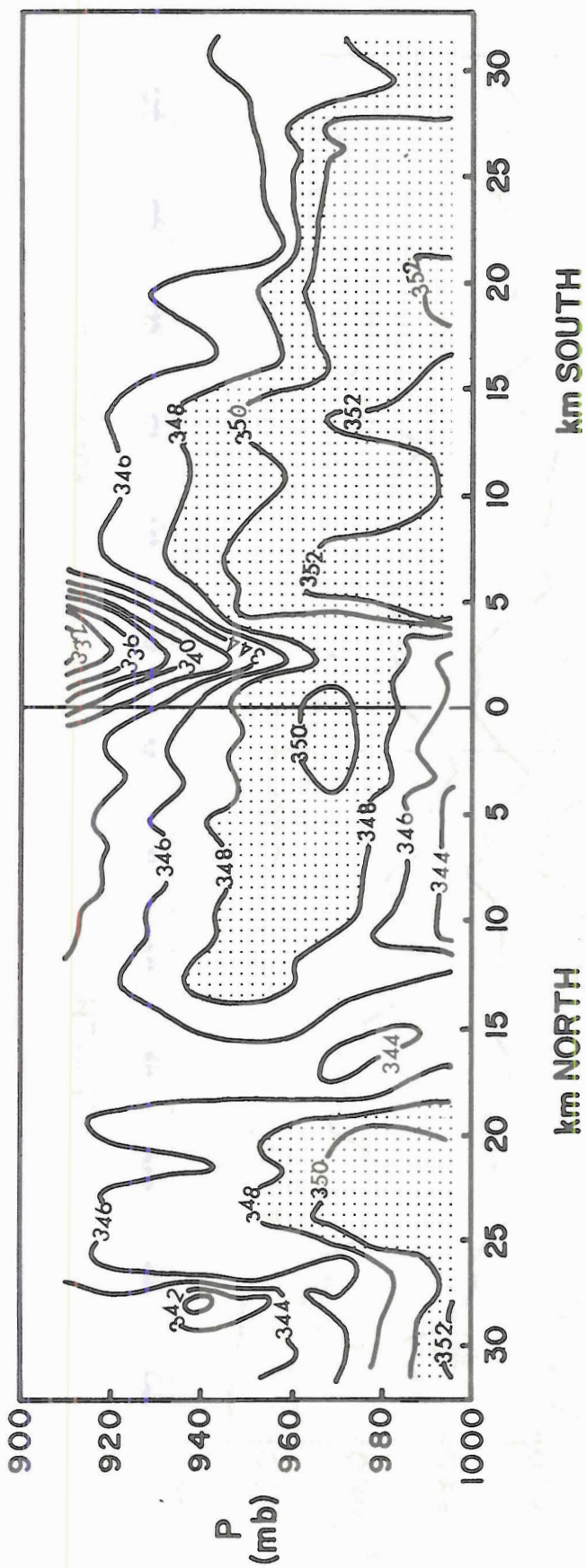


Figure 29. Equivalent potential temperature ( $\theta_E$ ) relative to the southern line from 3 minute Dallas BLIS data.

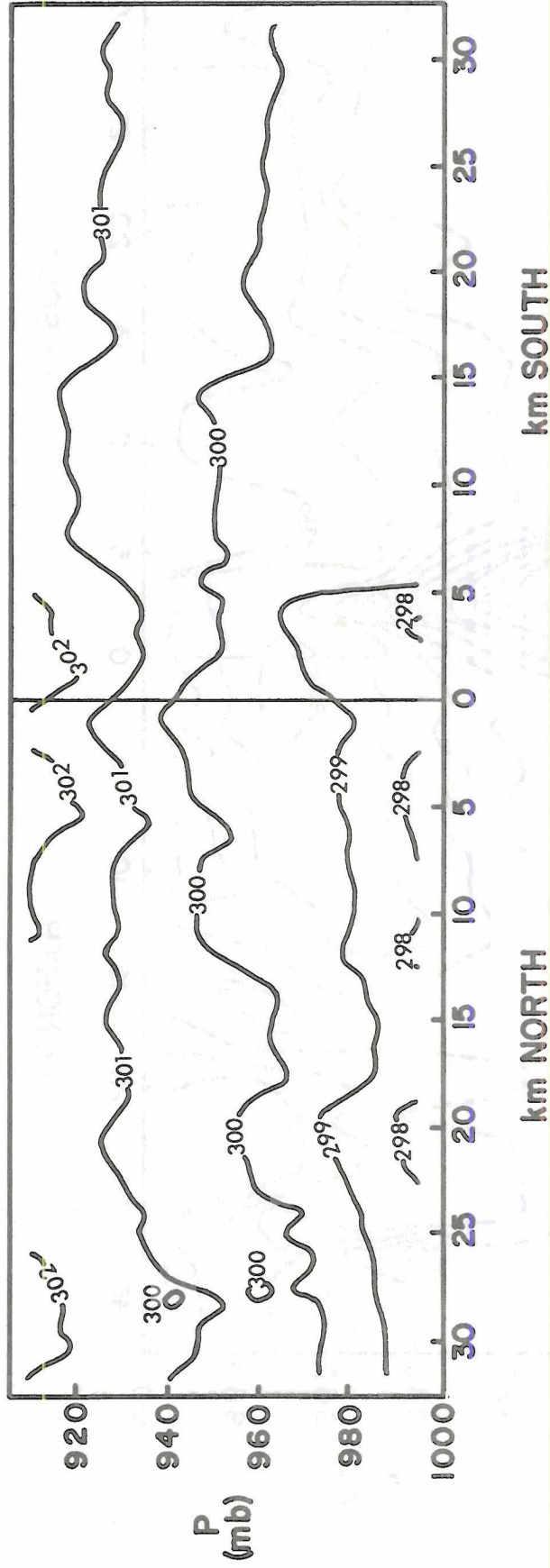


Figure 30. Potential temperature ( $\theta$ ) relative to the southern line from 3 minute Dallas BLIS data.

into the main updraft. With a block inflow of  $\sim 4 \text{ ms}^{-1}$  at all levels, this downdraft must be fed by air flowing into the line from the south. It is not descent between neighboring cells and is in no way associated with the tongue of dry air south of the line.

Figure 30 shows again that the descending air is associated with slightly higher temperatures (a result of dynamical descent) and the temperature drop across the line is about  $1.5^{\circ}\text{C}$ .

In conclusion, although the numerical values for the tethered balloon data may be slightly suspect, there is strong agreement between the three data sets discussed thus far, i.e. surface, aircraft and tethered balloon.

### 3.6 Vertical profiles

There have been several studies of squall-line systems based on 'before' and 'after' profiles using rawinsonde data, e.g. Betts, Grover and Moncrieff (1976); Betts (1976). It will, therefore, be instructive to construct vertical profiles representing mean inflow and outflow to the southern line.

The data from the Dallas boom and the aircraft shown in Figures 20-27 were averaged in the inflow and outflow regions. The averages, which were performed over distances of  $\sim 35 \text{ km}$  where possible, are thought to be representative of mean conditions in each region. Regions very close to the line at the surface where large gradients are observed have been omitted from the average.

It is important to note that most aircraft made sections through the line at at least two different levels and so data are not sampled simultaneously at each level. Consequently, data sampled on the first

traverse may possess different numerical values than data sampled at a later time. It is desirable, therefore, to examine the data for a trend in time and to correct for this by extrapolating to a common time before performing the average.

All parameters on both sides of the line were averaged and plotted against time. A trend was only observed in the wind components u and v and in both cases, the components appear to become more positive with time thus making it a simple matter to extrapolate to a common time - in this case, 1330Z. The corrections are found in Table 9.

Table 9. Corrections for the trends in u and v.

LEVEL	CORRECTION FOR TREND			
	LINE A		LINE B	
	u	v	u	v
	-(ms <sup>-1</sup> )-		-(ms <sup>-1</sup> )-	
sfc	-	-	0	0
985	+0.8	+0.4	-0.8	-0.5
969	-	-	+1.0	+0.5
946	-1.3	-1.1	-2.3	-1.8
903	0	0	+0.2	+0.4
810	-0.1	-0.5	-1.1	-0.8
720	0	+0.1	0	-0.6
640	0	-0.2	+0.8	+0.7
380	0	0	0	0
290	0	0	0	0
220	0	0	0	0

### 3.6.1 Wind profiles

Figures 31-35 show the vertical profiles of all parameters for in-flow (south of line) and outflow (north of line).

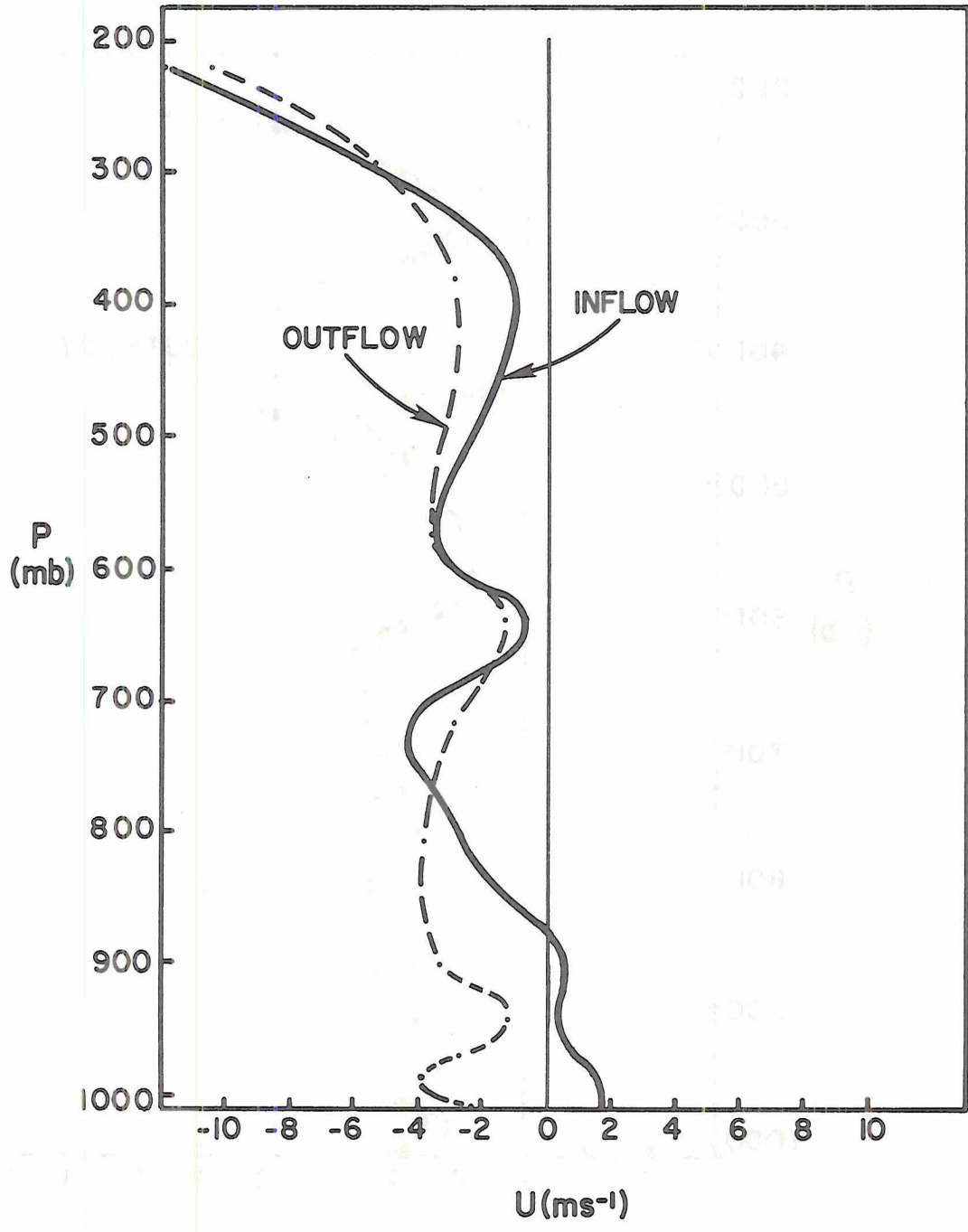


Figure 31. Average zonal wind component for southern line from aircraft data.

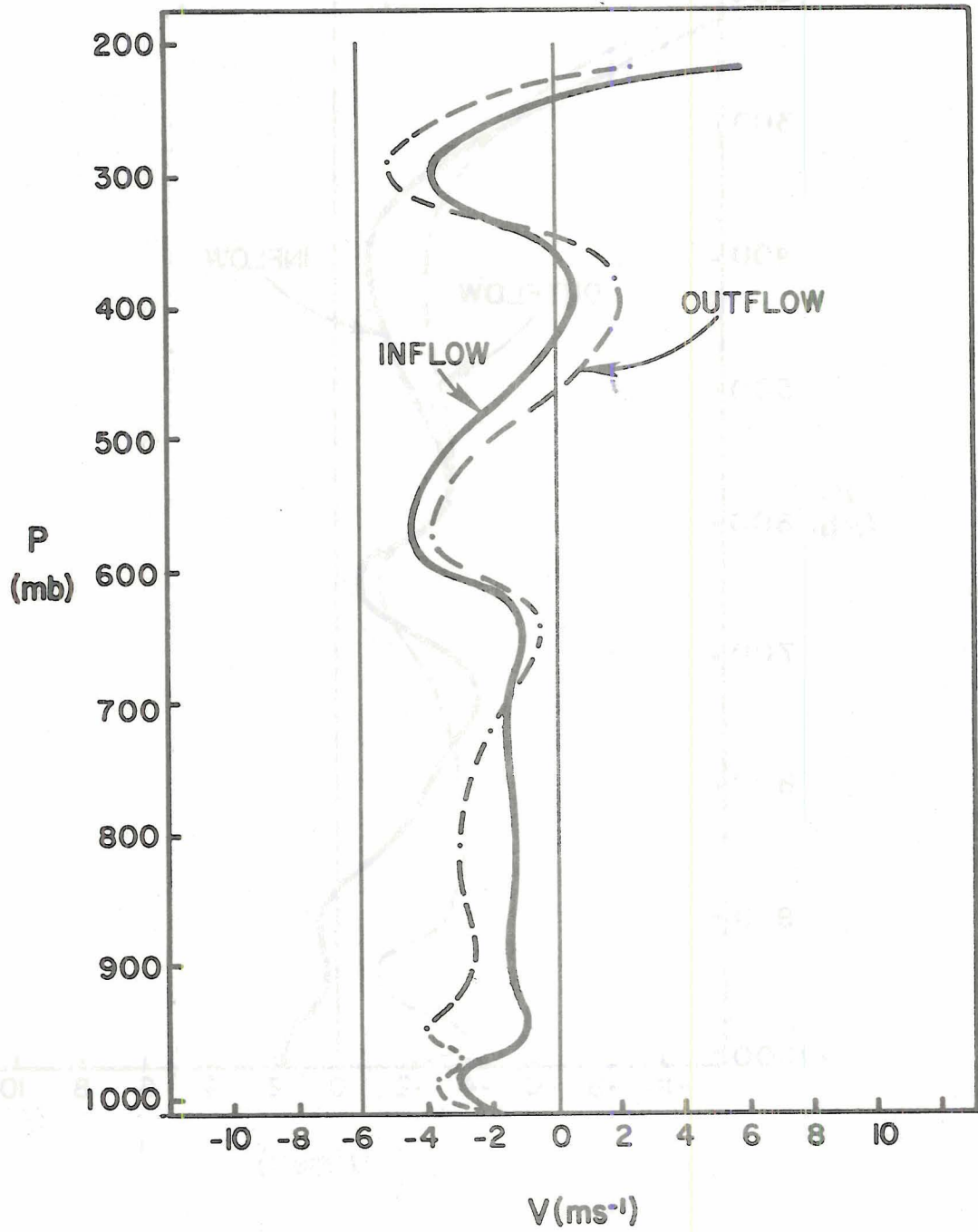


Figure 32. Average meridional wind component for southern line from aircraft data.

The u wind component shows weak surface westerlies ahead of the line. A large decrease in westerly momentum ( $\sim 3-4 \text{ ms}^{-1}$ ) is observed throughout a relatively deep layer from the surface to 750 mb. Above 300 mb the easterly flow increases rapidly with height.

The v wind component shows an increase in the northerly component of  $\sim 2 \text{ ms}^{-1}$  from the surface to 700 mb. Only at the highest level do we observe a southerly component. Both figures indicate little or no vertical shear in either component throughout most of the troposphere. At no level does v become equal to the line travel speed. Consequently, these are not steering-level systems. This contradicts a statement made by Pestaina-Haynes and Austin (1976).

Raymond (1975) represented a convective storm as a wave packet of forced internal gravity waves. The gravity waves are able to produce low-level convergence which, in turn, drives the wave itself. This model is capable of predicting accurate storm travel speeds, thereby eliminating any requirement for a steering-level. The low-level shear may, however, be a more fundamental feature for their propagation.

### 3.6.2 Thermodynamic profiles

Figures 33-35 show the distribution of the thermodynamic variables. Figure 33 indicates a drying of 2 g/kg in the lower troposphere with compensating moistening above. This change in the sub-cloud layer is also observed in the 'Dallas' BLIS data and similar trends have also been observed by Betts (1976) in VIMHEX but of larger magnitude. This lends support to the assertion that the atmosphere is overturned by mixing processes on the scale of the system (see Moncrieff and Green, 1972).

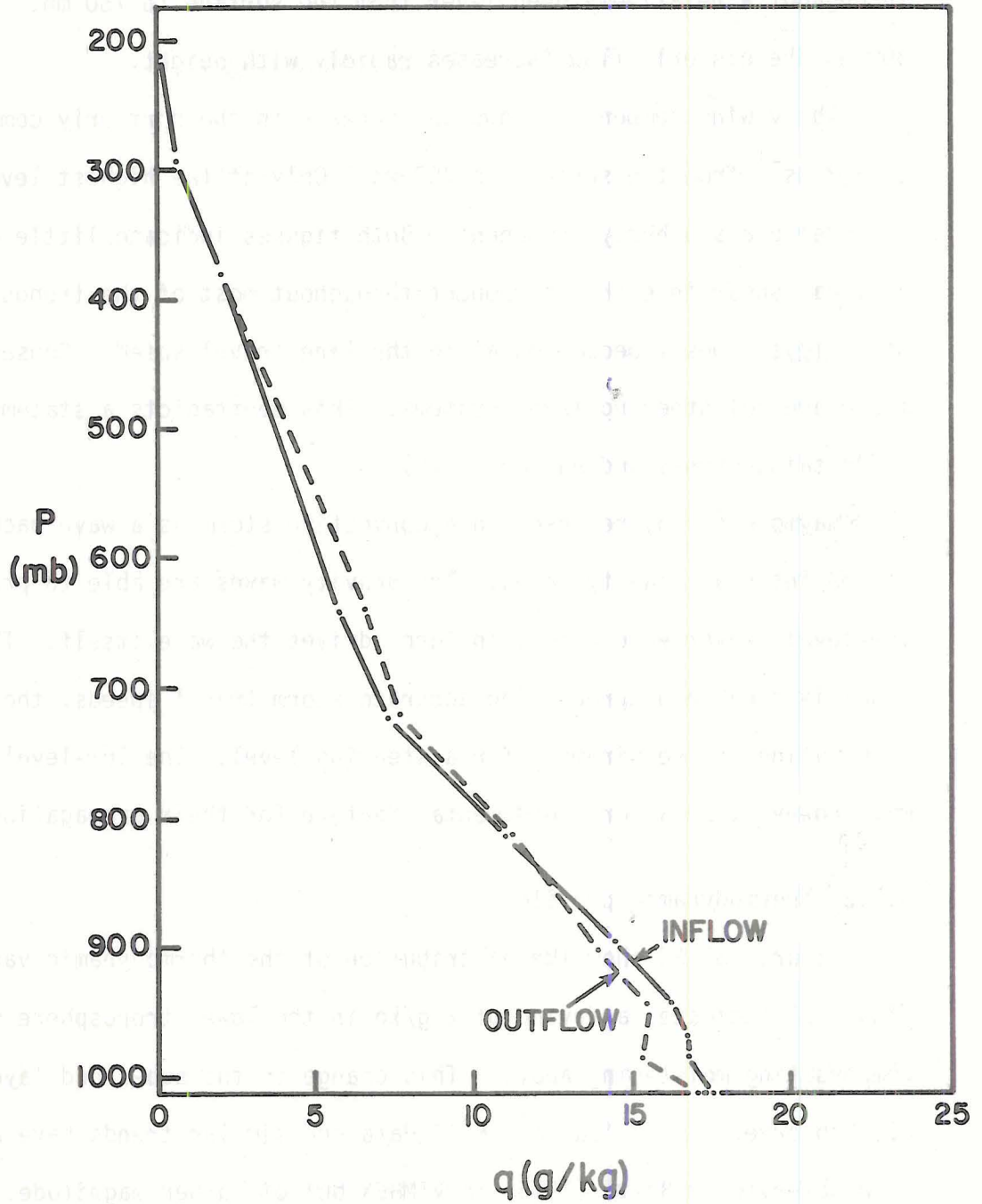


Figure 33. Average specific humidity for southern line from aircraft data.

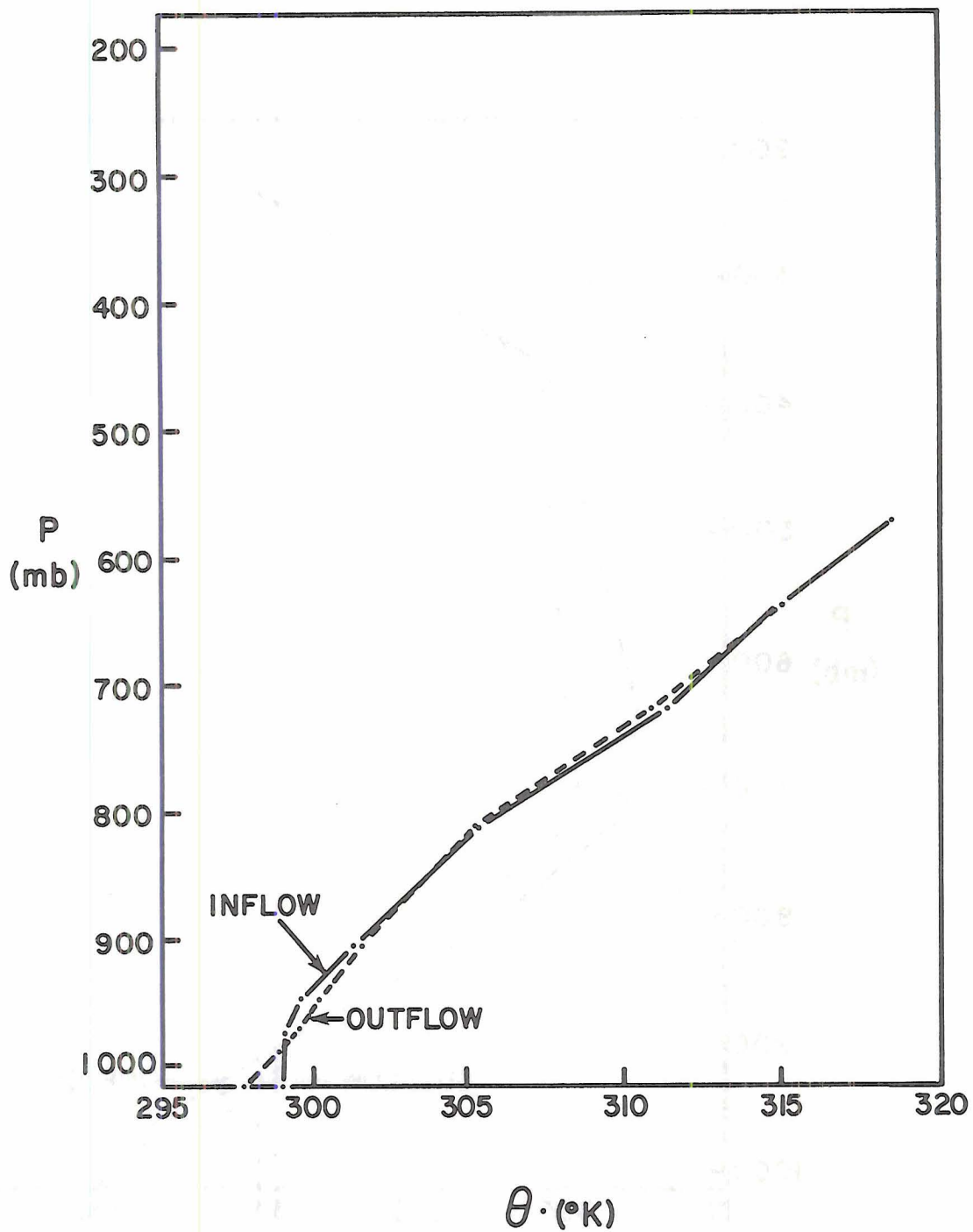


Figure 34: Average potential temperature for southern line from aircraft data.

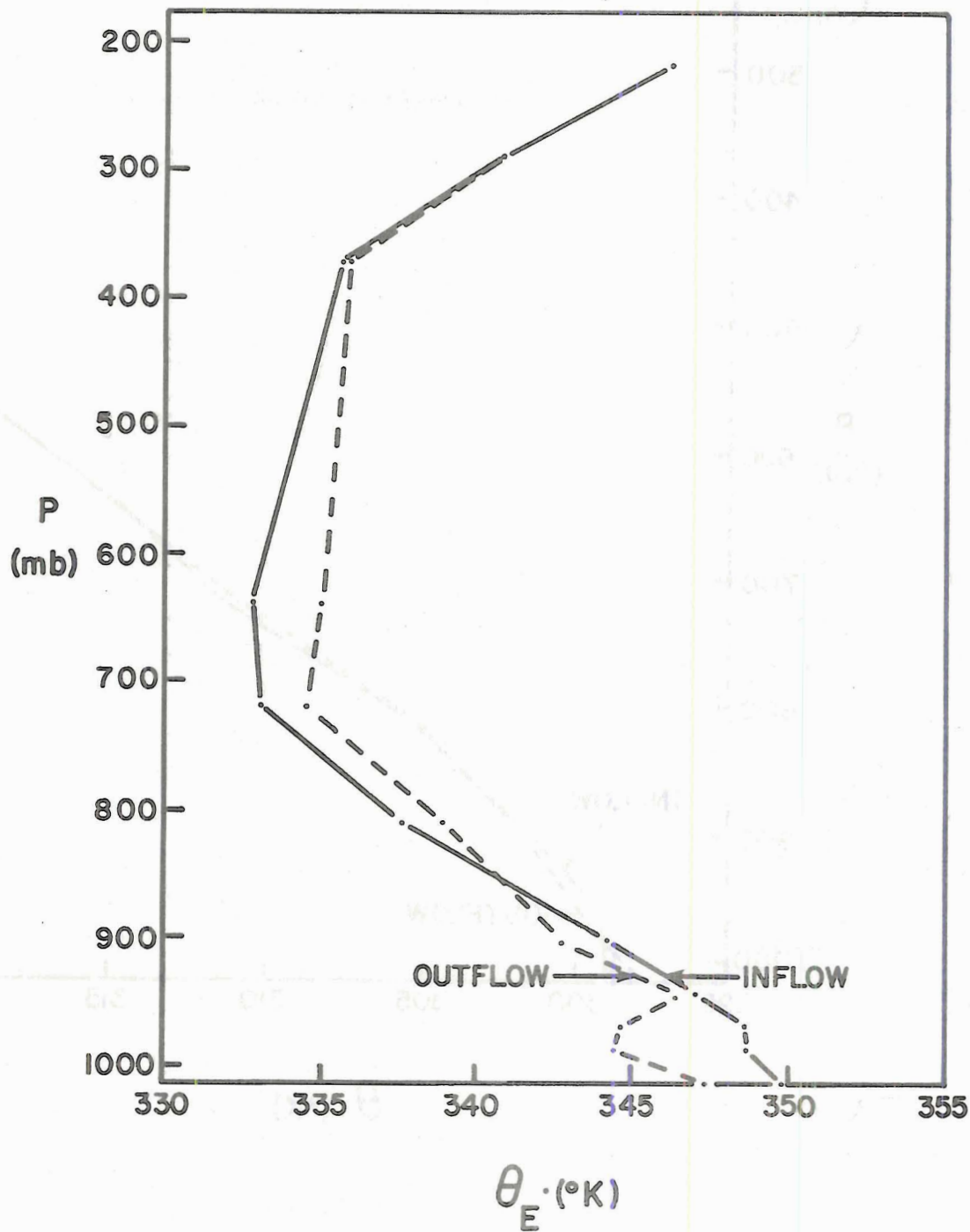


Figure 35. Average equivalent potential temperature for southern line from aircraft data.

Figure 34 indicates a cooling of  $1.5^{\circ}\text{K}$  confined to a shallow layer near the surface (250 m) with a slight warming trend above. No trend is observed at levels higher than this. The depth of the layer of cooling gives an indication of the depth of the outflowing, cold 'density' current.

The changes in  $\theta_E$  which are simply a composite of the changes in  $\theta$  and  $q$  indicate a large decrease in the mixed layer of  $\sim 5^{\circ}\text{K}$  and an increase of similar magnitude throughout the rest of the troposphere. This increase can be caused by mesoscale ascent to the rear of the line or simply higher humidity values in cloud (see Zipser, 1977). The large decrease in the mixed layer is the result of downdraft activity discussed earlier.

Generally speaking, these profiles agree well with the Dallas BLIS data in low-levels thus enabling high confidence to be placed on the qualitative arguments presented in this section.

### 3.6.3 Vorticity and divergence

As previously stated, the vorticity and divergence in the wind field is probably fundamental to the formation and maintenance of lines of this nature. The difference between the  $u$  and  $v$  profiles yields values for the 2-dimensional vorticity and 2-dimensional divergence respectively. The differences between profiles at 25 mb intervals were taken and they are shown in Figures 36 and 37.

Figure 36 shows that the divergence profile for the northern line does not satisfy mass-balance. This is probably because on earlier traverses the aircraft went through less active parts of the line. For the southern line, however, Figure 36 indicates strong convergence from

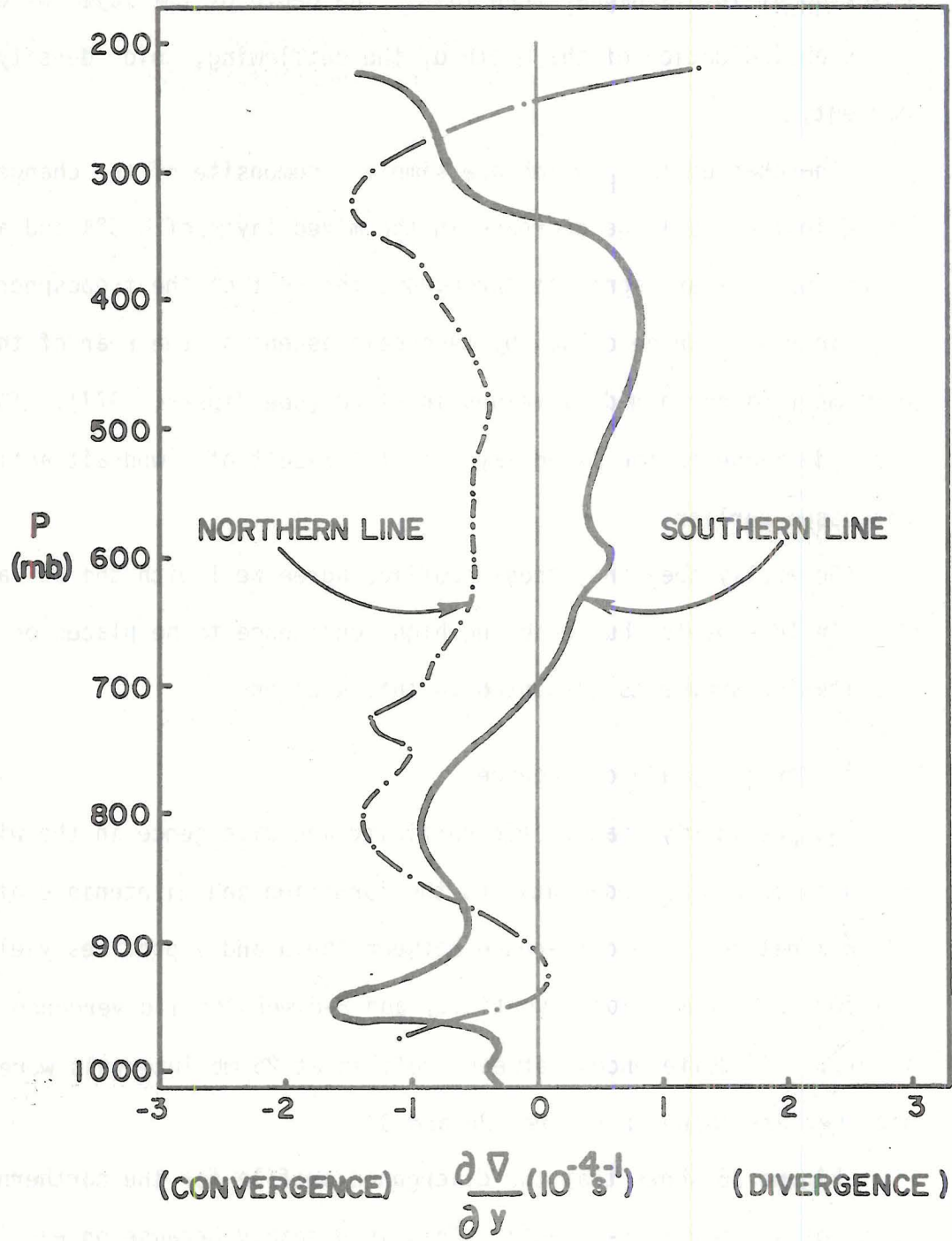


Figure 36. Mean 2-dimensional divergence computed from aircraft data.

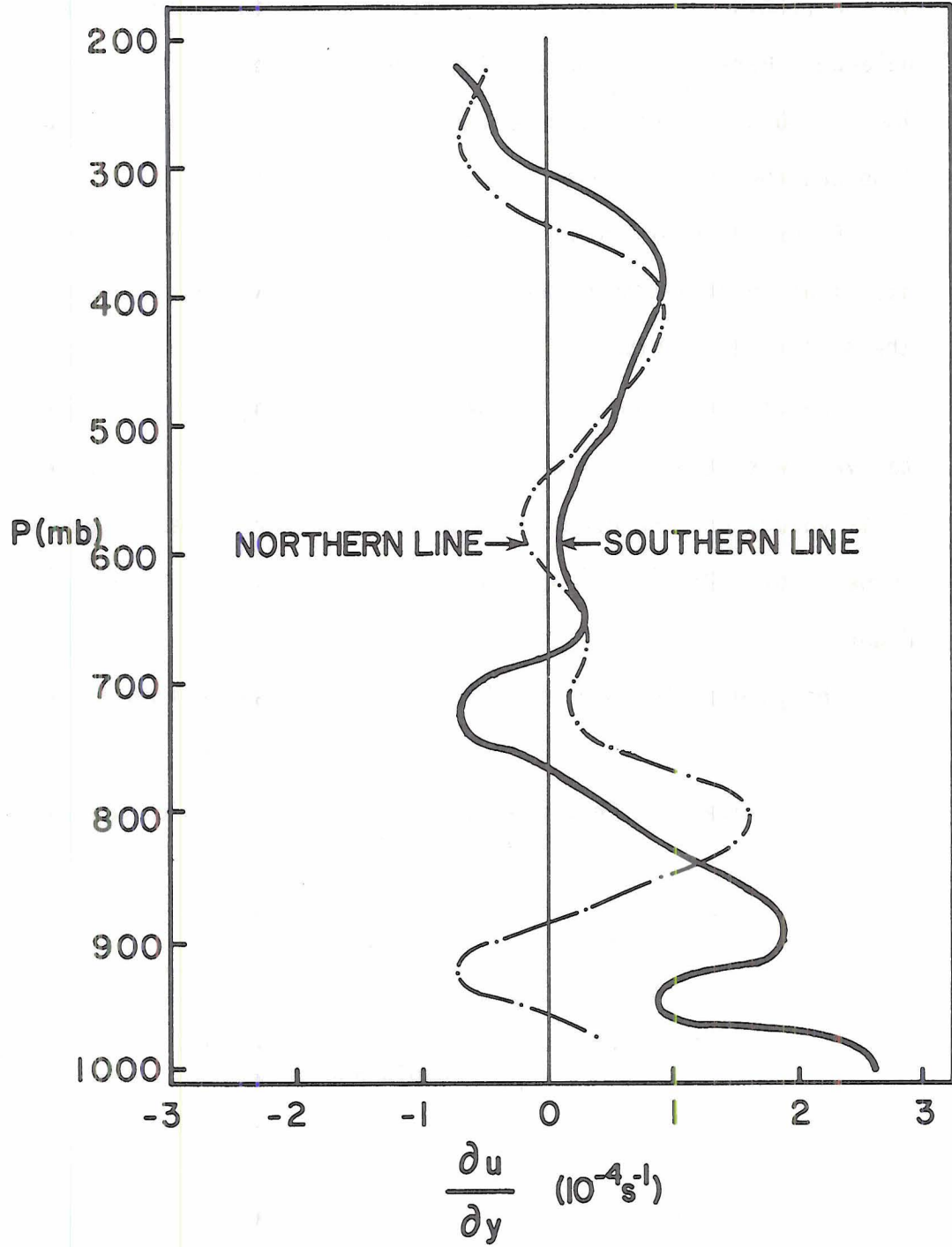


Figure 37. Mean 2-dimensional vorticity computed from aircraft data.

the surface to 700 mb ( $\sim 10^{-4} \text{ s}^{-1}$ ) with divergence in the middle troposphere ( $.5 \times 10^{-4} \text{ s}^{-1}$ ) and convergence aloft giving approximate mass-balance. Here we are considering mean values over a distance of approximately 60 km. [The sharp convergence ( $\sim 10^{-3} \text{ s}^{-1}$ ) just ahead of the line and the divergence to the rear partly cancel].

Figure 37 shows there to be a 'layered structure' in the vertical distribution of 2-dimensional vorticity with cyclonic vorticity from the surface to 750 mb ( $\sim 1.5 \times 10^{-4} \text{ s}^{-1}$ ).

The low-level values of both divergence and vorticity agree qualitatively with the synoptic-scale profiles of Reeves and Ropelewski 1976. Their values are one order of magnitude smaller, as expected, with convergence of  $\sim 2 \times 10^{-5} \text{ s}^{-1}$  and cyclonic vorticity of  $\sim 5 \times 10^{-5} \text{ s}^{-1}$ . (See Figure 7).

The general features in this section are summarized in Table 10.

Table 10. Characteristics of layers associated with this line of convection.

LAYER (mb)	CHARACTERISTICS
sfc - 750	Convergent, cyclonic cools and dries
750 - 500	Divergent, irrotational moistens
500 - 300	Divergent, weak cyclonic moistens
300 - 200	Convergent, anticyclonic

### 3.6.4 Discussion

The wind shift (being the most important feature of this line) is probably the source of maintenance and propagation. The convergent and cyclonic wind field, from the surface to 750 mb, in which the line is embedded provides a mechanism whereby warm, moist air in the sub-cloud layer is able to be fed into the system. The downdraft to the rear, which forms the gust front at the 'leading' edge of the line, provides an additional impetus to this air. The southerly propagation of the downdraft as it reaches the surface is thought to be the source of the observed convergence and is, therefore, a necessary component of the line.

Figure 38 shows the aircraft data in the inflow region plotted on a tephigram. The atmosphere in mid-levels is relatively moist with a mixing ratio of 6 g/kg at 650 mb. Large mid-level humidity is favorable to deep cumulus convection (a dry environment destroys buoyancy by entrainment into the cloud). Consequently, clouds during GATE frequently reached the upper troposphere with little vertical motion associated with them. This is a possible reason why cloud-tops in this study reached the 200 mb level.

### 3.7 Density current model

It is now of interest to see if a realistic travel speed for the southern line can be predicted from a simple density current model formulated by Miller and Betts (1977).

$$C_p^2 = -g \frac{\Delta\theta}{\theta} H$$

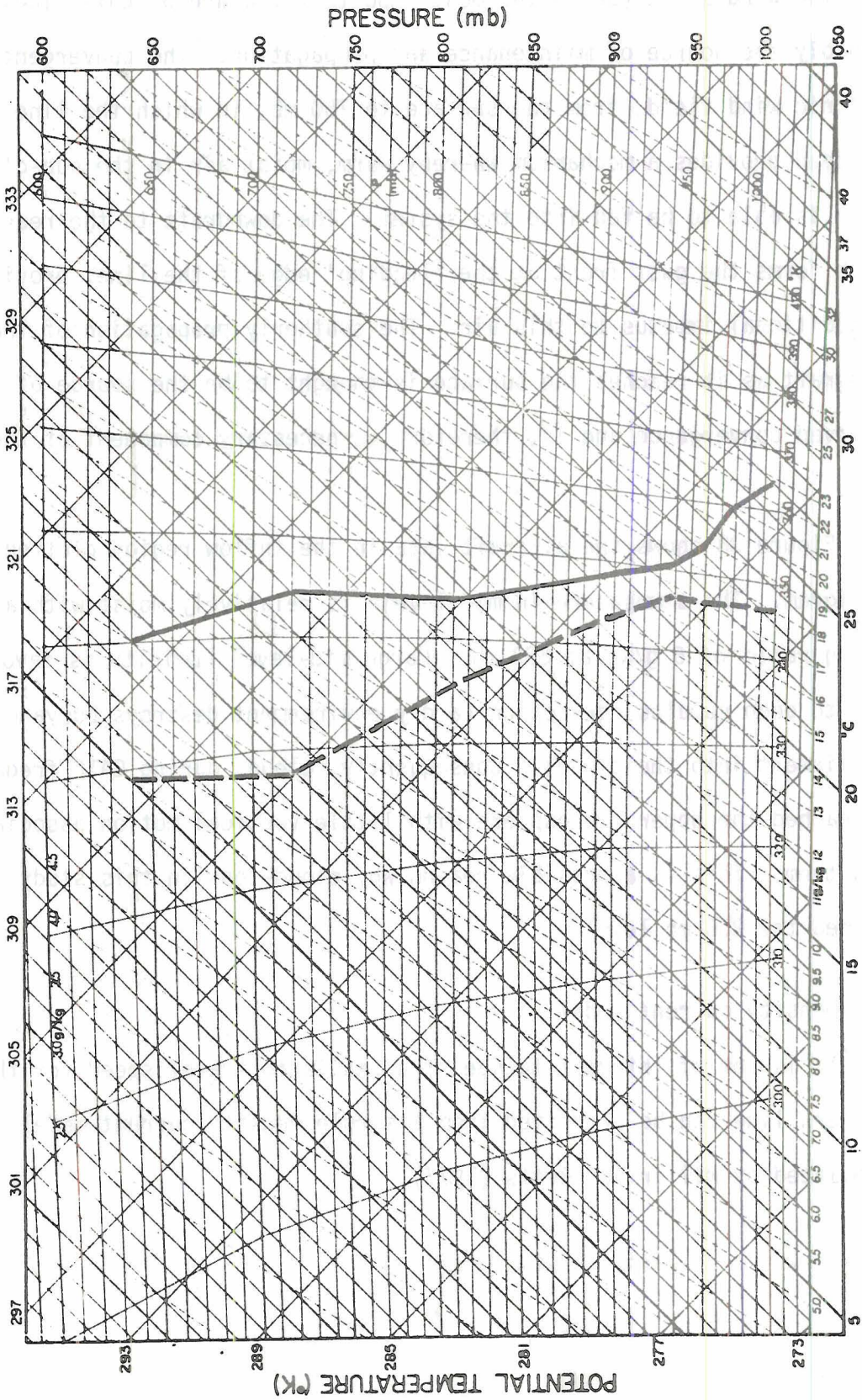


Figure 38. Mean inflow to southern line from Dallas boom and aircraft data.

where  $C_\rho \sim$  density current speed  
 $g \frac{\Delta\theta}{\theta} \sim$  buoyancy deficit  
 $H \sim$  depth of the density current  
 $\Delta\theta \sim$  observed potential temperature drop at the surface  
 $\theta \sim$  mean potential temperature within the density current  
 $g \sim$  acceleration of gravity

using  $g = 9.81 \text{ ms}^{-2}$

$$\Delta\theta = 1.2^\circ\text{K}$$

$$\theta = 298.3^\circ\text{K}$$

$$H = 232 \text{ metre}$$

gives  $C_\rho = -3.03 \text{ ms}^{-1}$ .

Now if the line travel speed is  $C$  and the mean velocity ahead of the line is  $\bar{V}_0$  (Miller and Betts, 1977) then

$$C = 0.42 \bar{V}_0 + 0.83 C_\rho$$

which gives, upon substitution,  $C \sim -3.5 \text{ ms}^{-1}$  which falls far short of the observed  $6 \text{ ms}^{-1}$ . It can only be concluded that the density current model applies only to the more intense Venezuelan squall-lines where the formation of a strong density current (or downdraft) is a necessary ingredient to their maintenance.

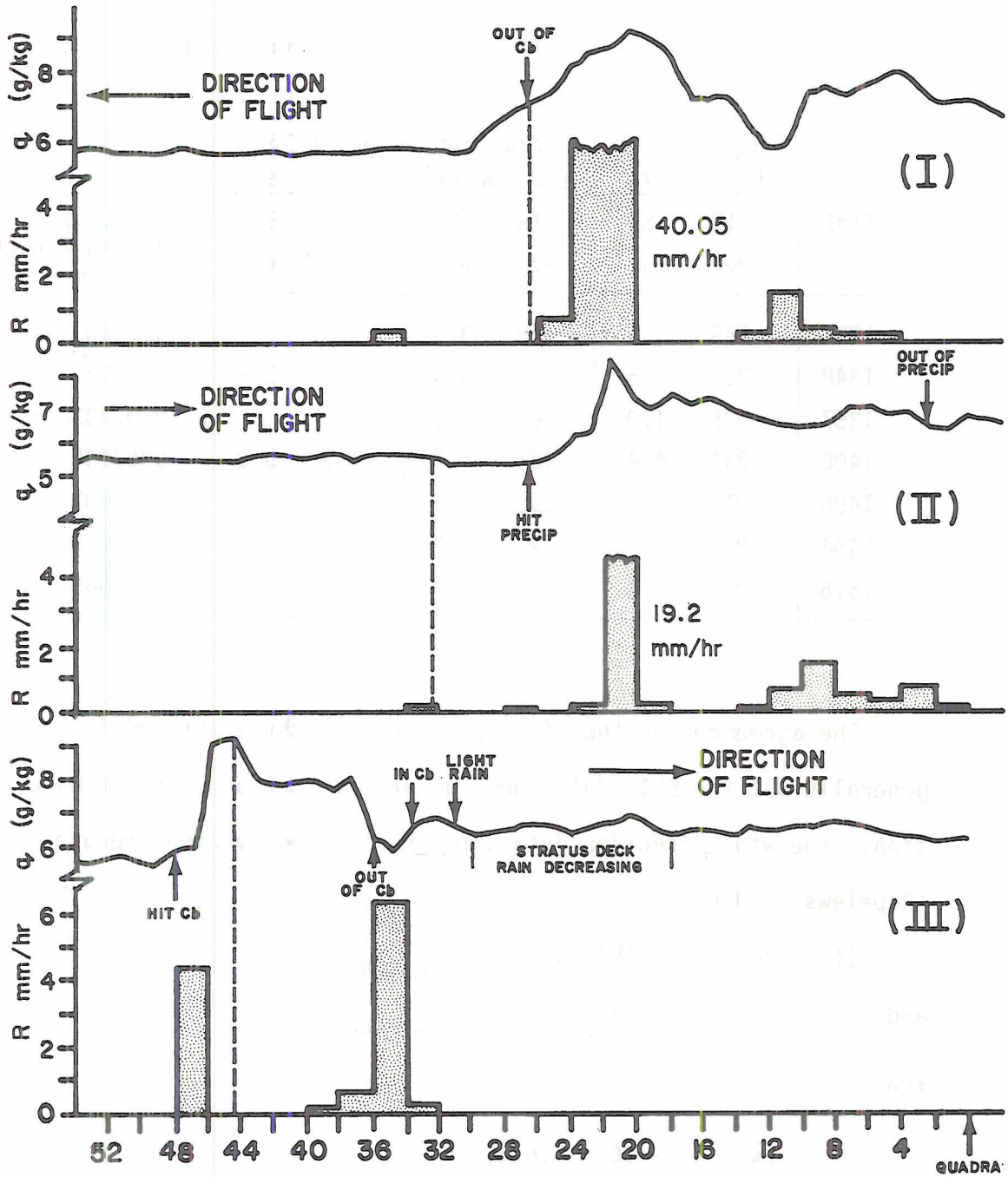
#### IV. DATA INTERCOMPARISON

##### 4.1 Aircraft and Quadra radar

The digital cross-sections from the Quadra radar along  $22.8^{\circ}\text{W}$  at 1214Z, 1229Z and 1314Z are compared to the ten second averaged data from the USC-130. The comparisons in Figure 39 are at a level of 4 km and consist of precipitation intensity (R) and specific humidity (q) from both systems for the southern line. The aircraft data were chosen so that they were closest in both space and time to the radar sections. At worst, the USC-130 was flying 5 km to the west of the sections. A characteristic feature of the precipitation data is that it is highly variable in space and, therefore, varies greatly from one grid point to the next. Since the grid spacing is 2 km for the Quadra radar, this could explain the small discrepancies between the two data sets. However, there appears to be a strong correlation between q and R at all times presented here. The vertical dashed line represents the RMS position of the southern edge of the line and the radar fix on this position is within two grid spaces. The observers' reports have also been included and they, too, show excellent agreement. The Quadra radar data will, therefore, be a useful tool in further case studies.

##### 4.2 Dallas BLIS - aircraft - Dallas boom

Aircraft point values were taken every time the aircraft crossed the latitude of the Dallas. Data from the BLIS and boom are averages of three, three minute values and correspond to approximately 3 km in space. A similar space average was calculated for the aircraft which involved taking three adjacent ten second averages. Values from all three sources were compared and tabulated at approximately the same levels.



km SOUTH OF QUADRA

Figure 39. Comparison of aircraft specific humidity and Quadra precipitation intensity at (I) 1214Z, (II) 1229Z, and (III) 1314Z at 4 km. The vertical dashed line is the r.m.s. fit for the southern line.

Table 11 shows the wind intercomparison.

Table 11. 3 km mean wind intercomparison.

TIME Z	DALLAS BLIS (9 min av)		AIRCRAFT (30 sec av)		DALLAS BOOM (9 min av)		LEVEL BLIS/A/C/BOOM (mb)
	DIR deg	SP ms <sup>-1</sup>	DIR deg	SP ms <sup>-1</sup>	DIR deg	SP ms <sup>-1</sup>	
1230	189	3.1	125	3.8			910/903/sfc
1348	228	5.5	170	4.4	185	5.3	995/985/sfc
1357	225	1.0	261	4.0			910/903/sfc
1400	231	4.4	185	5.1	195	5.0	995/985/sfc
1406	217	1.0	265	3.1			910/903/sfc
1454	239	2.1	193	1.8			950/945/sfc
1515	229	2.8	184	1.6			950/945/sfc

The agreement of the wind speed for all three systems is good generally but the BLIS data shows a large discrepancy in the wind direction. The wind direction data are contaminated by high-frequency noise (Ropelewski 1976).

$$\begin{aligned} \text{If } \Delta\alpha &= (\text{DIR})_{\text{BLIS}} - (\text{DIR})_{\text{AIRCRAFT}} \\ \text{and } \Delta w &= (\text{SP})_{\text{BLIS}} - (\text{SP})_{\text{AIRCRAFT}} \\ \text{then } \overline{\Delta\alpha} &= 25^\circ \pm 45^\circ \\ \overline{\Delta w} &= -.06 \pm 1.6 \text{ ms}^{-1}. \end{aligned}$$

The small difference between the boom and aircraft winds is probably the result of wind shear between the surface and 985 mb.

A similar averaging procedure was performed on q and  $\theta$  showing the agreement to be reasonably good (see Table 12).

Table 12. 3 km mean specific humidity and potential temperature intercomparison.

TIME	DALLAS BLIS		AIRCRAFT		DALLAS BOOM		LEVEL BLIS/A/C/BOOM (mb)
	q	θ	q	θ	q	θ	
	g/kg	°K	g/kg	°K	g/kg	°K	
1230	14.4	301.4	14.1	301.5			910/902/sfc
1257	17.4	299.6	16.5	298.6			970/970/sfc
1300	17.3	299.6	16.9	298.6			970/970/sfc
1348	16.0	298.4	16.4	298.5	16.6	297.6	995/985/sfc
1357	13.4	302.6	14.4	301.5			910/903/sfc
1400	16.0	297.8	17.4	297.8	16.4	297.4	995/985/sfc
1406	13.6	302.1	14.7	301.2			910/903/sfc
1454	16.2	300.4	15.7	300.3			950/945/sfc
1515	15.3	300.6	15.4	300.3			950/945/sfc

Similarly,  $\Delta q = (q)_{\text{BLIS}} - (q)_{\text{AIRCRAFT}}$

and  $\Delta \theta = (\theta)_{\text{BLIS}} - (\theta)_{\text{AIRCRAFT}}$

$$\overline{\Delta q} = -.02 \pm 0.9 \text{ g/kg}$$

$$\overline{\Delta \theta} = 0.5 \pm 0.5 \text{ °K.}$$

In tropical regions, differences of this order (in q and θ) are frequently observed locally and so the standard deviations listed above are acceptable.

#### 4.3 BLIS, aircraft and rawinsonde data

Figures 40 and 41 show the data from the Dallas 1221Z sounding, Dallas BLIS at 1221Z, Dallas boom at 1221Z and aircraft averages. At this time the Dallas was in the inflow to the southern line. Both aircraft averages are shown i.e. the larger-scale (~ 30 km) averages and the point (~ 3 km) averages mentioned earlier. All systems substantiate

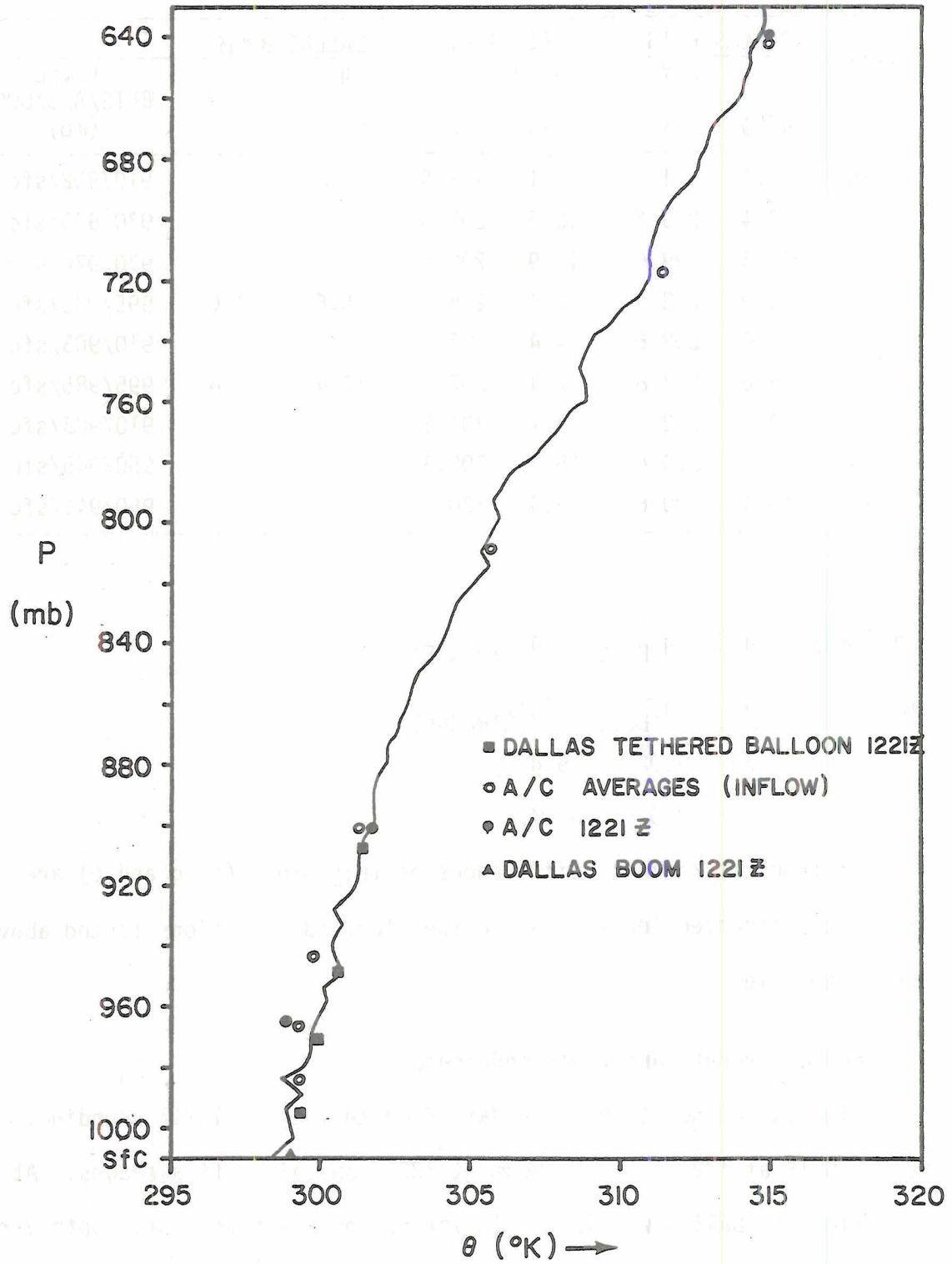


Figure 40. BLIS, aircraft, boom and rawinsonde  $\theta$  inter-comparison for 1221Z.

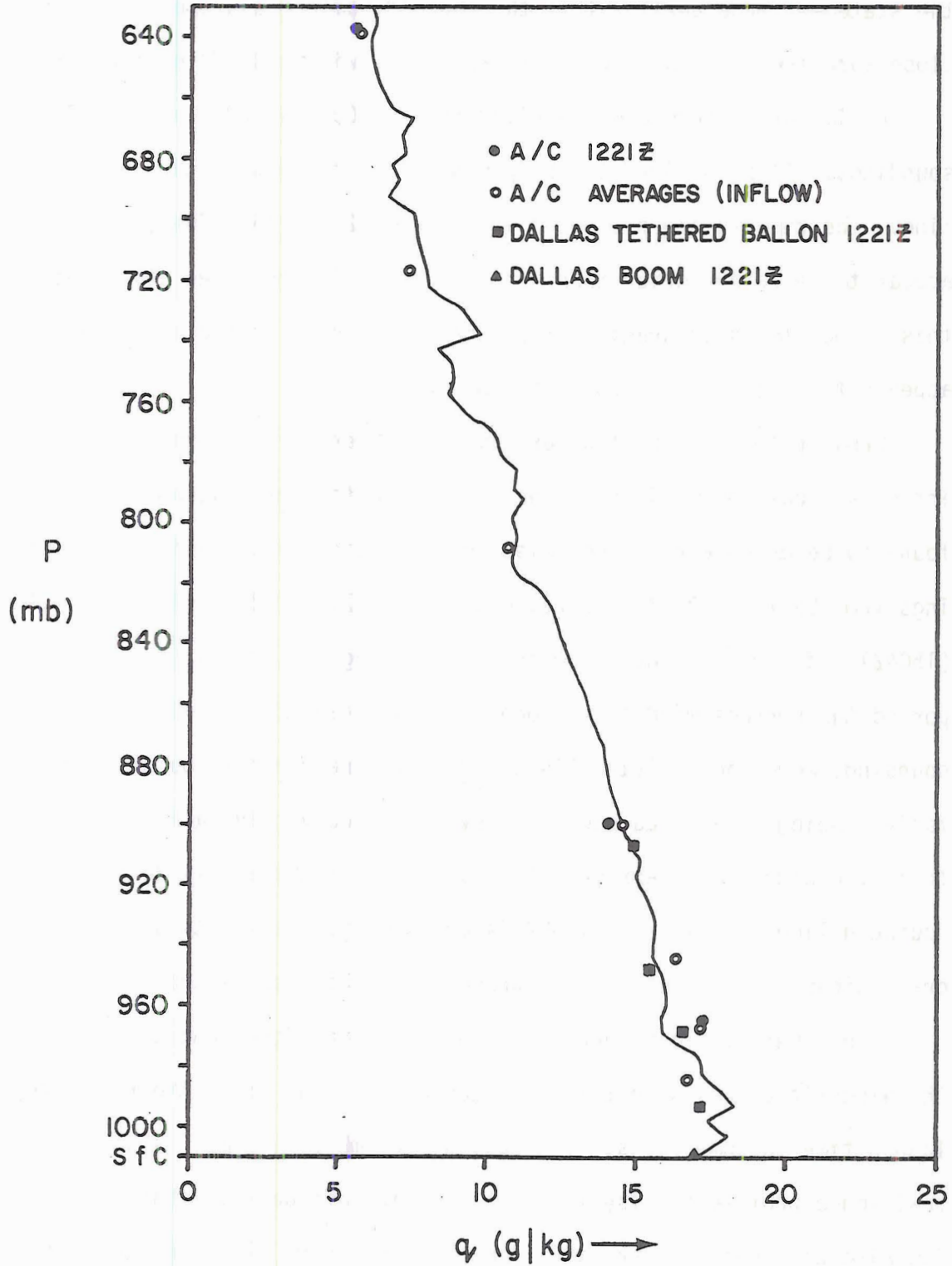


Figure 41. BLIS, aircraft, boom and rawinsonde  $q$  inter-comparison for 1221Z.

the statement made earlier that the thermodynamic measurements are in close agreement. Both aircraft averages are within  $0.5^{\circ}\text{K}$  of each other.

A similar procedure was applied for the Quadra 1202Z and 1505Z soundings. At both times the ship was in the outflow to the southern line. The results are presented in Figures 42 and 43. The averages appear to be rather drier than the rawinsonde in the mixed layer but this is not too discouraging since the Quadra data in the mixed layer appears to be slightly suspect in this case.

Great potential existed for computing average wind profiles in the inflow and outflow regions of the line but unfortunately, most data were found to be unrepresentative, missing or physically unrealistic. Soundings from Dallas (1221Z, 1502Z), Quadra (1202Z, 1505Z) and Oceanographer (1504Z) had large amounts of wind data missing and in most cases, reported the surface wind only. Oceanographer (1200Z) and all Meteor soundings were bad and Vize (1430Z, 2030Z) were found to be unrepresentative, being in an area showing very little convective activity in their vicinity. One representative sounding in the inflow to the southern line from Vize at 1130Z is compared to the thirty second aircraft winds in its vicinity and presented in Figures 44 and 45.

The zonal wind component shows good general agreement even though the aircraft values were taken as much as one hour after the rawinsonde launch time in some cases. The peak at 700 mb of  $-8\text{ ms}^{-1}$  shown in the rawinsonde profile is also found in the aircraft data at that level. The aircraft profile peaks at  $-4\text{ ms}^{-1}$  (see Figure 31). The rawinsonde also reports surface westerlies. The meridional wind component (Figure 45) shows little vertical shear from the surface to 400 mb and supports the aircraft data in a qualitative sense.

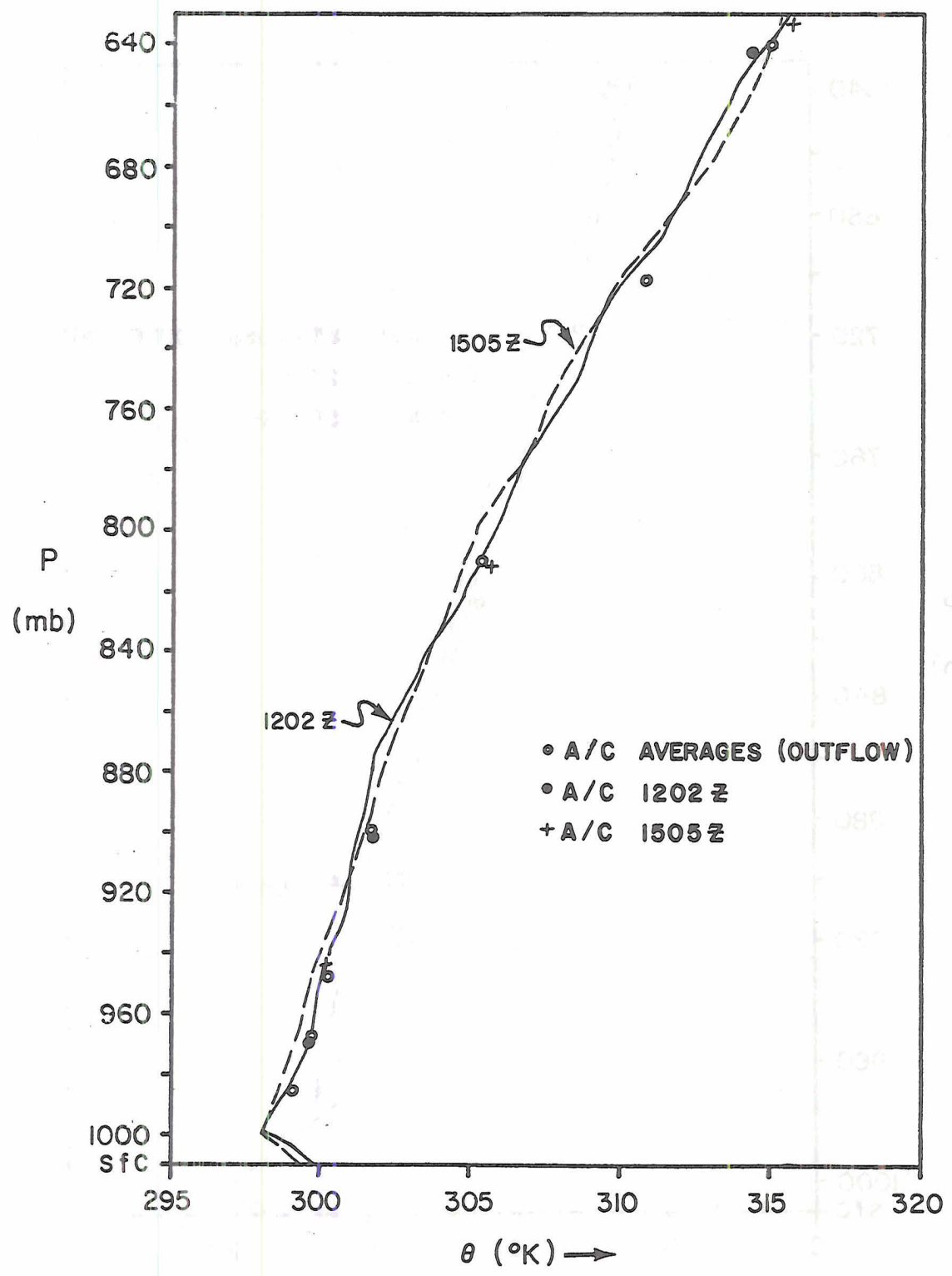


Figure 42. Quadra and aircraft potential temperature inter-comparison at 1202Z and 1505Z. Dashed line shows rawinsonde values.

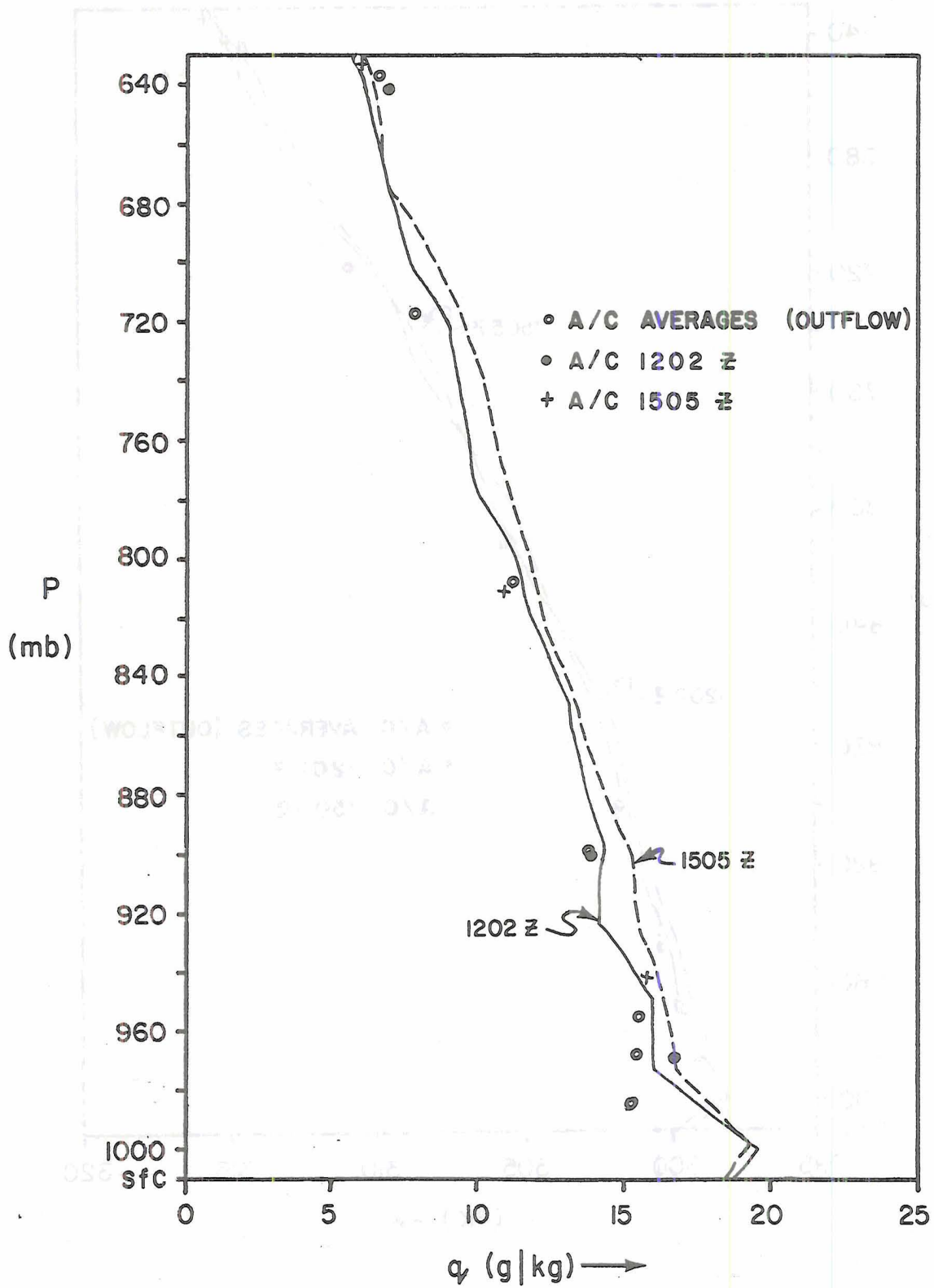


Figure 43. Quadra and aircraft specific humidity inter-comparison at 1202Z and 1505Z. Dashed line shows rawinsonde values.

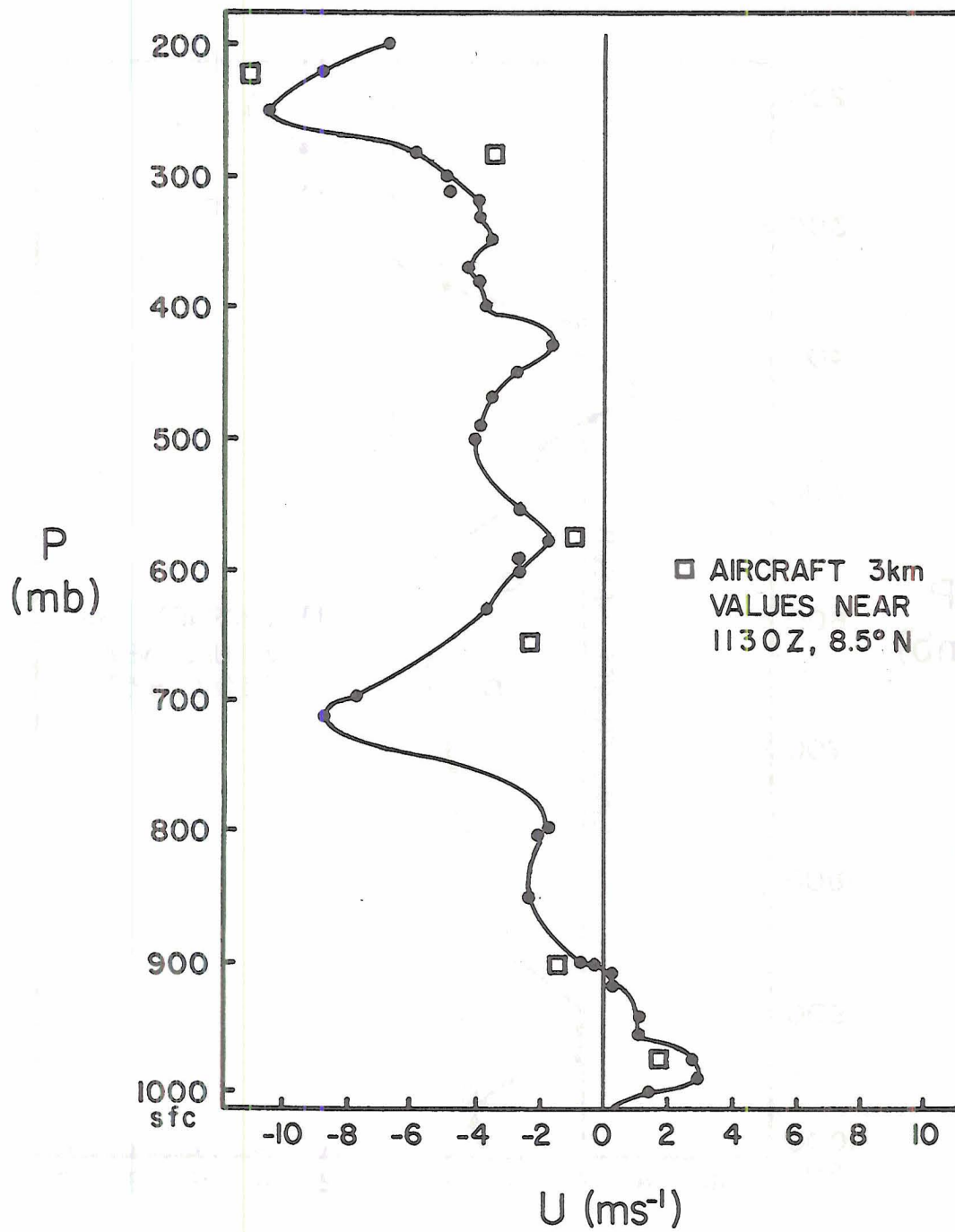


Figure 44. Comparison of zonal wind component from Vize at 1130Z and proximate aircraft data.

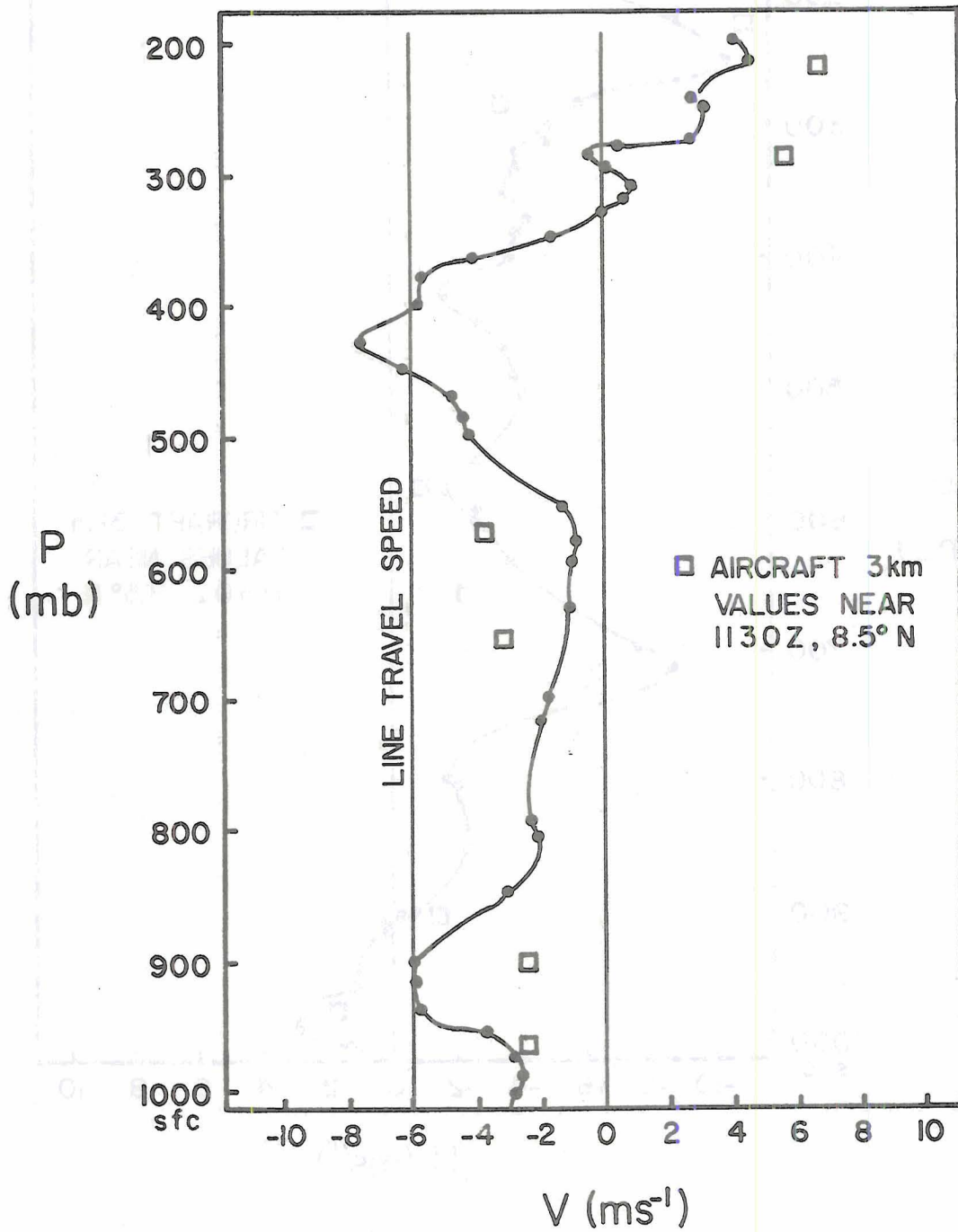


Figure 45. Comparison of meridional wind component from Vize 1130Z and proximate aircraft data.

In conclusion, then, this brief intercomparison has shown that the thermodynamic data from the systems presented here are in close agreement and gives confidence to the arguments presented in the previous chapter. The wind data from the BLIS should, however, be used with caution because of the directional problem. Winds derived from rawinsonde data seem to support the aircraft data but it is unwise, at this stage, to generalize from just one rawinsonde!

## V. CONCLUSIONS

The aim of this case-study was to attempt a semi-quantitative description of the typical lines of convection observed during the GATE, and to attempt a brief intercomparison between the different data sets. A line mission on 2nd September 1974 was flown close to the C-scale array where there were two lines which appeared to be components of a feeder band to a vortex to the NE. Aircraft, rawinsonde, radar and satellite data are used to describe the modifications of the immediate atmosphere surrounding the lines. Using high resolution aircraft data (10 sec) relative to the lines, there appeared to be very strong gradients in the vicinity of the 'leading edge' of the lines. Summarizing their basic features we have:

- a) Sharp convergence of high  $\theta_E$  air at the 'leading' edge of the lines ( $\sim 10^{-3} \text{ s}^{-1}$ )
- b) Strong divergence of slightly smaller magnitude to the rear
- c) Large drop in  $\theta_E$  indicating the presence of a downdraft at the surface with its origins in the 900-800 mb layer
- d) Cooling at the surface after the line passage of  $\sim 1.5 \text{ }^\circ\text{K}$  (small)
- e) Small, but sharp, pressure drop with a large decrease in incoming solar radiation, together with a lowering of cloud base.

From these line sections, the vertical profiles showed mean inflow and outflow. The wind profiles showed:

- a) Surface westerlies ahead of the line
- b) Very little vertical shear in both wind components
- c) No observable steering level

- d) Lines are embedded in a larger-scale motion field which is convergent and cyclonic from the surface to 700 mb.

The thermodynamic profiles showed:

- e) Drying in the lowest 50 mb resulting from the downdraft
- f) Drying at the surface and moistening above
- g) Cooling at the surface of 1.5°K with warming aloft
- h) A large  $\theta_E$  drop in the mixed layer.

From the wind fields relative to the line and the thermodynamic fields a schematic picture of the line is shown in Figure 46. The propagation of the downdraft after it has reached the surface forces additional mass up into the cloud layer from the surface layer. It is the downdraft which produces the sub-cloud layer convergence into the leading edge of the line, and, provided there is an abundant supply of warm, moist air in the mixed layer this may be the dominant driving mechanism for the lines. They can be maintained for a period of several hours until the supply of high  $\theta_E$  air has been extinguished.

A small pressure drop was observed after the passage of the gust front. This is unusual because the pressure normally rises at the gust-front to form a mesohigh (Zipser, 1977).

Since there is very little vertical shear in both the wind components, and therefore, no indication of a steering level, these systems must be self-propagating convective systems moving regularly through the basic large-scale flow field. A topic, which has not been the goal of this thesis, is to determine whether they are propagated by the downdraft alone or by the synoptic-scale flow field. Also, the fact that they may be forced gravity waves must not be overlooked. These questions may be answered by combining meso-scale and large-scale case

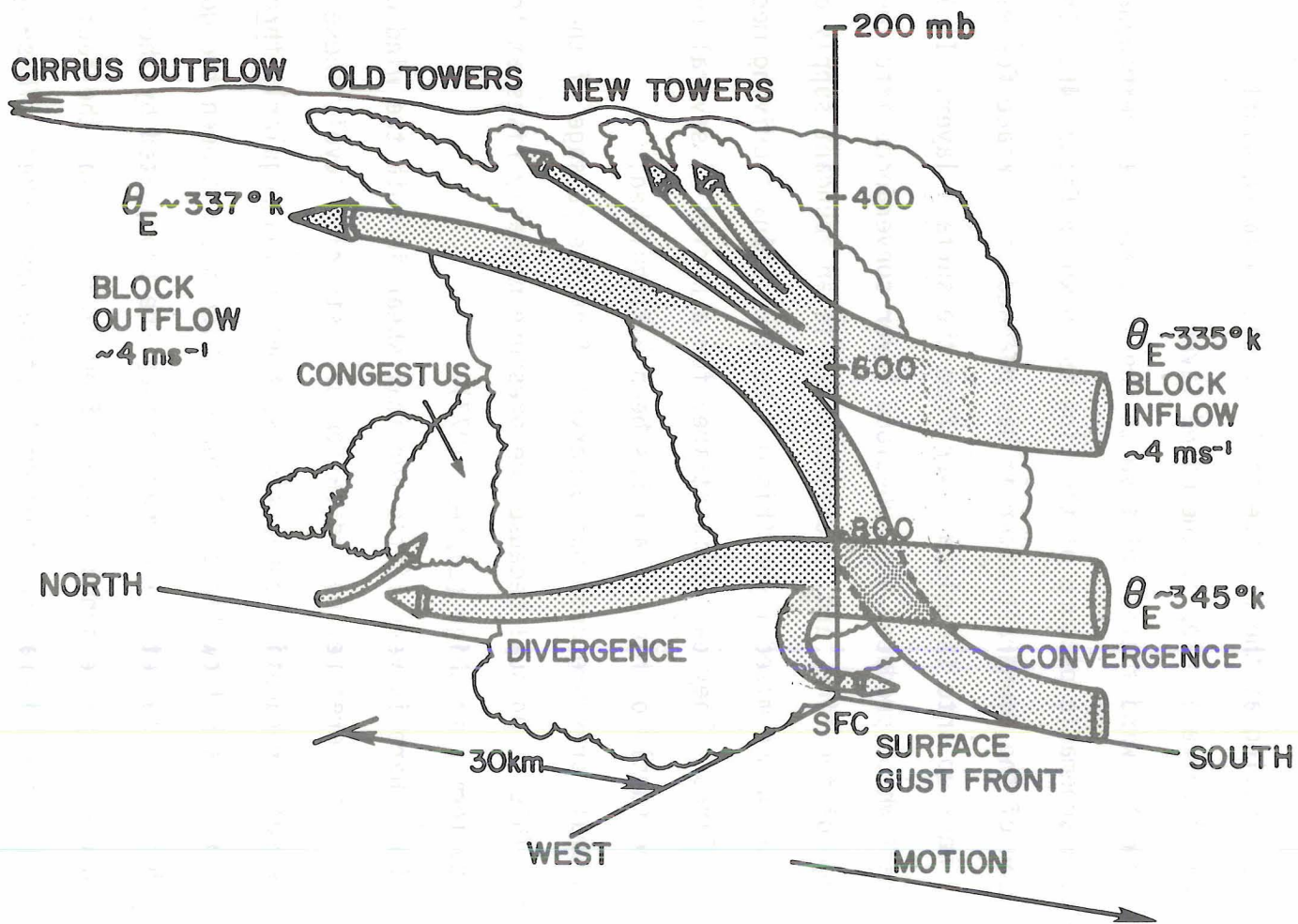


Figure 46. Schematic of stream tubes and characteristics of this line of convection.

studies with the objective of finding which scale is dominant. The interaction with the large-scale can possibly be studied by computing large-scale parameters over the GATE array such as a threshold value of divergence necessary for convection.

From various pieces of 'visual data' for this case, these lines appear to be spaced regularly (60 km) within the array and have constant velocity. Their spacing and velocity should be studied further - it is possibly a dynamical problem and is unfortunately, beyond the scope of this paper but provides avenues for future research.

In order to examine the generality of these lines, the author is currently investigating other days on which line convection was present. Personal observation of line-type systems at Dakar and a brief study of 13th July 1974 (Julian Day 194) seems to indicate that strong surface wind-shifts are a common occurrence within these types of systems.

REFERENCES

- Acheson, D.T., 1974: Omega windfinding and GATE. Bull. Amer. Meteor. Soc., 55, 385-397.
- Betts, A.K., and D.R. Rodenhuis, 1975: GATE convection subprogramme. Field Phase Report, 107 pp.
- \_\_\_\_\_, R.W. Groyer, and M.W. Moncrieff, 1976: Structure and motion of tropical squall lines over Venezuela. Quart. J. Roy. Meteor. Soc., 102, 395-404.
- \_\_\_\_\_, 1976: The thermodynamic transformation of the tropical subcloud layer by precipitation and downdrafts. J. Atmos. Sci., 33, 1008-1020.
- Browning, K.A., 1962: Air flow in convective storms. Quart. J. R. Met. Soc., 88, 117-135.
- Burpee, R.W., 1972: The origin and structure of easterly waves in the lower troposphere in North Africa. J. Atmos. Sci., 29, 77-90.
- \_\_\_\_\_, 1974: Characteristics of North African easterly waves during the summers of 1968 and 1969. J. Atmos. Sci., 31, 1556-1570.
- Grossman, R.L., 1976: A simple procedure for the correction of biases in winds measured from aircraft. GATE Information Bulletin No. 11, 29-45.
- Houze, R.A., 1976: GATE radar observations of a tropical squall line. Preprints 17th Radar Meteor. Conf., Seattle, Amer. Meteor. Soc., 384-389.
- Krishnamurti, T.N., 1968: A calculation of percentage area covered by convective clouds from moisture convergence. J. Appl. Meteor., 7, 184-195.
- Kuettner, J.P., 1959: The band structure of the atmosphere. Tellus, 11, 267-294.
- \_\_\_\_\_, 1971: Cloud bands in the earth's atmosphere. Tellus, 23, 404-425.
- Miller, M.J., and A.K. Betts, 1977: Travelling convective storms over Venezuela. Mon. Wea. Rev., July.
- Moncrieff, M.W., and J.S.A. Green, 1972: The propagation and transfer properties of steady convective overturning in shear. Quart. J.R. Met. Soc., 98, 336-352.

REFERENCES - Continued

- Moncrieff, M.W., 1975: Summary of a lecture delivered at the R.M.S. discussion meeting on GATE on 21/5/75.
- \_\_\_\_\_, and M.J. Miller, 1976: The dynamics and simulation of tropical cumulonimbus and squall lines. Quart. J. Roy. Meteor. Soc., 102, 373-394.
- Pennell, W.T., 1975: A study of the subcloud layer in the vicinity of an isolated line of cumulus. GATE Report No. 14, 276-286.
- Pestaina-Haynes, M., and G.L. Austin, 1976: Comparison between maritime tropical (GATE and Barbados) and continental mid-latitude (Montreal) precipitation lines. J. Appl. Meteor., 10, 1077-1082.
- Rasmusson, E., D. Acheson and J. Rasmussen, 1976: Summary of the Navaid upper air wind observing program from U.S. vessels in GATE. Informal preliminary report of U.S. GATE project office and the Center for Experiment Design and Data Analysis. 54 pp.
- Raymond, D.J., 1976: Wave - CISK and convective mesosystems. J. Atmos. Sci., 33, 2392-2398.
- Reed, R.J., and E.E. Recker, 1971: Structure and properties of synoptic-scale wave disturbances in the equatorial western Pacific. J. Atmos. Sci., 28, 1117-1133.
- \_\_\_\_\_, 1975: An example of a squall line in the B-scale network. GATE Report No. 14, 217-223.
- \_\_\_\_\_, N.E. LaSeur and D. Berrill, 1975: Aircraft observations of ITCZ structure on August 4, 1974. GATE Report No. 14, 211-217.
- \_\_\_\_\_, D.C. Norquist and E.E. Recker, 1977: The structure and properties of African wave disturbances as observed during Phase III of GATE. Mon. Wea. Rev., 105, 317-333.
- Reeves, R.W., and C.F. Ropelewski, 1976: Comparison of the vorticity and divergence derived from the ship surface, rawinsondes, and the boundary layer instrument system (BLIS). GATE Information Bulletin No. 14, Oct. 1976, 21-28.
- Riehl, H., 1945: Waves in the easterlies and the polar front in the tropics. Department of Meteorology, University of Chicago Misc. Report, 17, 79 pp.
- \_\_\_\_\_, 1954: Tropical meteorology. McGraw-Hill Book Co., Inc., New York, 394 pp.
- Ropelewski, C.F., 1977: Personal communication.

REFERENCES - Continued

- Ruiz, O., 1975: Mesoscale study of the tropical sub-cloud layer. Colorado State University, Atmospheric Science Paper No. 237, 133 pp.
- Smith, C.L., E.J. Zipser, S.M. Daggupaty and L. Sapp, 1975: An experiment in tropical mesoscale analysis: Part I. Mon. Wea. Rev., 103, 878-892.
- \_\_\_\_\_, 1975: An experiment in tropical mesoscale analysis: Part II. Mon. Wea. Rev., 103, 893-903.
- Seguin, W.R., and M. Garstang, 1976: Some evidence of the effects of convection on the structure of the tropical subcloud layer. J. Atmos. Sci., 33, 660-666.
- Williams, K.T., and W.M. Gray, 1973: Statistical analysis of satellite-observed trade wind cloud clusters in the western North Pacific. Tellus, 25, 313-336.
- Zipser, E.J., 1969: The role of organized unsaturated convective downdrafts in the structure and decay of an equatorial disturbance. J. Appl. Meteor., 8, 799-814.
- \_\_\_\_\_, 1977: Mesoscale and cloud-scale downdrafts as distinct components of squall-line structure. Submitted to Mon. Wea. Rev.

BIBLIOGRAPHIC DATA SHEET		1. Report No. CSU-ATSP-271	2.	3. Recipient's Accession No.
4. Title and Subtitle Case study of convection lines during GATE			5. Report Date June 1977	
7. Author(s) R. N. Mower			8. Performing Organization Rept. No. CSU-ATSP-271	
9. Performing Organization Name and Address Department of Atmospheric Science Colorado State University Foothills Campus Fort Collins, Colorado, 80523.			10. Project/Task/Work Unit No.	
			11. Contract/Grant No. OCD-74-21678	
12. Sponsoring Organization Name and Address Office for Climate Dynamics National Science Foundation 1800 G. Street NW Washington D.C.			13. Type of Report & Period Covered M.S. Thesis	
			14.	
15. Supplementary Notes				
16. Abstracts A semi-quantitative case study of 2 September 1974 (Julian Day 245) is presented. As many data sources as possible were used to describe the dynamics and thermodynamics of two lines of active convection located within the GATE B-scale ship array. Compositing data from 5 aircraft indicates a region of strong convergence near the surface ahead of the lines ( $\sim 10^{-3} s^{-1}$ ), with a somewhat weaker divergence to the rear associated with a region of downdraft air. The lines appear to be similar to tropical squall-lines with block inflow to the south and block outflow to the north. It is suggested that an adequate supply of high $\theta_E$ air below cloud base together with low-level divergence and vorticity seem to be important for the origin, formation and maintenance of these lines. The fact that the lines travel southwards at $6 m s^{-1}$ is not clearly understood except to comment that they appear to be embedded in feeder bands of a well defined vortex to the NE of the A/B-scale array; it is possible that their movement is related to the large scale dynamics of the vortex.				
17. Key Words and Document Analysis. 17a. Descriptors  Tropical squall-lines. Tropical mesoscale systems GATE data analysis Cumulus convection.				
17b. Identifiers/Open-Ended Terms				
17c. COSATI Field/Group				
18. Availability Statement			19. Security Class (This Report) UNCLASSIFIED	21. No. of Pages 92
			20. Security Class (This Page) UNCLASSIFIED	22. Price

